## SECTION 6                                                                129

## SECTION 7                                                                  161

FIGURE

# SECTION 6

# MINERAL POTENTIAL MODELLING
## Porphyry and Volcanogenic-hosted Massive Sulphides

M. Scott and summary of internal departmental report 'Mineral Prospectivity Analysis of the Yarrol Province using Probabilistic Neural Networks' prepared by D. Hedger, 2004

This section presents preliminary results of computer-based prospectivity modelling over the Yarrol Province. Mineral potential mapping is used to provide additional information to support estimates of the number of deposits (Section 7) for land-use decisions and to allow more focussed exploration targeting during reconnaissance tenement selection.

A Geographic Information System (GIS) forms the basic tool for the regional scale analysis of near surface mineralisation. The data themes in the Yarrol mineral potential GIS dataset have been sourced from the Department of Natural Resources, Mines and Water database interface MERLIN and include:

- Exploration Permit Minerals; Mineral Development Licences, Mining Lease (Natural Resources, Mines and Water Mining Tenure Database)

- Mineral Occurrences and Mines (MINOCC)

- Regional Geology (REGMAP)

- Regional Exploration Geochemistry

- Geophysics

- Infrastructure.

It should be noted that additional data from sources such as drilling, seismic and detailed structural interpretation, are required before a comprehensive assessment for the potential for mineralisation at depth can be made. Multiscale gravity wavelet (Worms) data, used to help delineate and characterise gradients in potential field data (gravity and aeromagnetics), is included in the Yarrol Data Package. The worm processing of gravity data for Yarrol was undertaken by Geoscience Australia, with post-processing by Dr Murphy, Department of Earth Sciences *pmd\*CRC*, University of Melbourne. The report and datasets that were generated, including a series of depth slices through the data at 900m, 2000m and 5000m levels of upward continuation are provided in the Data Package for interrogation by explorers. This dataset was not available at the time that prospectivity modelling was being undertaken for the Yarrol assessment.

Two computer-based modelling techniques have been applied to highlight areas favourable for mineralisation: weights of evidence (WOE) and probabilistic neural network (PNN). A preliminary example of WOE modelling using ArcSDM software is provided along with the software, included in the Yarrol mineral potential GIS dataset, to encourage more detailed interrogation by explorers. The following text provides an overview of the WOE and PNN methods, the analysis stages and results of the modelling for the Yarrol Province for VMS style deposits using both WOE and PNN, and porphyry style deposits using PNN. These deposit styles have been selected for the analyses because these types of mineralisation are known to occur in the area and because they are considered to have the greatest likelihood for discovery of a significant new economic resource. Studies of deposits such as Mount Morgan and Mount Chalmers in association with emerging models of caldera-forming processes for Kuroko-type VMS (Stix & others, 2003; Troll & others, 2002) and examples such as Develin Creek, described in this text as a Besshi/Cu-Zn subtype VMS, are used to define regional exploration criteria applied in the VMS prospectivity analyses.

Porphyry style deposits are included in this analysis because whilst most deposits known in

Queensland appear to be of smaller tonnages, none with the exception of Coulston Lakes have been fully assessed/drilled-out.

Local examples including Mount Cannindah, Moonmera and Riverhead are used in the PNN analysis of porphyry style deposits.

# WEIGHTS OF EVIDENCE

Weights of evidence is a data-driven or statistical technique, in the sense that statistical calculations are used to estimate the relative importance of evidence (the various geoscientific data themes) and to assign 'weights'. The importance of theme layers in delineating areas with potential for deposits is determined mathematically by how it compares with the areal distribution of a training set of known deposits. The odds of the association between the training set and each evidential data theme are measured and expressed as 'weights', defined as the natural log of the odds. When several themes are combined, the areas with the greatest coincidence of weights produce the highest ranking in terms of occurrence of undiscovered mineralisation. Detailed discussions of weights of evidence modelling to predict mineral potential have been presented by Bonham-Carter & others (1988, 1990), Agterberg (1989), Bonham-Carter & Agterberg (1990), Bonham-Carter (1994) and Wright & Bonham-Carter (1996). A summary of the technique is provided in Appendix 1 of this report.

## Method

This analysis aims to identify the combination of geological variables that control or point to the location of mineral deposits as defined by known historic sites of mineralisation. The analysis is not meant as an exhaustive treatment or to use all available data, but is meant to demonstrate the use of regionally applicable criteria through the application of weights of evidence in a relatively well-studied area.

The procedure followed in applying WOE analysis is carried out in five steps:

1.  development of a regional exploration model,

2.  selection of a training set,

3.  selection of evidence themes based on the descriptive model,

4.  testing of the evidence themes to qualify them as viable 'predictor' themes, and

5.  integration of the themes into a useful resource prediction model.

Definition of an exploration model is the first step in most prospectivity analyses. The exploration model used here is based on a range of published VMS models: USGS Bulletin 1693, UNE deposit model classification, Ozpot - Geoscience Australia, Stix & others, 2003 and characteristics of well-explored VMS style deposits known in the Yarrol Province — Taube & Van der Helder, 1983; Taube & McLeod, 1987; Golding & others, 1994; Horton & others, 1993. The exploration model is fundamental to the analysis process as it guides the selection of the training sites and determines the procedure for testing the evidence themes. The training set used consists of mines and non-producing prospects/occurrences of inferred VMS origin. The location and characteristics of these mines/occurrences were sourced from the GSQ MINOCC database. Mine and occurrence sites, and consequently the training sites are point datasets.

Evidence themes selected for testing include lithologic units, dykes and faults (including magnetic interpretations) all of which were defined as polygons or lines prepared as ArcView shapefiles from Arc/Info data. Subsets were derived as appropriate. For example, regional-scale faults and local-scale faults of various orientations were subsetted from the larger structural dataset in the Yarrol GIS. Shapefiles and point databases, such as line intersections, were reclassified from predetermined spatial criteria such as buffering, extrapolation/interpolation, or from expert-assigned attributes of genetic significance within the GIS data tables.

The testing of evidence themes involved comparison of the spatial distribution of the training set with the evidence themes. Testing produced weights, contrasts, and other statistical values calculated for each of the evidence themes. The weights express the

degree of spatial association between the training set and the evidence theme. The contrast value is the difference between the positive weight value and the negative weight value. The contrast describes the level of spatial correlation between an evidence theme and the training set. Based on the weight and contrast values generated, statistically significant evidence themes were selected as predictor themes.

In the final step the predictor themes are integrated into a VMS favourability model by the addition of values at each grid cell. The statistical significance of the contrast can be assessed to decide if the observed contrast is due to a random event or otherwise.

As a statistical approach, WOE is objective, avoiding to a large degree the subjective determination of weights. Disadvantages associated with this technique, however, include the assumption of conditional independence. Singer & Kouda (1999) compared neural networks with WOE and concluded that there is an inherent upward bias associated with multivariate methods founded on Bayes rule. They considered that probabilistic neural networks or logistic regression should be used where unbiased estimates are required, WOE being more appropriate to estimate thresholds between anomalies and background and for exploratory data analysis. WOE is also limited in its application to regions where the distribution of mineral occurrences is fairly well known. Appropriate control regions form the basis of the statistical models. Thus the validity of such methods depends on whether a well-known area exists which is representative of the area studied. This is often an obstacle as either there may be no similar well-known area, or data from a well-known area is insufficient for a statistical study.

## Application — Yarrol Province

Modelling was restricted to zone 56 of the Yarrol dataset.

## Generating regional search criteria

### VMS model

The Cu-Zn subtype model is characterised by thin, sheet like bodies of massive to well-laminated pyrite, pyrrhotite, chalcopyrite and sphalerite ± magnetite ± galena ± gold-electrum ± molybdenite. Ores may be localised within permeable sediments or in fractured/brecciated rocks. Deposits are associated with oceanic rifting environments and maybe proximal to continental and island arc sources, but range from mid-ocean to back-arc settings. Host rocks include thinly laminated clastic sediments, mafic tuffs and submarine basaltic volcanics that are commonly MORB type. Overlying and distal exhalites may be rich in iron.

Key features that can be extracted from regional datasets are:

1. tectonic setting — extensional environments such as backarc basins, oceanic ridges proximal to continental and island arcs,

2. extensional structures that allow fluid circulation,

3. areas of increased fault density and intersection,

4. occurrences of mafic tuffs and submarine basaltic volcanics, and

5. geochemical signatures: Cu, Zn, Ag, Co/Ni>1, Mn halos, Mg enrichment.

The Zn Pb (Cu) type or Kuroko VMS model is characterised by zoned massive sulphides, in some cases with underlying ore stockwork, stringers or disseminated sulphides. Overlying and distal exhalites may be rich in iron (magnetite, hematite), manganese and silica. The USGS Bulletin 1693 describes deposits as being located near centres of felsic volcanism toward the more felsic top of volcanic or volcanic-sedimentary sequences and may have brecciated or felsic domes nearby. Some deposits are described as being possibly gravity-transported and deposited in paleo-depressions in the seafloor. The University of New England deposit model description discusses formation in arc-related rifts (island arc or continental margin) associated with submarine rift grabens and/or calderas, felsic domes, dykes and underlying intrusives.

Recent models in the development of some ore-forming VMS systems emphasis a relationship with calderas that provide a heat source and magmatic volatiles to drive hydrothermal systems, structural permeability facilitating fluid flow and focussing mineralisation in a narrow zone and
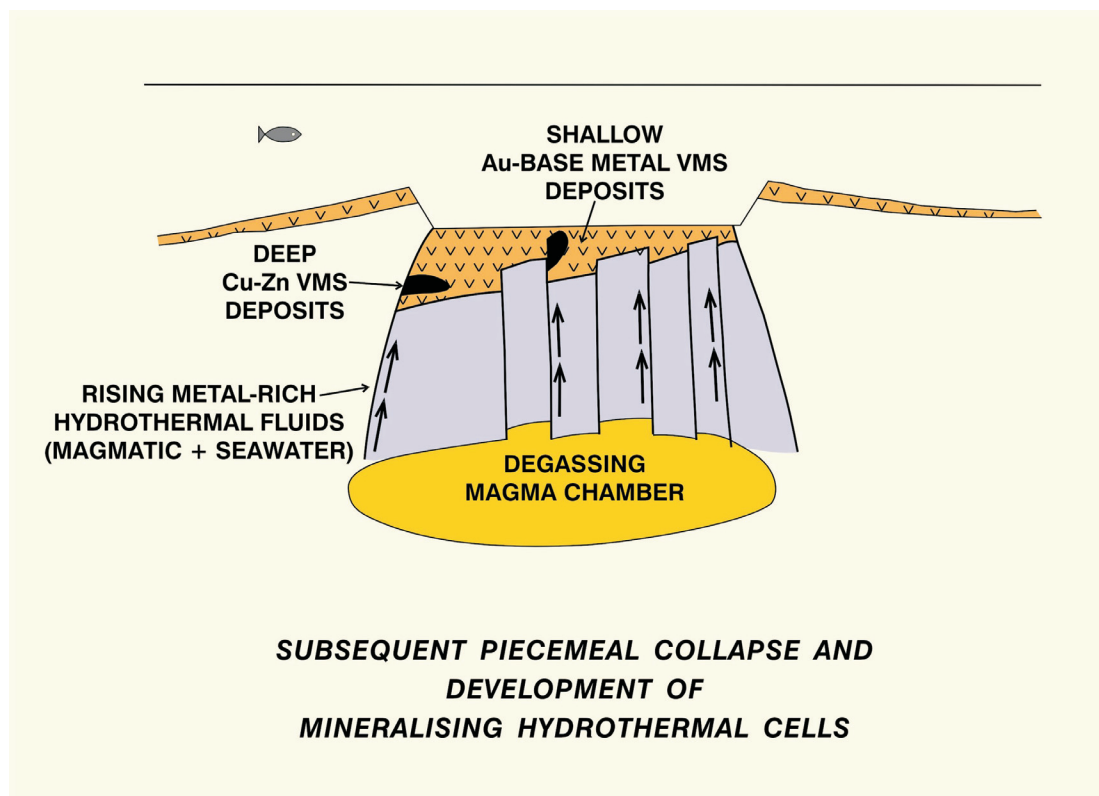
*Figure 34: Diagrammatic representation of caldera-related VMS mineralisation*

accumulations of significant thicknesses of permeable unwelded low-density pyroclastic debris as host rock. Stix & others (2003) discuss that in areas of extension and transtension main caldera faults may not be circular but instead form a series of connecting linear or accurate structures. Where these structures intersect are areas considered to be favourable for the formation of mineral deposits. In relatively undeformed successions, gravity signatures can aid in the identification of caldera structures. On a Bouguer gravity anomaly map, negative values are suggestive of low-density pyroclastic deposits. An asymmetric caldera should exhibit a large negative anomaly on one side, whereas steep gradients associated with the negative anomaly are indicative of a major caldera fault (Stix & others, 2003).

Key features of a caldera related VMS that can be readily extracted from regional data sets are:

1.   localities where dominant rock types are felsic volcanics,

2.   areas of increased fault density and intersection,

3.   extensional and transtensional settings,

4.   steep gravity contours,

6.   presence of a sub-volcanic granitoid, and

7.   geochemical signature showing: Zn, Hg and Mg halos; and anomalous Cu, Ag, As, Pb.

## Training sets

Training sets were defined using mines, prospects and mineral occurrences that have characteristics in common with those sought. The WOE methodology is reliant on the known examples used in training, in this instance mineral occurrences and deposits. Problems may arise due to the misclassification of deposits/occurrences. The use of mineral occurrences in the training set also means that the targets generated will include areas potentially hosting both relatively weak ore forming processes and those that may be economic. Fifty-one sites in total from the Yarrol Province were inferred, based on MINOCC investigations, to be related to VMS mineralisation. Five of the 51 training sites are currently prospects or former producers (eg Mount Morgan, Mount Chalmers, Tea Tree, Drive Prospect). The remainder of the training set consists of small to very small occurrences or abandoned producing sites. Mineral occurrences are small and uneconomic but importantly indicate where mineralisation has occurred, and as such provide a focus for initial

exploration investigations. Some occurrences are described as vein-type rather than stratabound and are considered to represent feeder zones.

## Analysis of geological patterns

Based on the descriptive model, themes were assembled and/or generated and tested as possible predictor themes. This involved calculating the spatial relationships of the selected themes to the known mineral occurrences.

The themes investigated were:

• geology — to determine the lithological units nearest to known mineralization. This establishes the areal association between the training set and the geological units that occur at the surface.

• faults — regional scale features interpreted as representing deep crustal structures that could provide fluid circulation pathways and local linear features that may act as potential localisers for ore deposition were analysed in terms of proximity to known mineralisation. Both mapped and interpreted faults were used.

• geochemistry — stream sediment, rock chip and soil sample anomalies for indicator elements Cu, Zn and Pb were analysed. Other potential indicator elements (eg Ba, As, Ag, Au and halo enrichment in Mg) available in the regional geochemical database were not included because of quality issues (refer Section 5).

Whilst gravity data is considered to be a valuable regional dataset in the prospecting for cauldera related VMS deposits and as an indicator of subsurface structures, formatting of the data became an issue within the timeframe allowed for the mineral potential analysis. Multiscale gravity wavelet (Worms) data, however, have been included in the Yarrol mineral potential GIS and an accompanying report that discusses these data (Murphy, 2005) is included in the Yarrol Data Package.

The following hypotheses were tested:

1.  Lithological control — rock types identified in island arc and backarc basins with either significant tholeiitic or felsic

volcanism are good indicators of VMS mineralisation in Yarrol

2.  Fault orientation — normal faults of particular orientation control mineralisation

3.  Fault density — the density of faulting is a good indicator of mineralisation

4.  Fault intersections — intersecting linear features control mineralisation

5.  Regional geochemical data for Cu, Pb and Zn can be used as a predictor.

In some instances reclassification of data was required to test a hypotheses. For example, fault data required subsetting by orientation, which allowed specific combinations of fault intersections and density themes to be generated. For both the linear orientation and point intersection themes buffering was done to enable determination of the optimum distance for the greatest spatial association of training sites and a selected feature. Buffering was at 500m intervals over 10km for regional structures and 250m intervals over 4km for local scale faulting. Intersections of faults were buffered at 250m intervals over 4km. Fault density patterns were derived by generating points every 1km along linears and gridding the density of the number of points per unit cell using an Arc script (refer Figure 35 and Yarrol mineral potential GIS -WOE scripts). The resultant data layers (Table 7), defined by specific attributes, were processed using Arcview 3.2 and the ArcSDM extension software (Kemp & others, 2001) to assess the spatial correlation of each variable with the training dataset.

In the spatial correlation calculation a cell size of ~1km was used. The size of the grid was chosen to allow a broad target area for indicators associated with potential mineralisation. The correlations were calculated assuming the known deposits have a sphere of influence of 0.5km. The spatial correlation (prior probability) of a feature can be calculated by using the relationship of the area covered by the data variable being tested and the number of training data points. This produces a W+ result for when the feature is present and a W- result when the feature is absent (refer Appendix 1). A contrast value C is then calculated from the difference. The standard deviations of Ws and Cs are calculated, from which the studentised value of

## Table 7: Subsetted map layers processed using ArcSDM extension software

| Map Layer | Attribute |
|---|---|
| Geology of the Yarrol Province 1:100 000 scale | Lithology |
| Tectonic Faults — regional scale | Trend |
| Faults — local scale | Trend |
| Faults — magnetic interpretation | Trend |
| Tectonic Faults — regional scale | Distance from fault |
| Faults — local scale | Distance from fault |
| Faults — magnetic interpretation | Distance from fault |
| Faults | Distance from intersection |
| Tectonic Faults — regional scale | Intensity of occurrence |
| Faults — local scale | Intensity of occurrence |
| Geochemical data — regional scale | Regional anomalies |

the contrast (StudC) can then be calculated (the ratio of the standard deviation of the contrast Cs to the contrast C). StudC gives an informal test of the hypothesis that C=0 and as long as the ratio is relatively large, implying the contrast is large compared to the standard deviation, then the contrast is more likely to be real. Ideally a StudC value larger than (-)1.5 can be considered as a positive or negative correlation (Bonham-Carter, 1994, Partington & Rattenbury, 2003). This ratio is best used as a relative indicator of spatial correlation, rather than an absolute sense. In this study a strong correlation is inferred from StudC values >4.0, moderate correlations inferred from StudC values between 4.0–1.5, weak correlations inferred from StudC values between 1.5–0.5, and poor correlations inferred from StudC values <0.5.

*Hypothesis 1: Lithological control*

Strong host rock controls are evident using the regional datasets. VMS mineralisation is associated with rock units identified as island arc and back arc basin settings with either significant tholeiitic or felsic volcanism — Capella Creek Group (Mount Warner Volcanics, Mount Dick beds, Marble Waterhole beds, Raspberry Creek Formation, Ginger Creek member); Three Moon Conglomerate, Mount Hoopbound Formation, Balacava Formation, Lochenbar Formation, Owl Gully Volcanics, Rookwood Volcanics, Berserker Group (Chalmers Formation and Sleipner member).

Themes tested and accepted as predictor themes are the Marble Waterhole beds, Chalmers Formation, Mount Dick beds, Mount Warner Volcanics, Rookwood Volcanics, Ellrott Rhyolite. Table 8 shows high positive weights

(inside the pattern) that indicate a lithology as a strong targeting pattern. The strong negative weightings (outside the pattern) indicate that unfavourable lithologic units are not associated with the training set. These results were anticipated since these units are known to host 36 of the 51 training sites.

The Three Moon Conglomerate, Mount Hoopbound Formation and the Sleipner member returned contasts and stud(C) values that indicated they were moderate predictors, with the Raspberry Creek Formation, Ginger Creek member, Lochenbar and Balaclava Formations as poor predictors.

Grouping units by lithological descriptors such as 'felsic volcanics' and 'mafic volcanics' reduced the effectiveness of the prediction but would broaden the scope of an analysis if lithologically similar units were considered to be under-explored.

It is recognised that geological units in the subsurface may differ from surface units.

*Hypothesis 2: Faults of particular orientation control mineralization*

Faults are considered as potential localisers for ore deposition providing increased permeability and pathways for mineralising fluids. The hypothesis was tested that faults of particular orientations influenced deposition using WOE cumulative proximity analysis.

Faults trending 60–80° and buffered at 250m intervals showed a strong association with training sites within the first 500m as did faults trending between 80–120° at an increased buffer distance of ~1.5km (Tables 9, 10, 11).

## Table 8: Lithological predictor themes

| Rock unit | Area km² | Number points | W+ | W- | Contrast (C) | Stud(C) | Ranking |
|---|---|---|---|---|---|---|---|
| Marble Waterhole beds | 58.37 | 10 | 4.80 | 0.330 | 5.060 | 13.70 | high |
| Chalmers Formation | 203.70 | 10 | 3.40 | -0.210 | 3.690 | 10.47 | high |
| Mount Dick beds | 22.70 | 3 | 4.48 | -0.060 | 4.540 | 7.60 | high |
| Mount Warner Volcanics | 62.33 | 4 | 3.70 | -0.070 | 3.870 | 7.29 | high |
| Rookwood Volcanics | 292.13 | 6 | 2.61 | -0.110 | 2.720 | 6.27 | high |
| Ellrott Rhyolite | 102.46 | 3 | 2.90 | -0.057 | 3.025 | 5.07 | high |

## Table 9: Faults trending 60–80

| Area km² | Area Units | #Points | W+ | s(W+) | W- | s(W-) | CONTRAST | s(C) | stud(C) |
|---|---|---|---|---|---|---|---|---|---|
| 796.5116 | 12744.1855 | 11 | 2.0590 | 0.3016 | -0.2200 | 0.1601 | 2.2790 | 0.3415 | 6.6732 |
| 2387.5921 | 38201.4732 | 19 | 1.5074 | 0.2295 | -0.3901 | 0.1796 | 1.8975 | 0.2914 | 6.5115 |
| 3264.7262 | 52235.6190 | 24 | 1.4281 | 0.2042 | -0.5317 | 0.1961 | 1.9597 | 0.2831 | 6.9222 |
| 4311.8475 | 68989.5605 | 28 | 1.3040 | 0.1890 | -0.6561 | 0.2132 | 1.9601 | 0.2849 | 6.8791 |
| 5560.0395 | 88960.6317 | 28 | 1.0496 | 0.1890 | -0.6028 | 0.2132 | 1.6524 | 0.2849 | 5.7995 |
| 6908.2811 | 110532.4970 | 29 | 0.8676 | 0.1857 | -0.5883 | 0.2182 | 1.4559 | 0.2866 | 5.0807 |
| 7819.4126 | 125110.6010 | 29 | 0.7437 | 0.1857 | -0.5449 | 0.2182 | 1.2886 | 0.2866 | 4.4968 |
| 8682.9478 | 138927.1640 | 34 | 0.7980 | 0.1715 | -0.7739 | 0.2500 | 1.5719 | 0.3032 | 5.1846 |
| 9258.9616 | 148143.3860 | 34 | 0.7337 | 0.1715 | -0.7442 | 0.2500 | 1.4779 | 0.3032 | 4.8747 |

## Table 10: Faults trending 80–100

| Area km² | Area Units | #Points | W+ | s(W+) | W- | s(W-) | CONTRAST | s(C) | stud(C) |
|---|---|---|---|---|---|---|---|---|---|
| 832.4518 | 13319.2281 | 2 | 0.3094 | 0.7072 | -0.0110 | 0.1443 | 0.3204 | 0.7217 | 0.4440 |
| 2626.5456 | 42024.7289 | 12 | 0.9523 | 0.2887 | -0.1773 | 0.1622 | 1.1295 | 0.3312 | 3.4106 |
| 3626.0705 | 58017.1276 | 19 | 1.0894 | 0.2295 | -0.3412 | 0.1796 | 1.4306 | 0.2914 | 4.9095 |
| 4882.0333 | 78112.5323 | 27 | 1.1434 | 0.1925 | -0.5876 | 0.2085 | 1.7310 | 0.2838 | 6.0998 |
| 6304.0979 | 100865.5660 | 28 | 0.9240 | 0.1890 | -0.5696 | 0.2132 | 1.4936 | 0.2849 | 5.2421 |
| 7853.4101 | 125654.5610 | 29 | 0.7393 | 0.1857 | -0.5433 | 0.2182 | 1.2826 | 0.2866 | 4.4759 |
| 8884.9897 | 142159.8350 | 30 | 0.6498 | 0.1826 | -0.5404 | 0.2236 | 1.1902 | 0.2887 | 4.1228 |
| 9944.6891 | 157515.0240 | 31 | 0.5800 | 0.1796 | -0.5412 | 0.2294 | 1.1212 | 0.2914 | 3.8479 |
| 10486.7550 | 167788.0810 | 31 | 0.5168 | 0.1796 | -0.5059 | 0.2294 | 1.0227 | 0.2914 | 3.5098 |

## Table 11: Faults trending 100–120

| Area km² | Area Units | #Points | W+ | s(W+) | W- | s(W-) | CONTRAST | s(C) | stud(C) |
|---|---|---|---|---|---|---|---|---|---|
| 1270.5331 | 20328.5301 | 4 | 0.5798 | 0.5000 | -0.0375 | 0.1474 | 0.6173 | 0.5213 | 1.1841 |
| 3606.6434 | 57706.2938 | 13 | 0.7151 | 0.2774 | -0.1651 | 0.1644 | 0.8802 | 0.3224 | 2.7298 |
| 4858.7207 | 77739.5318 | 26 | 1.1104 | 0.1961 | -0.5461 | 0.2041 | 1.6565 | 0.2831 | 5.8512 |
| 6324.4963 | 101191.9410 | 31 | 1.0226 | 0.1796 | -0.7153 | 0.2294 | 1.7379 | 0.2914 | 5.9643 |
| 8000.0848 | 128001.3560 | 33 | 0.8500 | 0.1741 | -0.7474 | 0.2425 | 1.5975 | 0.2986 | 5.3506 |
| 9750.4676 | 156007.4810 | 35 | 0.7110 | 0.1690 | -0.7827 | 0.2582 | 1.4937 | 0.3086 | 4.8398 |
| 10866.5552 | 173864.8820 | 37 | 0.6582 | 0.1644 | -0.8639 | 0.2774 | 1.5221 | 0.3224 | 4.7207 |
| 11914.6478 | 190634.3650 | 38 | 0.5928 | 0.1622 | -0.8822 | 0.2887 | 1.4749 | 0.3311 | 4.4540 |
| 12572.2556 | 201156.0890 | 38 | 0.5390 | 0.1622 | -0.8413 | 0.2887 | 1.3804 | 0.3311 | 4.1684 |

## Table 12: Regional faults trending 60–80

| Area km² | Area Units | #Points | W+ | s(W+) | W- | s(W-) | CONTRAST | s(C) | stud(C) |
|---|---|---|---|---|---|---|---|---|---|
| 206.8987 | 3310.3799 | 6 | 2.8018 | 0.4086 | -0.1205 | 0.1508 | 2.9224 | 0.4355 | 6.7097 |
| 618.7535 | 9900.0563 | 7 | 1.8594 | 0.3781 | -0.1288 | 0.1525 | 1.9882 | 0.4077 | 4.8766 |
| 828.5663 | 13257.0613 | 7 | 1.5672 | 0.3781 | -0.1212 | 0.1525 | 1.6884 | 0.4077 | 4.1417 |
| 1140.3715 | 18245.9437 | 9 | 1.4991 | 0.3334 | -0.1574 | 0.1562 | 1.6565 | 0.3682 | 4.4992 |
| 1470.6324 | 23530.1182 | 9 | 1.2446 | 0.3334 | -0.1452 | 0.1562 | 1.3899 | 0.3682 | 3.7751 |
| 1879.5731 | 30073.1695 | 10 | 1.1046 | 0.3163 | -0.1546 | 0.1581 | 1.2592 | 0.3536 | 3.5610 |
| 2135.0396 | 34160.6339 | 10 | 0.9771 | 0.3163 | -0.1449 | 0.1581 | 1.1220 | 0.3536 | 3.1731 |
| 2575.0637 | 41201.0193 | 12 | 0.9721 | 0.2887 | -0.1793 | 0.1622 | 1.1513 | 0.3312 | 3.4765 |
| 3100.5671 | 49609.0735 | 12 | 0.7863 | 0.2887 | -0.1587 | 0.1622 | 0.9450 | 0.3312 | 2.8534 |
| 3475.5104 | 55608.1657 | 12 | 0.6721 | 0.2887 | -0.1437 | 0.1622 | 0.8158 | 0.3312 | 2.4635 |
| 3846.5682 | 61545.0911 | 12 | 0.5707 | 0.2887 | -0.1287 | 0.1622 | 0.6993 | 0.3312 | 2.1117 |
| 4449.7800 | 71196.4804 | 12 | 0.4250 | 0.2887 | -0.1038 | 0.1622 | 0.5287 | 0.3312 | 1.5965 |
| 4790.7258 | 76651.6135 | 12 | 0.3511 | 0.2887 | -0.0894 | 0.1622 | 0.4405 | 0.3312 | 1.3302 |
| 5343.4272 | 85494.8349 | 12 | 0.2419 | 0.2887 | -0.0657 | 0.1622 | 0.3076 | 0.3312 | 0.9288 |
| 5649.4042 | 90390.4672 | 12 | 0.1862 | 0.2887 | -0.0523 | 0.1622 | 0.2385 | 0.3312 | 0.7202 |
| 6386.6631 | 102186.6090 | 1 | 0.2177 | 0.2673 | -0.0733 | 0.1677 | 0.2910 | 0.3150 | 0.9240 |
| 6882.0545 | 110112.8710 | 14 | 0.1430 | 0.2673 | -0.0505 | 0.1677 | 0.1935 | 0.3150 | 0.6144 |
| 7274.4821 | 116391.7140 | 19 | 0.3930 | 0.2294 | -0.1816 | 0.1796 | 0.5746 | 0.2914 | 1.9720 |
| 7794.1574 | 124706.5180 | 19 | 0.3240 | 0.2294 | -0.1567 | 0.1796 | 0.4806 | 0.2914 | 1.6494 |
| 8340.0592 | 133440.9470 | 19 | 0.2562 | 0.2294 | -0.1298 | 0.1796 | 0.3860 | 0.2914 | 1.3247 |

## Table 13: Cumulative analysis for fault density grid

| Area km² | Area Units | #Points | W+ | s(W+) | W- | s(W-) | CONTRAST | s(C) | stud(C) |
|---|---|---|---|---|---|---|---|---|---|
| 363.1875 | 726.3750 | 1 | 0.4311 | 1.0007 | -0.0071 | 0.1429 | 0.4382 | 1.0108 | 0.4335 |
| 178.6875 | 357.3750 | 2 | 1.8377 | 0.7091 | -0.0344 | 0.1444 | 1.8722 | 0.7236 | 2.5871 |
| 1354.6875 | 2709.3750 | 6 | 0.9073 | 0.4087 | -0.0782 | 0.1508 | 0.9854 | 0.4356 | 2.2621 |
| 1355.2500 | 2710.5000 | 6 | 0.9068 | 0.4087 | -0.0782 | 0.1508 | 0.9850 | 0.4356 | 2.2611 |
| 1356.3750 | 2712.7500 | 6 | 0.9060 | 0.4087 | -0.0781 | 0.1508 | 0.9841 | 0.4356 | 2.2590 |
| 1358.3125 | 2716.6250 | 7 | 1.0591 | 0.3785 | -0.1011 | 0.1526 | 1.1602 | 0.4080 | 2.8432 |
| 1362.0000 | 2724.0000 | 7 | 1.0564 | 0.3785 | -0.1009 | 0.1526 | 1.1573 | 0.4080 | 2.8362 |
| 1372.0625 | 2744.1250 | 7 | 1.0490 | 0.3784 | -0.1005 | 0.1526 | 1.1495 | 0.4080 | 2.8172 |
| 1409.2500 | 2818.5000 | 10 | 1.3799 | 0.3168 | -0.1715 | 0.1582 | 1.5514 | 0.3541 | 4.3816 |

Large regional faults were analysed separately, at 500m buffer intervals. North-easterly trends, between 40–80°, showed significant association to VMS style mineralisation within a 1km buffer zone (Table 12).

*Hypothesis 3: Fault density is a good indicator for mineralisation.*

Density patterns for faults and fault intersections generated (Figures 35 and 36) were found to have a significant association using the WOE cumulative descending analysis (Table 13).

Fault intersections were generated by selecting faults within a trend range and generating point intersections with all other faults in the dataset. Point intersections were then buffered at 500m intervals.

A significant association was found with a stud(C) value of 5.3 generated for intersections made with faults trending between 135–145° (Figure 36).

Intersections were also similarly generated for regional faults. Results indicated a strong association between regional faults trending 40–60° and mineralisation within a 500m buffer zone and at an increased buffer size of 2km for faults trending 60–80°.

*Hypothesis 4: Regional geochemical data for Pb, Zn, and Cu are good predictors of VMS mineralisation.*

These elements were selected based on regional search criteria discussed above and because of quality issues with the available regional geochemical data.
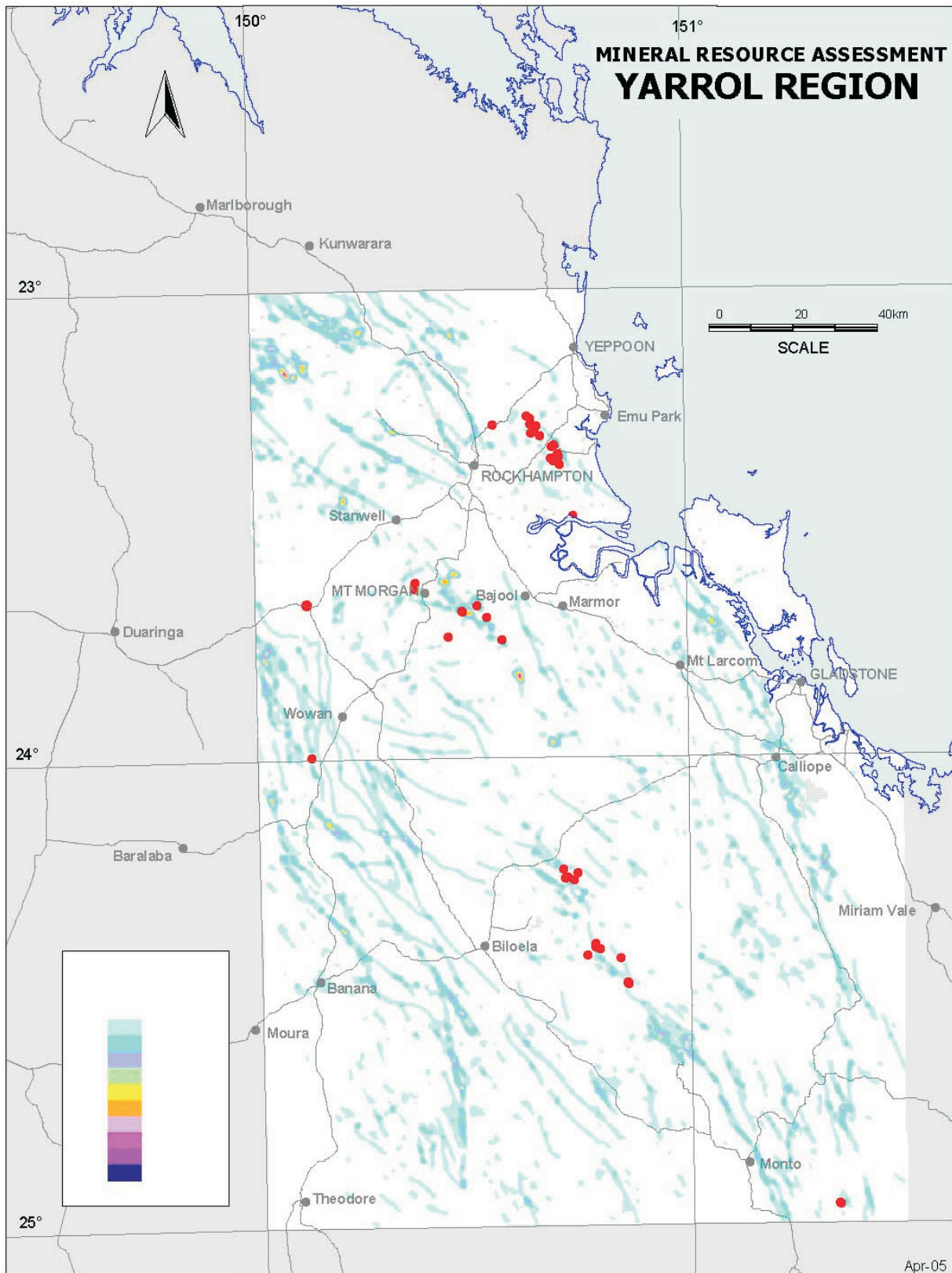
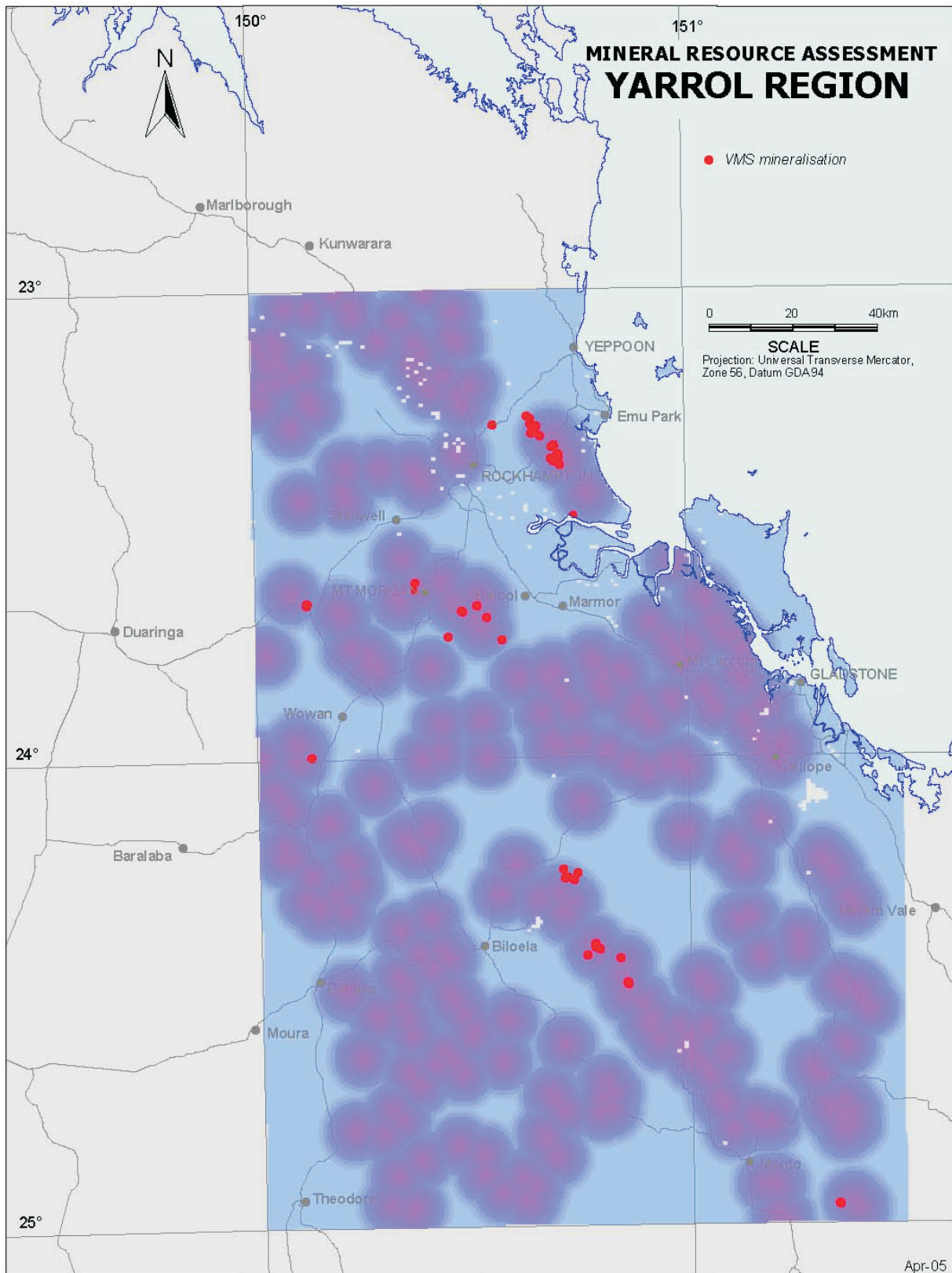*Figure 35: Regional fault density pattern*

*Figure 36: Intersections of faults trending 135–145° (10km buffer at 500m intervals)*

Cu and Zn regional geochemical patterns were found to have significant spatial correlation to the training dataset using the WOE cumulative descending analysis.

*Results*

The determination of predictor themes provides a ranked exploration model highlighting important spatial controls on VMS mineralisation in the Yarrol assessment area based on known mineralisation in the area and the datasets available.

To generate a final prospectivity map the *predictor* themes and *attribute fields* that contain the classes to analyse are combined to generate a response grid (or unique conditions grid ) and attribute table. Weights, variances and contrasts are calculated for each predictor theme and written to a *weights table* (woe#.bdf) and a *variances table* (woevar#.dbf). Arc-SDM calculates a number of statistics for each unique condition (eg posterior probability, sum of weights, uncertainty).

The response grid is symbolised using the 'posterior probability' attribute, using 7 classifications defined by ArcView's natural breaks method. It should be noted that whilst 'posterior probabilities' are generated, issues of upward bias (Singer & Kouda, 1999) and very often conditional independence, means that these values are better treated as rankings. A major benefit of this process is that it readily allows numerous scenarios to be run and examined.

## Integrating patterns — VMS targets

In this assessment a single scenario is used to demonstrate the process. The objective of this preliminary modelling is to encourage explorers to further interrogate the datasets rather than to undertake a comprehensive analysis here. To facilitate further investigation the raw datasets are provided in an accompanying GIS (Yarrol_WOE) along with the SDM software (ArcSDM, Kemp & others, 2001).

Scenario:
The patterns for three predictor themes (lithology, structure, geochemistry) are combined to suggest possible regional VMS target areas.

The Marble Waterhole beds, Mount Dick beds, Mount Warner Volcanics, Rookwood Volcanics, Ellrott Rhyolite and Chalmers Formations make-up the lithology theme. These units were selected as strong predictors from the earlier hypothesis testing, producing high contrast values of about 5 to 3 (Table 8).

Fault density and the copper regional geochemistry predictor themes are combined with the lithology theme to create a response theme – sdmu3 (refer Figure 37).

The additive results of the predictor themes expresses the ranking of the unit cell in terms of the likelihood of mineralisation.

The map generated in this preliminary scenario consistently highlights areas of known mineralization, but also includes an area with no recorded workings.

The Mount Morgan area and an elongate zone extending to the south-east, including the Grillo and Drive prospects, are ranked as highly prospective. High regional copper geochemistry is recorded west and north of Mount Morgan. Both areas are associated with predictive rock units, including the Mount Warner Volcanics and the Mount Dick beds, and both are associated with zones of structural intersection.

South-west of Westwood a cluster of VMS-type occurrences are associated with Rookwood Volcanics and some moderate copper values.

On the west of the Bajool sheet an area is identified as prospective within Raspberry Creek Formation. This area continues the zone of structural intersections identified in the Grillo and Drive prospect area. This area also corresponds with 'Area 26' in the PNN modelling (refer Figure 48).

Occurrences in the Mount Fane area are associated with elevated copper values and structural intersections within Three Moon Conglomerate. Further south, in the Kroombit area, the Karita prospect is associated with Marble Waterhole beds and some elevated copper geochemistry. This area has also been identified as prospective, but for porphyry style mineralization, in the PNN modelling (refer Figure 48).

Parts of the Glassford Igneous complex are identified as favourable, and this aberation is attributed to the effect of elevated regional copper values in the area.
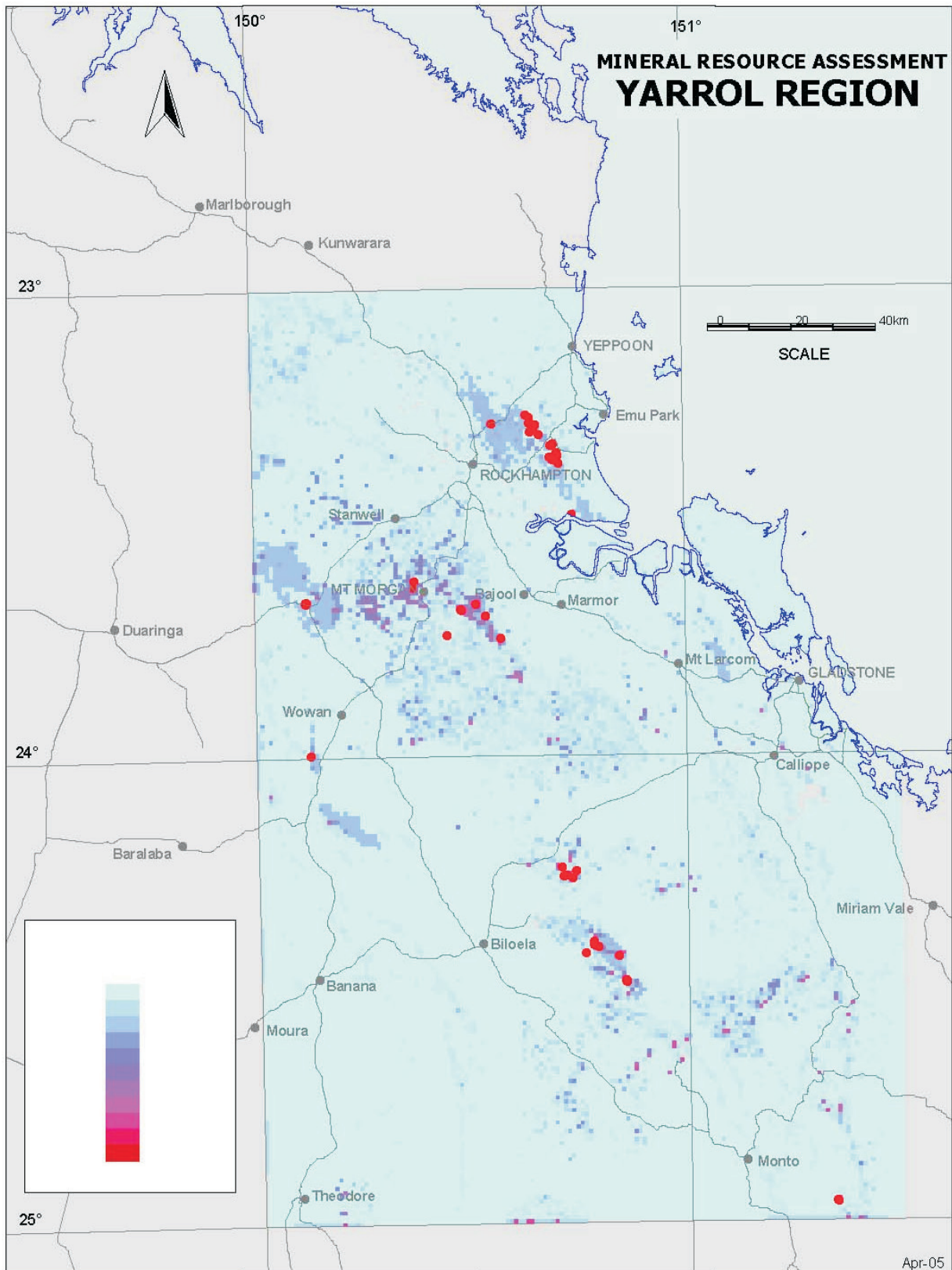
*Figure 37: Integration of Cu geochemistry, predictor lithologies and regional fault density for prospectivity ranking*

Ranked as moderately prospective are felsic rock units in the Mount Warminster area.

## Discussion

The scenario run for zone 56 of the Yarrol dataset provides an example of the application of WOE with the objective of focussing regional targeting for further exploration, such as more detailed geochemical sampling.

The preliminary analysis identified areas with similar combinations of geological and geochemical variables that have recorded VMS style mineralization in the past. Included is an area on the Bajool sheet covering Raspberry Creek and Ginger Creek beds where no historical workings are known. This area corresponds with target area 26 generated in the PNN analysis (refer following section). An interesting result recognising that the datasets used in both modelling session had significant differences.

The WOE modelling readily supports the development of multiple scenarios that can be compared to assess the validity of a model and those features that should be concentrated on during exploration (Partington & Rattenbury, 2003). Further VMS scenarios should be tested using the datasets provided in the Yarrol GIS and the gravity worm data included in the Data Package.

# PROBABILISTIC NEURAL NETWORK (PNN)

The following analyses use a PNN to integrate the Yarrol GIS data for the classification of potential mineral occurrences and to identify regional exploration targets.

Probabilistic neural networks are powerful intrinsic classifiers that can handle complex data and multi-modal class distributions (Masters, 1995), making them very suitable tools for integrating geological data. Singer & Kouda (1997) successfully used a PNN to classify deposit types from complex and incomplete mineralogy assemblages. PNNs can handle independence and sampling bias in geological data better than weights of evidence (Singer & Kouda, 1999). PNNs have also been found to be a more accurate classifier of mineralisation compared to logistic regression, discriminate analysis and a generalized regression neural network (Harris & Pan, 1999). In addition to this, the PNN can generate robust probabilities that can be used for predictive purposes. A summary of the concepts underlying PNNs, based on the work of Masters (1995) is presented in Appendix 1.

PNNs use known examples to learn and recognise patterns. Learning is based on a process of training and is heavily reliant on the set of known examples, in this instance mineral occurrences and deposits. Therefore the selection of training data and the independent validation of the trained network (testing with classified data not used in training) is integral to the process of modelling with the PNN.

The Yarrol PNN analysis considers 9 mineral types: *Low sulphidation epithermal; Au on low angle faults; Low sulphide Au quartz veins; Magmatic Au veins; Polymetallic veins; Porphyry Cu-Au-Mo; Cu Skarn; Besshi massive sulphide; Kuroko massive sulphide*. However, the target generation focuses on Kuroko volcanogenic massive sulphides (Kuroko VMS) and Cu-Au-Mo porphyries which are currently considered to be the most prospective deposit types for economic finds in the Yarrol Province.

The following text outlines the:

1.  raw data used in the analysis

2.  sampling of the data

3.  interpreting the data

4.  design of the analysis

5.  interpretation of Yarrol PNN results

Parts 1, 2 and 3 set the scene of the analysis in terms of outlining the type of data used in the analyses, explaining how these data are prepared for analysis so as to maximise information retention whilst addressing operational issues, and defining the modelling approach used in the prospectivity analysis. Part 4 outlines the design of the analysis and the PNN model and part 5 presents and discusses the results of the Yarrol PNN prospectivity analysis.

Additional more detailed discussion and the associated mathematics are presented in the report — Application of the Probabilistic Neural Network to Mineral Prospectivity of the Yarrol Province, Queensland (Refer Data Package — Reports).

## *Data*

Raw data for the assessment were extracted from the Yarrol Geographical Information Systems (Yarrol GIS). In addition to these data, digital elevations for the 1:100 000 sheets that cover the Yarrol Province were acquired from the Geoscience Australia (GA) elevation database.

Nine data layers formed the core dataset for the prospectivity analysis: mineral occurrence; geology; linear and fault features; airborne radiometrics; digital elevation; aeromagnetic: total magnetic intensity (TMI); aeromagnetic: 1st vertical derivative of the TMI; gravity (ground stations); gravity gradient.

To improve the classification ability of the PNN the geological data were resampled to produce 29 binary geological layers.

Descriptions of the nine data layers, and the rationale for their inclusion in the assessment are provided in the PNN report (refer Data Package – Resource Assessment Report, Additional Documents, Hedger, Appendix III).

### Sampling the data layers

The data are in four topologies: points, lines, polygons and raster. Each of these topologies represents different degrees of support or information that can be attributed to their respective spatial features. To standardise the different levels of support all layers were reduced to point values within cells prior to analysis by the PNN.

The unit cell size used is equal to the 2 minute tenement blocks used by the Queensland Department of Natural Resources, Mines and Water (NRMW) to administer land usage. At the latitude of the Yarrol Province these blocks project as 1.7 x 1.7km cells and cover an area of 2.89km$^2$. This cell size was selected because tenement blocks provide a scaled grid for sampling, processing and presenting the data that conforms to a standard set by the Queensland government and used by the exploration industry. The centre point of the unit cell is referred to in the following text as

an 'observation' because it determines the view of the underlying geological data layer. The observations used in the PNN analyses are described as either 'classified' or 'unclassified' observations. The classified observations are those that correspond to known mineral occurrence and deposit observations that have an assigned deposit model. These classified observations are used to train and validate the probabilistic neural network (PNN). The unclassified observations are located at the centres of the 1.7km x 1.7km tenement blocks for which no mineral deposit model has been assigned. These unknown observations are the data that are to be classified by the trained PNN. The total number of tenement blocks in the unknown dataset is 8674.

It needs to be recognised that the conversion of line, polygon and raster data to point values involved a reduction in spatial information. For example the transfer of shape and boundary information from a rock type polygon to a point that lies inside or outside the polygon results in some loss of spatial information. To manage the uncertainty associated with this loss, fuzzy set theorem is used in the sampling process. Cell based output themes are expressed as fuzzy sets. These fuzzy set themes are later combined to produce a data vector for input to the PNN.

### *Line data*

The structural layer contains linear features that have both a length and direction or strike. An issue for linear data in grid-based sampling is the retention of length information, as only a portion of the structure is represented. Whilst a length attribute can be assigned to each structural feature and this length could be recorded at the cell, linear features in GIS are often captured as a series of smaller segments and the true length of a structure is not known or at best is an approximate figure. Consequently, the sampling method used in these analyses focuses on the distance to the closest structure and the strike of the structure. In this process the closest structure to the centre of the cell is selected and the distance between the cell centre and the closest point on the structure is measured. A fuzzy membership function 'Close' is generated from this distance using a Gaussian function that ensures that a fuzzy membership grade of 0.5 is returned for a distance half way between the cell centre and the side of the cell. The strike of the closest structure is also recorded. Directional fuzzy sets are used, 'EW', 'NW',

'NS' and 'NE'. Each fuzzy set is based on a Gaussian function centred at 0/180°, 45°, 90° and 135°, with a spread that results in a fuzzy membership grade of 0.5 at the half points of 27.5°, 62.5°, 117.5° and 152.5°.

The mathematics applied and maps of the five fuzzy structural variables Close, EW, NW, NS and NE, in the unclassified dataset, are presented in the PNN report (Refer Data Package – Resource Assessment Report, Additional Documents, Hedger, appendix VI).

## Polygon data

The binary geological layers were sampled using the distance from the centre of the unit cell to the closest boundary of the polygon feature. A fuzzy membership function was applied using this distance, such that if the unit cell is completely in or complete outside the geological feature the cell is assigned 0 or 1 respectively. If the cell intersects the geological feature and the cell centre is not totally outside the feature, then the value assigned to the cell is >0 but <0.5, depending on the distance. If the cell centre is inside the polygon, but not completely, then the value assigned to the cell is >0.5 but <1. A value of 0.5 is generated in the cell if the cell centre is on the polygon boundary.

Maps and detailed discussion of the fuzzy sets describing the 29 binary geological features are in the PNN report (Refer Data Package — Resource Assessment Report, Additional Documents, Hedger, appendix VI).

## Raster data

To maximise the retention of raster information in the sampling process two values were calculated for each unit cell; the fuzzy centroid and the fuzzy entropy.

Calculation of the fuzzy centroid uses a weighted average that weights the $k^{th}$ value at each pixel $x_k$ by its fuzzy distance $fD_k$ from the cell's centre. The centroid is calculated by averaging the sum of weight values (numerator) over the sum of the weights (denominator). The fuzzy distances $fD_k$, used as weights, are calculated with the same Gaussian function used for the line layers. The Gaussian function is centred over the cell centre. Pixel values close to the cell centre are given greater weight than those further away. At a distance half way between the cell centre and the edge of the cell the weight is 0.5. The

advantage of this approach compared to averaging the pixel values within the unit cell is that it is not affected by isolated high values that may occur at the cell edges that bias the averages.

To quantify the change in the pixel values within the unit cell a measure of fuzzy entropy is calculated for each cell. The closer the values are to the value of 0.5 the higher the fuzzy entropy indicating that the cell is very fuzzy and correspondingly, the further the values are from 0.5 the lower the fuzzy entropy. For example, a cell centred over part of a magnetic high or low will have low fuzzy entropy, as all the pixel values are further away from the value of 0.5. If the cell is centred over an area between a magnetic high and low, and contains both high and low values, the fuzzy entropy of the cell will be high. Fuzzy entropy has an advantage over using pixel variance in that it returns a value in the unit interval 0 to 1. Maps displaying the fuzzy centroid and the fuzzy entropy, in the unclassified dataset, for the eight raster data layers are presented in the PNN report (refer Data Package — Resource Assessment Report, Additional Documents, Hedger, appendix IV).

## The input vector

The input vector is a list of data values that are provided to the PNN for analysis. Input vectors are generated for each classified and unclassified observation using the sampling methods described above. Each vector contains 50 values quantifying the following fuzzy set variables:

- 29 Geological variables

  1. Recent_rocks
  2. Young_rocks
  3. PR_granites
  4. PR_granodiorites
  5. PR_diorites
  6. PR_monzonites
  7. PR_gabbros
  8. PR_felsic_volcanics
  9. PR_mafic_volcanics
  10. PR_sediments
  11. SD_lCeP_marine_felsic_pyroclastics
  12. SD_lCeP_marine_mafic_extrusives
  13. SD_lCeP_marine_felsic_extrusives
  14. SD_lCeP_marine_fine_sediments
  15. SD_lCeP_marine_felsic_breccia_ volcaniclastics
  16. SD_lCeP_marine_mafic_breccia_ volcaniclastics

## Table 14: PNN results for the 70:30, training to validation split

**Predicted Class**

|  | Cover | EpioCC | LaaufOcc | LsauvOcc | MmauvOcc | PmVOcc | PorpOcc | SkarnOcc | VmsbOcc | VmskOcc | %Correct |
|---|---|---|---|---|---|---|---|---|---|---|---|
| Cover | **12** | 1 |  |  |  |  |  |  |  |  | 92% |
| EpiOcc |  | **7** |  |  |  |  | 1 |  |  |  | 88% |
| LaaufOcc |  |  | **7** |  |  | 3 |  |  |  |  | 70% |
| LsauvOcc |  |  | 1 | **8** |  |  |  |  |  |  | 89% |
| MmauvOcc | 1 |  |  |  | **9** | 1 |  | 1 |  |  | 75% |
| PmVOcc |  |  | 1 | 1 |  | **17** |  |  |  |  | 89% |
| PorpOcc |  |  |  |  |  | 2 | **7** | 1 |  |  | 70% |
| SkarnOcc |  |  |  |  | 1 |  |  | **12** |  |  | 92% |
| VmsbOcc |  |  |  |  |  |  |  | 1 | **5** |  | 83% |
| VmskOcc |  | 1 |  |  |  |  |  |  |  | **5** | 83% |
| **MisClass** |  | 18% | 12% | 6% | 6% | 35% | 6% | 18% |  |  |  |

| Observations: 106 | Total Incorrect: 17 | Total Correct: 89 | Total % Correct: | 84% |
|---|---|---|---|---|

17. SD_lCeP_marine_felsic_intrusive_domes
18. SD_lCeP_marine_chert_jasper
19. SD_plutons
20. lCeP_pillows
21. lCeP_sub-aerial_sediments
22. lCeP_sub-aerial_mafic_volcanics
23. lCeP_sub-aerial_felsic_volcanics
24. Limestone
25. Oolitic limestone
26. lDeC plutons
27. lDeC marine sediments
28. Metamorphics_serpentinites
29. Accretionary sediments

• 5 Structural variables

30. EW
31. NW
32. NS
33. NE
34. Close

• 6 Radiometric variables

35. Uranium_centroid
36. Uranium_entropy
37. Potassium_centroid
38. Potassium_entropy
39. Thorium_centroid
40. Thorium_entropy

• 2 Elevation variables

41. Elevation_centroid
42. Elevation_entropy

• 8 Geophysical variables

43. TMI centroid
44. TMI entropy

45. 1st VD_centroid
46. 1st  VD_entropy
47. Gravity_centroid
48. Gravity_entropy
49. Gravity_gradient_centroid
50. Gravity_gradient_entropy

## Interpreting the data

A confusion matrix (Table 14) indicates how well each PNN is classifying on a class-by-class basis. The rows in the matrix show the known PNN class for an observation while the columns indicate the PNN class into which the observation is placed. The diagonal cells of the matrix contain the number of correct classifications for each PNN class. This number is used to calculate the percent correctly classified, shown at the end of each row as a percentage of all the observations in the class. The off diagonal cells contain the number of misclassifications for a class relation. For example in Table 14, two Cu-Au-Mo porphyry occurrences observations were misclassified as Polymetallic veins observations. The total percentage of misclassifications for each class is shown along the bottom. The total percentage of correct classifications is shown in the bottom left hand corner. The matrix is used to indicate the overall performance PNN and is used below to examine sets of multiple PNN tests.

## Application — Yarrol Province

### PNN classes

The 9 mineral deposit types considered in the PNN analysis have been used to define 11 of the classes shown in Table 15. Nine of the

## Table 15: PNN classes

| Yarrol PNN Classes | Description |
| --- | --- |
| EpiOcc | Low sulphidation epithermal occurrences |
| LaaufOcc | Au on low angle fault occurrences |
| LsauvOcc | Low sulphide Au vein occurrences |
| MmauvOcc | Magmatic Au vein occurrences |
| PmvOcc | Polymetallic vein occurrences |
| PorpOcc | Cu-Au-Mo porphyry occurrences |
| SkarnOcc | Cu-Au skarn occurrences |
| VMSbOcc | Besshi massive sulphide occurrences |
| VMSkOcc | Kuroko massive sulphide occurrences |
| PorpDep | Cu-Au porphyry deposits |
| VMSkDep | Kuroko massive sulphide deposits |
| Cover | Recent sediments (Tertiary-Quaternary) |

classes describe minerals occurrences and are used in the first part of the PNN analysis to model mineral occurrences. Two of the classes described mineral deposits. The deposit classes are used, in conjunction with the 9 occurrence classes, in the second part of the analysis to model potential target areas. In both the mineral occurrence and targeting aspects of the PNN analysis, known observations in the classified dataset are assigned to only one of these PNN classes.

The class referred to as 'Cover' is used in both analyses to model concealed areas. 'Cover" was generated by arbitrarily selecting 44 observations from areas of thick cover. These additional observations were added to the classified dataset and used in the training and validation of the PNN analyses.

## PNN Model

The Yarrol analysis uses PNN algorithms developed by Masters (1995). The mathematics behind these algorithms is presented in the PNN report (Refer Data Package — Resource Assessment Report, Additional Documents, Hedger, appendix V, source of PNN coding — Masters, 1995).

Masters' algorithms use three different PNN models:

1.    single sigma

2.    multivariate sigma

3.    multiclass sigma.

Each model incorporates different approaches to finding the optimal weight density functions during the training process. These density functions are used by the PNN to classify the training observations and define the probability estimates. The PNN training process involves optimising the spread of the weighted density functions. This spread is referred to as the smoothing parameter or sigma. An optimal sigma is one that is just wide enough to minimise the misclassifications of the training data.

The three sigma models were trialed using Yarrol data, with the results indicating that the single sigma model used in conjunction with PNN class prior probability weighting produced the best outcomes (refer PNN report in Data Package — REPORTS)).

## Training and validation

PNN performance is highly dependent on the quality of the training dataset. Independent validation is necessary and generally done by randomly excluding part of the training dataset from the training process. These excluded data are then processed by the trained PNN and because the excluded data, or validation data, also contains classified observations, the network's independent performance can be gauged by counting how many observations the trained network correctly classifies. The process of independent validation via exclusion can, however, cause problems because the training process potentially can be denied relevant information. In such a situation different combinations of observations in the training and validation datasets may produce quite different levels of network performance. This is the case in many exploration applications where the modelling must address complex natural systems with brief class definitions and a finite number of labelled observations. In the case of the Yarrol
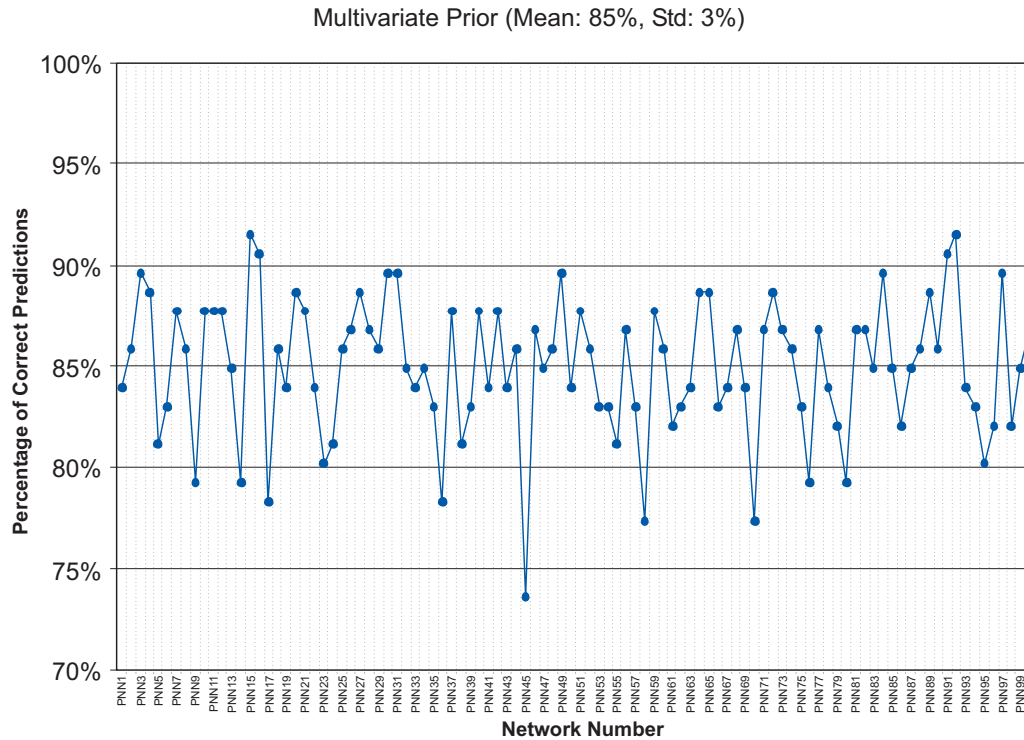
Multivariate Prior (Mean: 85%, Std: 3%)



*Figure 38: Independent validation results for 100 single sigma PNN tests*

Province, the geological data is complex and mineralisation is not always well understood. Consequently, the classification of mineral observations is vulnerable to errors and relies heavily on finding appropriate training and validation datasets. In this situation, the random selection of training data gives no assurance that it is more appropriate than any other possible training set. To address this fundamental problem more than one randomly selected training and validation dataset has be used to assess performance of the PNN.

In the following analysis, multiple PNNs are exposed to various combinations of the training data and tested with different validation datasets. In geological terms this is analogous to training the PNN with a range of possible mineralisation and cover patterns. Because independent validation requires the exclusion of some classified observations, these mineralisation patterns assume that a proportion of the known mineralisation has not been discovered. Hence, the independent validation datasets represent sets of possible undiscovered mineralisation observations within the Yarrol Province. The multiple PNNs are linked through the training data, which are randomly selected from the same set of classified mineral occurrence observations using a constant ratio of training to validation observations (70:30, ratio of training to validation for each of the 10 mineral occurrence PNN classes). Consequently, an

observation has the same probability of occurring in the training or validation dataset for each PNN. Within each training or validation dataset the prior probability that an observation will occur within a given PNN class is constant for all PNNs.

In the analysis of the Yarrol Province the number of splits and tests used in the multiple PNN test was set at 100 (refer Data Package — Resource Assessment Report, Additional Documents, Hedger, appendix VI).

The issues of over-representation and bias in classifications also need to be addressed. The cause of classification bias is generally over representation of one or more classes in the training dataset. This problem is exacerbated if the training observations for a particular PNN class are heavily clustered in an area, reinforcing one geological pattern over all others. This can occur with deposit types such as polymetallic veins where numerous small occurrences are spatially and genetically associated. To overcome this problem, Bayesian weights are used during the training of the PNN. This involves applying different prior probabilities for each of the PNN classes (refer Data Package — Resource Assessment Report, Additional Documents, Hedger, appendix V).
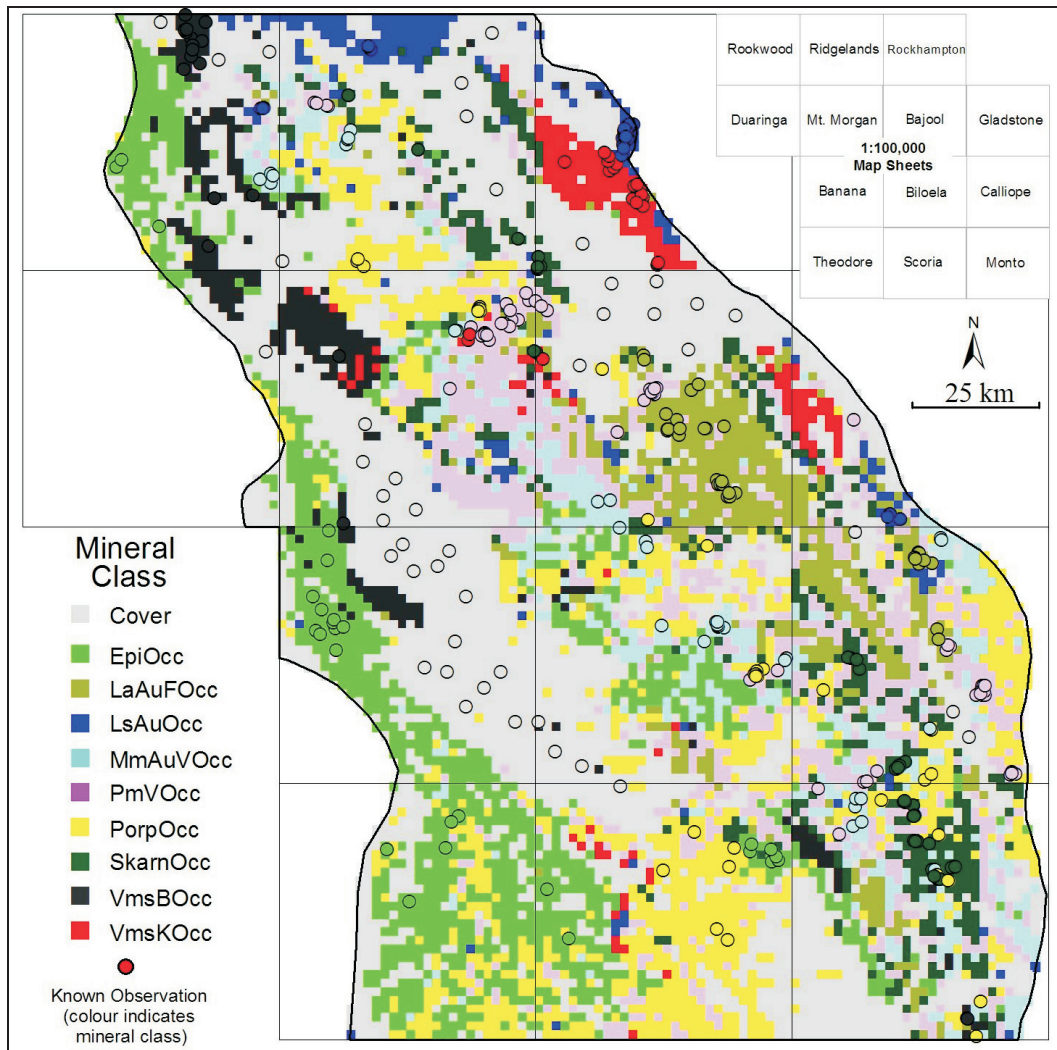
*Figure 39: Tenement classification map based on the average PNN class probability estimates in 100 single sigma PNN tests*

## Yarrol PNN analysis

The independent validation results for the 100 PNN single sigma tests are shown in Figure 38. The tenement block classification map (Figure 39) shows classifications based on the average probability estimate of the 100 PNN tests.

A determination of how well each model is classifying on a PNN class basis can be obtained using composite confusion matrices. A composite confusion matrix is calculated by summing all the test confusion matrices on a cell by cell basis. The sum in each cell is then normalised to the total number of observations in that cell's known PNN class, multiplied by the number of networks in the test. The cells values now represent the proportion, or percentage, of observations classified correctly.

Like the standard confusion matrix, the diagonal cells contain correct PNN class predictions, though in this case it is a

percentage that indicates the rate of correct classifications per PNN class. Off diagonal cells now indicate the percentage rate of misclassifications. The matrices presented in the following also show the error rate for each PNN class, under the bottom row of the matrix.

The independent composite confusion matrix for the 100 PNN test is shown in Table 16.

Independent validation indicates that the PNN tests are performing well, with an average of 85% for correct classifications.

The results are discussed below.

## Regional mineral occurrence potential

Figure 39 shows the tenement block classifications along with the known observations used in training. An excellent spatial correlation between PNN classes in the training observations and the tenement block classifications is apparent. Away from known

**Table 16: Independent composite confusion matrix for 100 single sigma PNN tests**

| | Cover | EpioCC | LaaufOcc | LsauvOcc | MmauvOcc | PmVOcc | PorpOcc | SkarnOcc | VmsbOcc | VmskOcc |
|---|---|---|---|---|---|---|---|---|---|---|
| Cover | **99%** | | | | | | 1% | | | |
| EpiOcc | | **96%** | | | 3% | | 2% | | | |
| LaaufOcc | | | **80%** | 10% | | 11% | | | | |
| LsauvOcc | | | 8% | **90%** | 1% | 1% | | | | |
| MmauvOcc | 1% | 5% | 5% | | **66%** | 10% | 9% | 5% | | |
| PmVOcc | 2% | 0% | 9% | 1% | 2% | **75%** | 4% | 6% | | |
| PorpOcc | 6% | | 0% | | 4% | 5% | **78%** | 6% | 1% | |
| SkarnOcc | | 0% | 1% | | 4% | 1% | | **94%** | | |
| VmsbOcc | | | 2% | | 1% | | 0% | 6% | **92%** | |
| VmskOcc | 3% | | | | 0% | 1% | 0% | | | **96%** |

| | |
|---|---|
| 🟨 | 5%–10% |
| 🟩 | ≥10% |

observations, classifications in the tenement blocks show a strong correlation between PNN classes, or combinations of classes, and major geological features[1].

Cu-Au-Mo porphyry, Magmatic Au and polymetallic veins tenement classifications are indicated over some of the major plutonic centres; as in the case of the Wingfield Granite on the Scoria sheet, the Galloway Plains Igneous Complex in the north-east corner of the Biloela sheet, and the Bouldercombe Igneous Complex at the northern edge of the Mount Morgan sheet. A number of tenements along the western edge of the Province, in the Bowen Basin and Tertiary cover sediments, have Cu-Au-Mo porphyry occurrence classifications. Whilst some correlate with magnetic highs, most do not. These classifications may be caused by the number of known porphyry observations in the trained data that have a close spatial relationship with covered areas, for example Limonite Hill.

Other features in the tenement classifications include:

1. Tenements along the western side of the Province, around the edges of the Gogango Overfold Zone, exhibit a strong Besshi VMS pattern. Tenements cover the mafic members of the Rookwood Volcanics, in particular its basalt and pillow lava members. A small belt of Besshi VMS classified tenements are mapped on the eastern side of the Wingfield Granite (north-west corner of the Monto sheet). These tenement blocks contain the Permian Owl Gully Volcanics, a unit of andesitic lavas and sediments.

2. Two belts of Kuroko VMS occurrences classified tenements occur in the east of the Yarrol Province. Tenement blocks in both areas cover rocks of the late Carboniferous to early Permian Mount Chalmers Formation and Beserker Group. The Beserker Group hosts the Mount Chalmers Au-Cu deposit. Tenement blocks in the southern Kuroko VMS occurrences belt also cover members of the Rockhampton Group.

3. A scattering of Kuroko VMS occurrences tenements can be seen on the western side of the Wingfield Granite, on the Scoria sheet. These tenements blocks are over the late Carboniferous to early Permian Yaparabra Volcanicsin a heavily faulted, late Carboniferous to early Permian extensional basin. No known Kuroko VMS occurrences are documented in the area. Another scatter of Kuroko VMS occurrences classed tenements lie to the south of Mount Morgan over southern extensions of the Mount Morgan Trondjemite, rocks of the Mount Warner Volcanics and the Mount Dick beds.

4. Low sulphide epithermal classed tenement blocks are associated with the Mount Benmore, Leura, Camboon and Torsdale Volcanics. Some of these classified tenement blocks also contain late Permian sediments of the Barfield Formation and the Oxtrack Formation. Low sulphide epithermal are also classified in tenements

---

1    Reference to the GIS tectonic map, the dominant lithology map in appendix II and the geological layers shown in appendix III of Hedger's report is recommended (Resource Assessment Report, Additional Documents, Hedger).
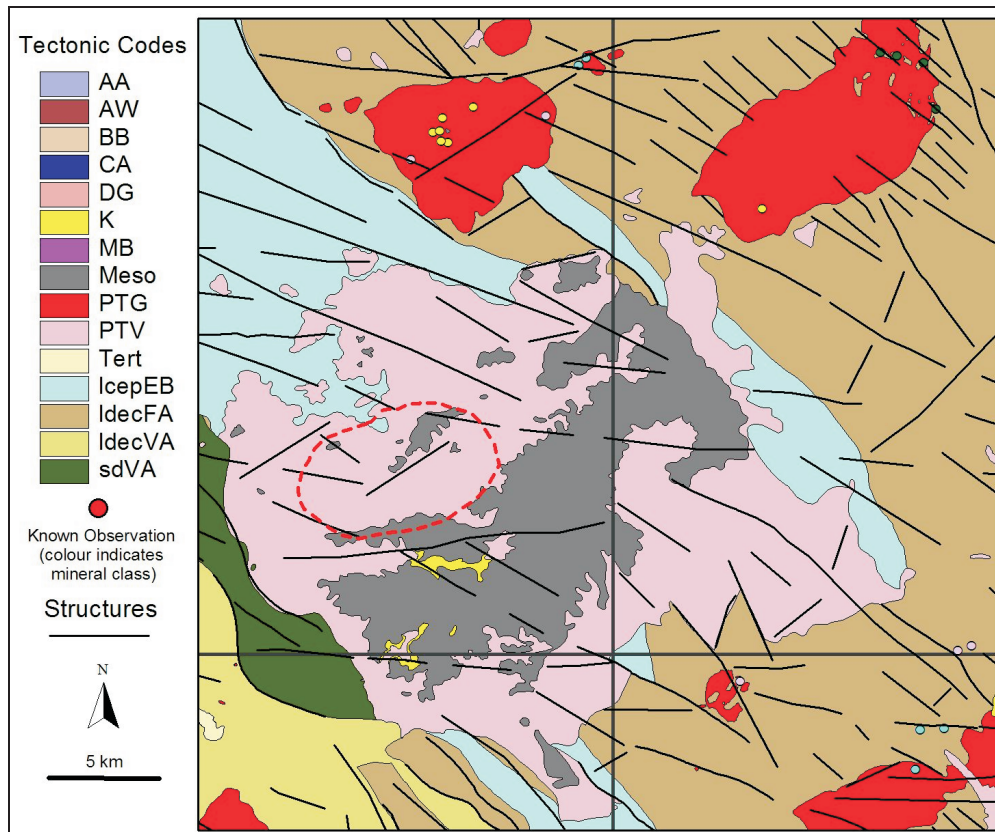
*Figure 40: Kroombit area, structure and tectonics map, red dashed outline of a possible subvolcanic intrusive*

hosting the late Carboniferous to early Permian rocks of the Youlambie Conglomerate along the western edge of the Gogango Overfold Zone.

5.  A large zone of Au on low angle faults tenements occurs on the Bajool sheet extending south onto the Calliope sheet. These tenement blocks cover mostly marine sediments of both the Silurian to Devonian volcanic arc and late Carboniferous to early Permian forearc tectonic environments.

6.  Tenement blocks classified as Cu-Au skarn show a close association with exposed and buried igneous bodies, both calc-alkaline and the more mafic systems. The small belt of Cu-Au skarn classifications in the north-east corner of the Ridgelands sheet are in tenements that cover small, late Permian to early Triassic gabbro and diorite intrusions. These intrude structurally deformed late Devonian to early Carboniferous sediments of the Rockhampton Group and Mount Alma Formation.

A review of the Yarrol PNN GIS, included in the Yarrol Data Package, is recommended.

Before completing this section it is important to point out that the classification produced by the 100 single sigma PNN test set does contain inaccuracies. For example there are some tenement blocks classified as LsauvOcc that contain mostly igneous rocks. Whilst some inaccuracies are evident they are not common and do not effect the overall assessment.

### Areas of High Mineral Potential

Several of the areas outlined above are considered to warrant further field checking: 1. Kuroko VMS occurrences classified tenements on the Scoria sheet and along the Mount Morgan mine corridor; 2. the belt of Kuroko VMS occurrences classed tenements in the Mount Chalmers area, and 3. Cu-Au skarn/Cu-Au-Mo porphyry occurrence classified tenements in the Mount Cannindah area. These examples occur in well-explored areas. The Kroombit area, however, is also considered to have high potential for Cu-Au-Mo porphyry occurrence classified tenements, but has not been as extensively explored. The Kroombit area covers the south-eastern corner of the Biloela sheet and north-eastern corner of the Scoria sheet. This area contains a cluster of porphyry occurrence classed tenements blocks that cover late Permian to early Triassic Winterbourne
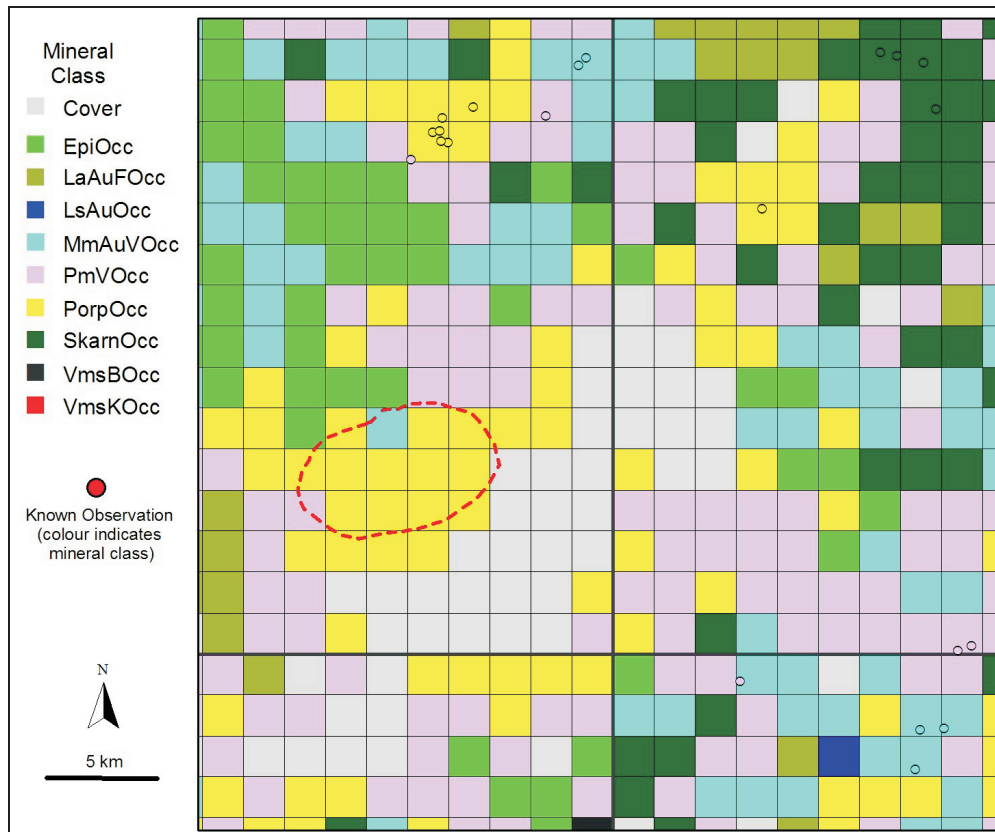
*Figure 41: Kroombit area, tenement classifications, red dashed outline of a possible subvolcanic intrusive*

Volcanics and a remnant cap of the Jurassic Precipice Sandstone. The nearest known porphyry system is the Mount Seaview Complex to the north where a cluster of porphyry occurrences are hosted by a late Permian to early Triassic granite, which is part of a larger intrusive body.

Total magnetic intensity in Figure 42 shows a subtle ovate feature (red dashed line), which is interpreted as a possible subvolcanic intrusive, within a large ovate feature. The potassium radiometrics show a strong potassic high in the overlying felsic volcanics. The potassic response also appears out to the north-west in the older late Carboniferous to early Permian sub-aerial sediments suggesting possible potassic alteration of the basement. A number of tenement blocks over these sub-aerial sediments have Low sulphide epithermal classifications, which could be interpreted as associated high-level mineralisation. A weaker potassic response can be seen to the north-east over the Mount Seaview Complex (and the Diglum Granodiorite).

A number of Cu-Au skarn classed tenement blocks also occur to the south-east in late Devonian to early Carboniferous sediments

and limestone. The area is considered to have potential for a porphyry Cu-Au-Mo occurrence and quite possibly associated skarn and epithermal occurrences.

## Yarrol mineral deposit exploration targets

The preceding work focused on mineral occurrences as a tool for identifying broad regions that may be favourable for mineralisation. This section includes data about known deposits and focuses on generating regional exploration targets. The distinction occurs because mineral occurrences are a weak manifestation of an ore forming process, whilst mineral deposits are larger, well known examples of a deposit type that would be considered possibly economic.

The Yarrol Province historically contains one large (>150t Au) Au-Cu deposit, Mount Morgan, and a medium Au-Cu deposit, Mount Chalmers. A number of small Au or Cu-Au deposits, some of which have produced and others that are still being explored (prospects) also exist in the terrane. The Mount Cannindah deposit and the Riverhead Prospect are examples.
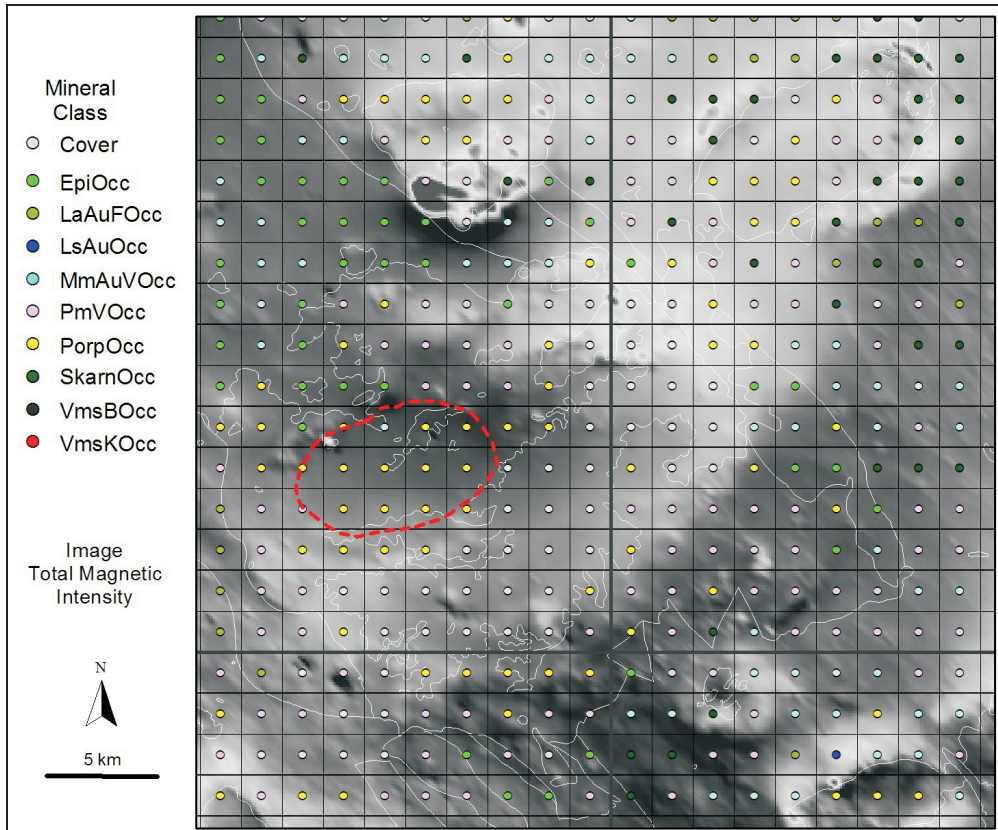
Figure 42: Kroombit area, tenement classifications over aeromagnetics, (TMI). White outlines marks tectonic units and the red dashed outline highlights a possible subvolcanic intrusive
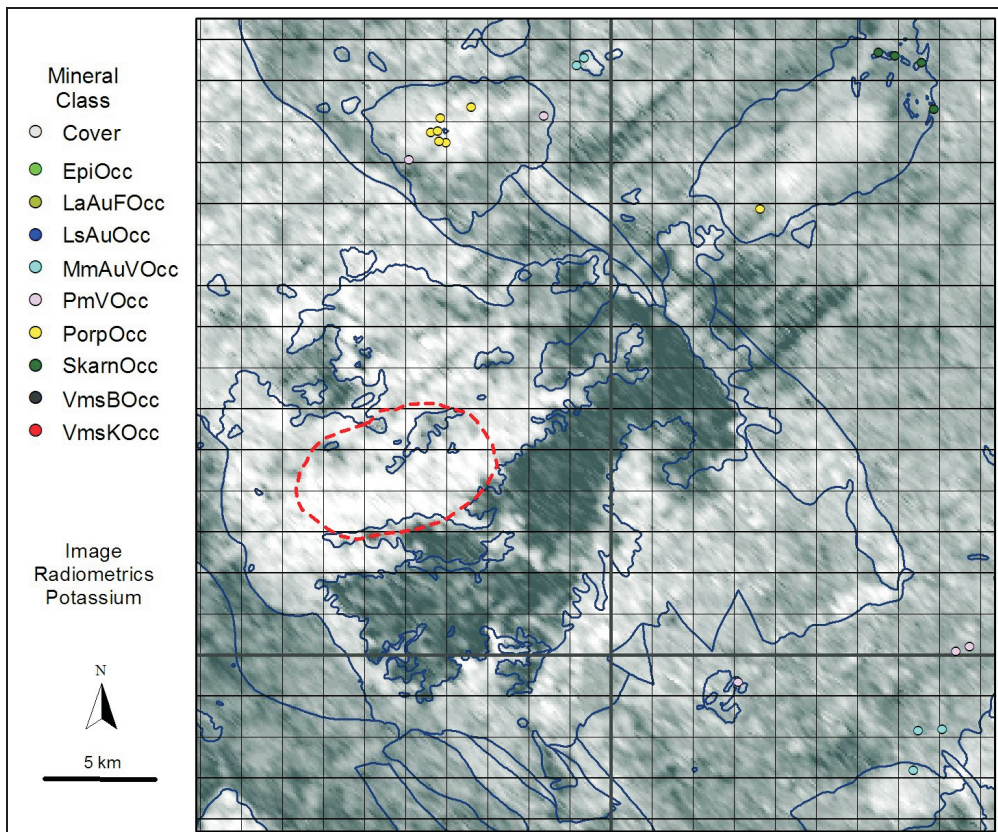


Figure 43: Kroombit area, classifications over potassium radiometrics. White outline marks tectonic units and the red dashed outline shows a possible subvolcanic intrusive
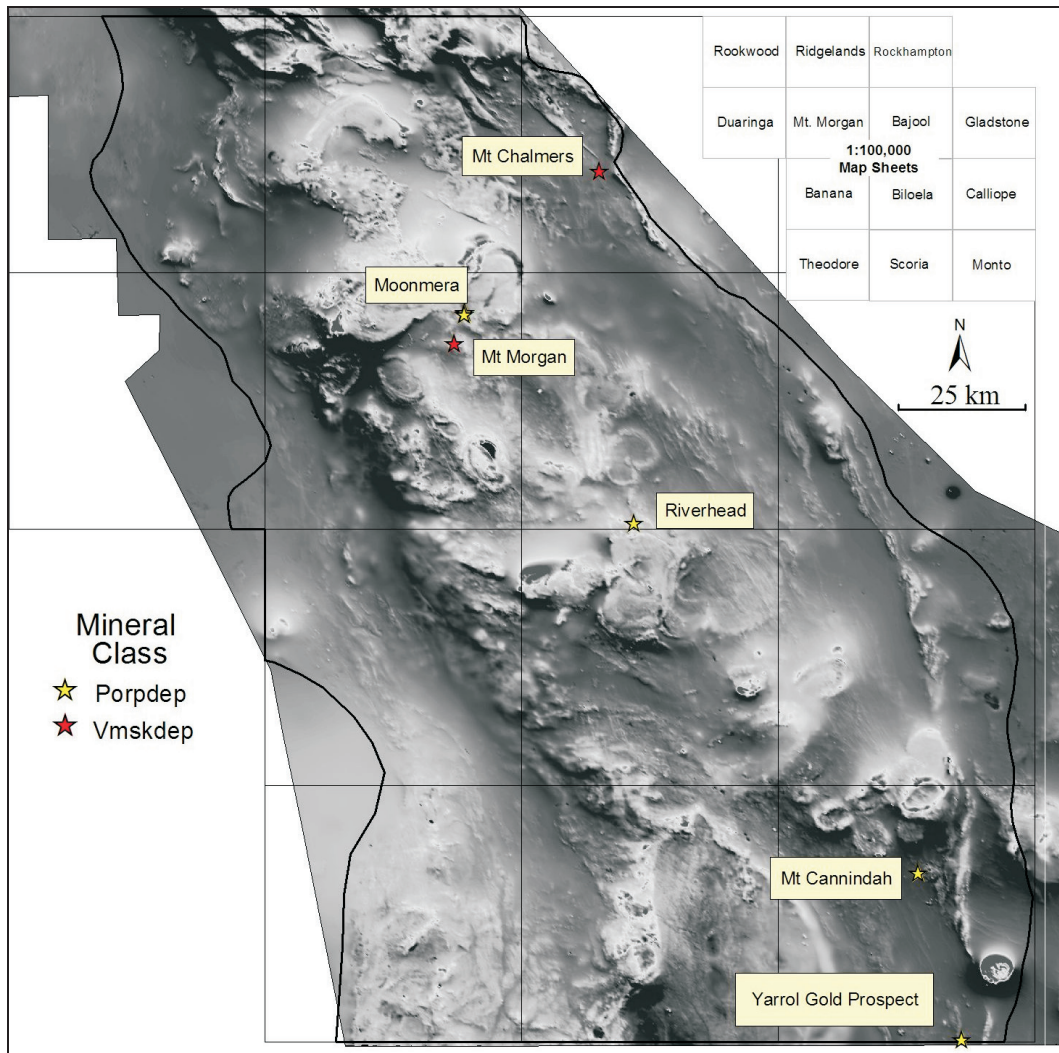
*Figure 44: Location of the six deposit observations over total magnetic intensity*

## Table 17: Mineral deposits used in the Target Assessment

| NAME | MINOCC Model |
|------|--------------|
| Mount Morgan | kuroko massive sulphide |
| Mount Chalmers | kuroko massive sulphide |
| Mount Cannindah | Cu-Au-Mo porphyry |
| Yarrol Gold Prospect | Cu-Au-Mo porphyry |
| Riverhead | Cu-Au-Mo porphyry |
| Moonmera | Cu-Au-Mo porphyry |

The 6 data sites listed in Table 17[2] and Figure 44 are recorded in the GSQ MINOCC database as having been large mines or significant prospects and as such are used in the following as examples of porphyry and Kuroko VMS occurrences deposits.

An immediate problem for PNN analyses is the small number of deposit observations, making independent validation almost impossible. To overcome this issue dummy deposit observations were placed randomly around each of the known deposit observations to act as possible variations in the location of each deposit. Dummy observations were placed inside a 250m radius of the documented deposits ensuring that appropriate rock type and age was maintained. Two dummy points were placed around each of the porphyry deposit observations and three around the

2    In the previous PNN tests, the Mount Cannindah Cu deposit was classified as a Cu Skarn occurrence. Mineralisation at this site has been described by Creenaune & Harvey (1996) as porphyry copper, skarn and late stage fissure-vein gold).
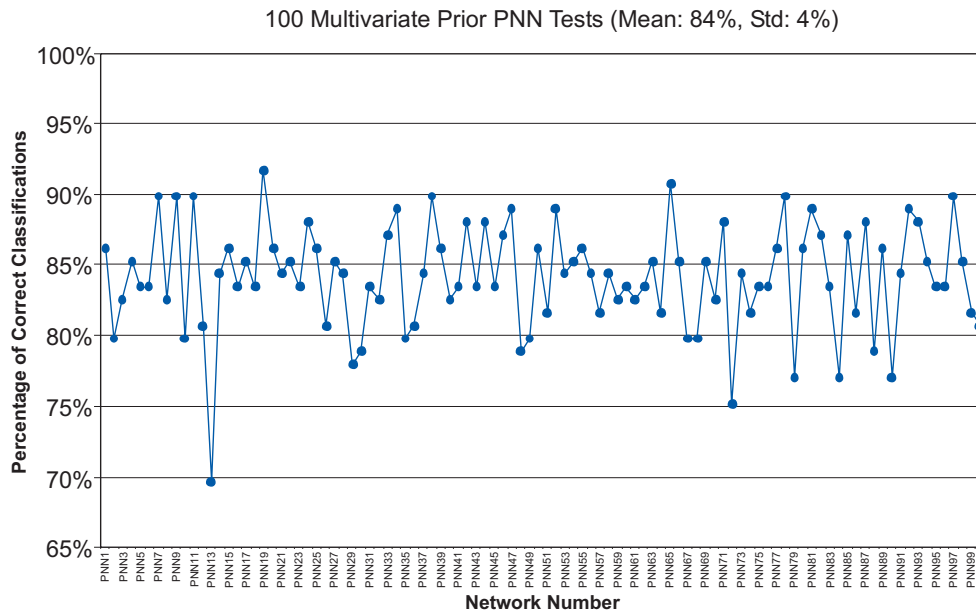
*Figure 45: PNN class numbers for the 12 classes*

Kuroko deposit observations, shown in Figure 44. The Kuroko deposits were given a higher number of dummy points as they are not as well represented in the classified dataset. Two Cu-Au-Mo porphyry occurrences close to Moonmera were also used as dummy points to reinforce the porphyry deposit class. By making these additions the number of known observations in the classified dataset changed from 356 to 364. The number of PNN classes within the classified data increased from 10 to 12. Class data is shown in Figure 45.

A multivariate PNN model, trained with class prior probabilities, was used to create a set of 100 PNN tests. Results for two other models trialed are shown in the PNN report (refer Data Package — Reports).

The training and validation split in the classification dataset was set at 70:30 (see Figure 46) and selection was carried out randomly. An average percentage of 85 was obtained for correct classifications.

Independent misclassification rates in the composite confusion matrix (Table 18) shows the Cu-Au porphyry deposits class has relatively low misclassification rates in both the Cu-Au-Mo porphyry occurrences and Cu-Au skarn classes. The high misclassification rate of Cu-Au-Mo porphyry occurrences as Cu-Au porphyry deposits in Table 12 suggests that some of the Cu-Au porphyry deposits are likely to be Cu-Au-Mo porphyry occurrences.

**Table 18: Independent composite confusion matrix for 100 multivariate sigma PNN tests (0% represents percentage <1% but > 0%, blank cells indicate no misclassifications)**

| | Cover | EpioCC | LaaufOcc | LsauvOcc | MmauvOcc | PmVOcc | PorpOcc | SkarnOcc | VmsbOcc | VmskOcc | PorpDep | VmskDep |
|---|---|---|---|---|---|---|---|---|---|---|---|---|
| Cover | **96%** | 0% | 0% | 0% | 1% | 0% | 0% | 1% | | | 1% | |
| EpiOcc | 2% | **85%** | 0% | | 7% | 2% | 2% | 3% | 0% | | 1% | |
| LaaufOcc | | | **85%** | 5% | | 10% | | 0% | 0% | | | |
| LsauvOcc | 0% | 0% | 9% | **88%** | 1% | 1% | 0% | | | 0% | | |
| MmauvOcc | 0% | 6% | 1% | 0% | **74%** | 5% | 5% | 5% | 0% | 0% | 3% | 0% |
| PmVOcc | 0% | 0% | 7% | 1% | 3% | **81%** | 1% | 4% | | 1% | 1% | 1% |
| PorpOcc | 2% | 2% | 1% | 1% | 7% | 6% | **64%** | 10% | | 0% | 8% | |
| SkarnOcc | 0% | | 1% | | 4% | 1% | 0% | **92%** | 0% | 0% | 0% | 0% |
| VmsbOcc | 0% | 0% | 0% | 0% | 1% | 1% | | 3% | **93%** | 2% | | |
| VmskOcc | 3% | 0% | 4% | | 0% | 2% | 0% | | 1% | **70%** | 0% | 18% |
| PorpDep | 1% | | | | | 0% | 4% | 5% | | | **91%** | |
| VmskDep | | | | | | | | | | 8% | | **93%** |

| | | |
|---|---|---|
| | 5%–10% | |
| | >10% | |

*Figure 46: Independent validation, showing total percentage of correct classifications, in 100 multivariate sigma PNN tests*
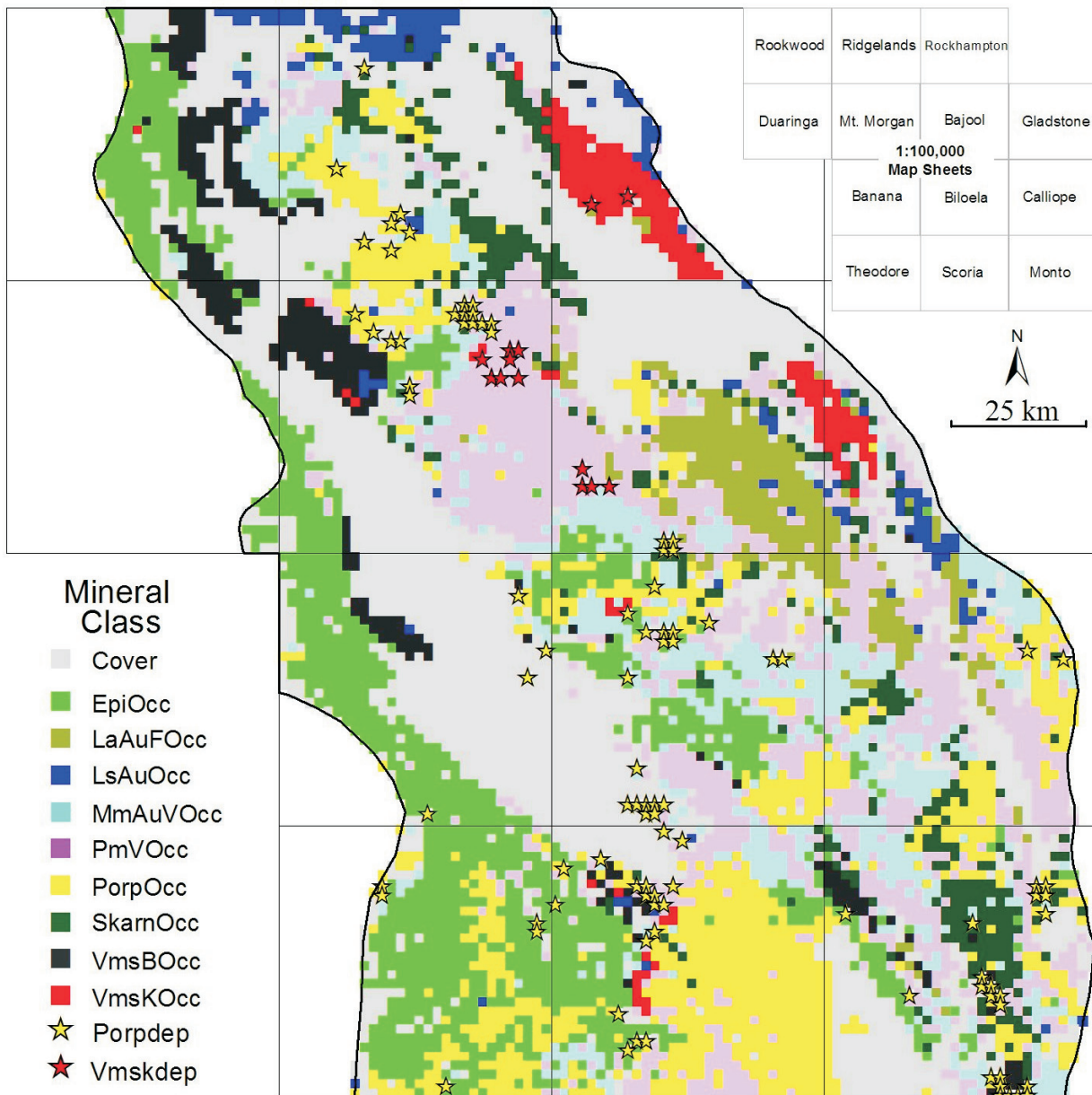


*Figure 47: Tenement block classifications based on the average probability in 100 multivariate sigma PNN tests*
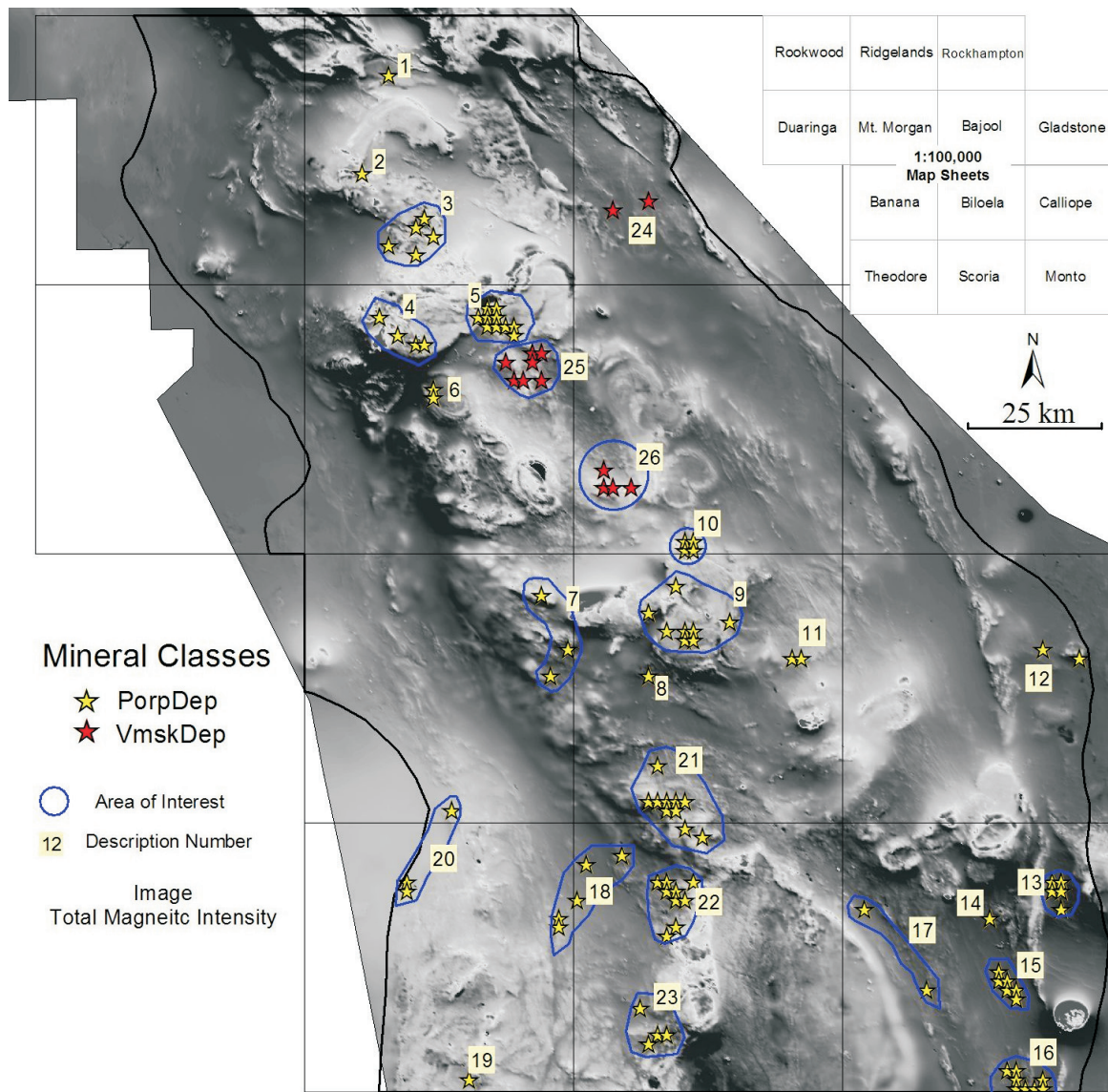
*Figure 48: Tenement blocks classified as deposit classes based on the average probability in 100 multivariate sigma PNN tests*

The Kuroko VMS deposits class in Table 18 shows a high misclassification rate of Kuroko deposits as Kuroko occurrences and visa versa. This is interpreted to be the result of low deposit observation numbers and a lack of good contrast between the two PNN classes.

The tenement classifications for a set of 100 multivariate PNN tests (Figure 47) displays PNN class patterns similar to those described in the mineral occurrence PNN tests.

The tenements classified as deposit classes and potential regional exploration targets are shown in Figure 48. A total of 26 targets were generated. These targets are discussed below, using the description number shown in Figure 48:

1. Single tenement block classified as Cu-Au porphyry deposit over the late Permian to early Triassic Wattlebank Granodiorite. The tenement also covers a large east west structure. No mineralisation is known to be associated with the Wattlebank Granodiorite.

2. Single Cu-Au porphyry deposit classed tenement block over the Cretaceous Mount Salmon Volcanics. The late Cretaceous Alton Downs Basalt and Lorray Formation crop out nearby. The nearest granitoid is the late Permian to Early Triassic Ridgelands Granodiorite, located 5km to the west. Polymetallic quartz veins have been recorded in the Craigilee beds in the headwaters of Seven Mile Creek, at the contact of the Craigilee beds and Lorray Formation (eg the **Alliance, Mount Mornish, Copper Shafts** mines); and associated with magnetic interpreted linears within Mount Mount Alma

Formation (**Welcome** mine). All three groups of occurrences are in or in close proximity to the target area.

3.  A spaced cluster of Cu-Au porphyry deposits tenements over mostly Cretaceous to late Cretaceous Alton Downs Basalt and Mount Salmon Volcanics. The **Golden Spur** and **Native Cat** mines are in the area and have been described as part of a hydrothermal system, possibly a high-level porphyry system associated with an unnamed Triassic diorite body that intrudes the local andesite (Burrows, 2004).

4.  A spaced cluster of Cu-Au porphyry deposit tenements over late Cretaceous basalt and some Jurassic Precipice Sandstone to the south. The tenements are concentrated along the edge of the cover where it contacts Permian and late Permian to early Triassic granitoids (Flaggy Quartz Monzonite and the Umbrella Granodiorite). An ovate potassium anomaly is evident in the northern tenement. The Umbrella Granodiorite is known to be associated with localised alteration systems, brecciation and intrusion of small porphyry plugs. The Flaggy Quartz Monzodiorite has local pegmatitic patches that contain magnetite crystals.

5.  A tight cluster of Cu-Au porphyry deposit tenements occur in the Moonmera area. The southern two Cu-Au porphyry deposits tenements cover the Moonmera deposit observations. The bulk of the Cu-Au porphyry deposits tenements are to the north-west and cover the contact between the Bundaleer Tonalite and Jurassic Precipice Sandstone and minor Cretaceous basalt

6.  Two adjacent tenements classified as Cu-Au porphyry deposits cover the north-western edge of the Permian Kyle Mohr Igneous Complex. The Westwood Group (**Westwood Gold mine, Westwood palladium prospect**), with vein style quartz, arsenopyrite, gold and palladium in a zone of fracturing within the gabbro, occurs in the target area.

7.  Three broadly spaced Cu-Au porphyry deposit tenements lie along the edge of the Tertiary covered basin. The two northern most tenements cover partially

exposed late Permian granitoid, which intruds partially exposed Smokey beds and Youlambie Conglomerate. The southern most tenement lies out in the Tertiary basin. A diffuse ovate magnetic feature can be seen in the aeromagnetics for this area. Some large north-west trending structures also underlie tenements in this area.

8.  A single Cu-Au porphyry deposit tenement is located in Three Moon Conglomerate. A small stock of Permo-Triassic diorite occurs almost at the centre of the tenement. The only other granitoid in the area is the Rocky Point Granodiorite, 6km to the north-east. No mineralisation is known in the target area. The Mount Rainbow Goldfield is associated with the Rocky Point Granodiorite.

9.  A broadly spaced cluster of Cu-Au porphyry deposits classed tenements which cover the central part of the Rocky Point Granodiorite. The northern most tenement covers the north edge of the Dumgree Tonalite. The granodiorite displays magnetic zoning and possible multiple intrusions. The tenements all lie over north-west trending structures that cut the granitoids.

10. A tight cluster of tenements near the Riverhead prospect.

11. Two adjacent Cu-Au porphyry deposit tenements cover the southern contact of the Bocoolima Granodiorite and the Three Moon Conglomerate and some rocks of the Mount Alma Formation. Aeromagnetics in the area of the tenements show that the contact is magnetic and cut by north-north-west trending dykes.

12. Two isolated tenements are classified as Cu-Au porphyry deposits. The western tenement covers the contact between the Castletower Granite and the Miriam Vale Granodiorite. The eastern tenement covers the Miriam Vale Granodiorite and Coulston Volcanics. A subsurface intrusive body is interpreted from the magnetics data.

13. Cluster of four adjacent Cu-Au porphyry deposits classed tenements with a fifth lying just to the south. All tenements cover Wandilla Formation. The four

adjacent tenements occur around two small late Permian to early Triassic granite stocks, a larger pluton of the same granite crops out 2km to the west. Aeromagnetics suggest several other small unmapped stocks. **Many Peaks** copper-gold-pyrite mineralisation is located in this region.

14. A single Cu-Au porphyry deposit tenement covers the Mount Cannindah deposit observation.

15. A cluster of Cu-Au porphyry deposit tenements lie in a north-north-east belt of Lorray Formation. No granitoids crop out in the area with the exception of a small Permo-Triassic granitic stock to the north.

16. A cluster of adjacent tenements classed as Cu-Au porphyry deposits cover the area about the Yarrol Gold Prospect and extended north following the Lorray Formation.

17. Two isolated Cu-Au porphyry deposits tenements. The southern tenement covers Rockhampton Formation. A number of small Permo-Triassic granitic stocks also crop out in this area. The northern tenement covers Youlambie Conglomerate and some Yarrol Formation. No granitoids are exposed in the north.

18. A broad cluster of Cu-Au porphyry deposit tenements. The southern three, cover mafic members of the Camboon Volcanics. No granitoids are exposed. The northern two tenements cover parts of the Lookerbie Igneous Complex where it intrudes the Back Creek Group. The area is strongly faulted. Mineralisation known in region includes **Scoria** (Cu) and **Prospect Park** (Cu-Au-Ag).

19. An isolated tenement classified as a Cu-Au porphyry deposits. The tenement covers part of the Carboniferous Hutchinson's Granite.

20. Three tenements classified as Cu-Au porphyry deposits. All three cover the contact between sediments of the Bowen Basin and the volcanics of the Auburn Arch. The aeromagnetic data shows buried ovate features but no granitoids are recorded in the area.

21. A cluster of Cu-Au porphyry deposit tenements, all are situated over the Tertiary basin overlying Lochenbar Formation. The Kariboe Layered Gabbro crops out outside of the tenement area. Aeromagnetics show a large diffuse ovate feature lying under the area, with a magnetic high under the central cluster of tenements. The Cu-Au occurrence, **Old Kroombit**, is the closest known mineralisation.

22. Two clusters of Cu-Au-Mo porphyry occurrence tenements are identified. These tenements are located 3km north of the Harrami Igneous Complex.The southern tenement cluster has two adjacent Cu-Au porphyry deposits tenements covering Tertiary basalt and Yaparabra Volcanics. Potassium radiometrics are elevated in the area. The northern cluster forms a north-west trending belt over and about the Lookerbie Igneous Complex. The aeromagnetics indicate some structural deformation and the tenements in the south are over a potassium anomaly. No mineralisation is known in the area.

23. A broad cluster of Cu-Au porphyry deposits classified tenements over a fault block of late Carboniferous to early Permian volcanics, volcaniclastics and sediments on the north-western edge of the Wingfield Granite. All tenements show a strong spatial association with exposed Permo-Triassic plutons. A large potassium high is located under the northern tenement block. Known mineralisation in the area includes **Valencia** (Au), **Rawbelle** (Ag-Pb), and **Ringwood** (Au-Cu). **Whitewash**, a porphyry prospect to the east of the target area was not identified.

24. The Mount Chalmers Au-Cu deposit is situated at the corner of four tenement blocks all of which are classed as Cu-Au-Mo porphyry occurrences, although each have high probabilities for the Cu-Au porphyry deposits class. The two widely spaced tenements classified in the Mount Chalmers area are not however near the deposit. The eastern tenement is situated 4km south-west of the Mount Chalmers deposit over sediments and felsic volcanics of the Chalmers Formation and the Sleipner member. This area contains a number of mineral occurrences, all of which had uncertain deposit model classifications, and were not included in the PNN tests. Recent fieldwork suggests that these occurrences are possible VMS
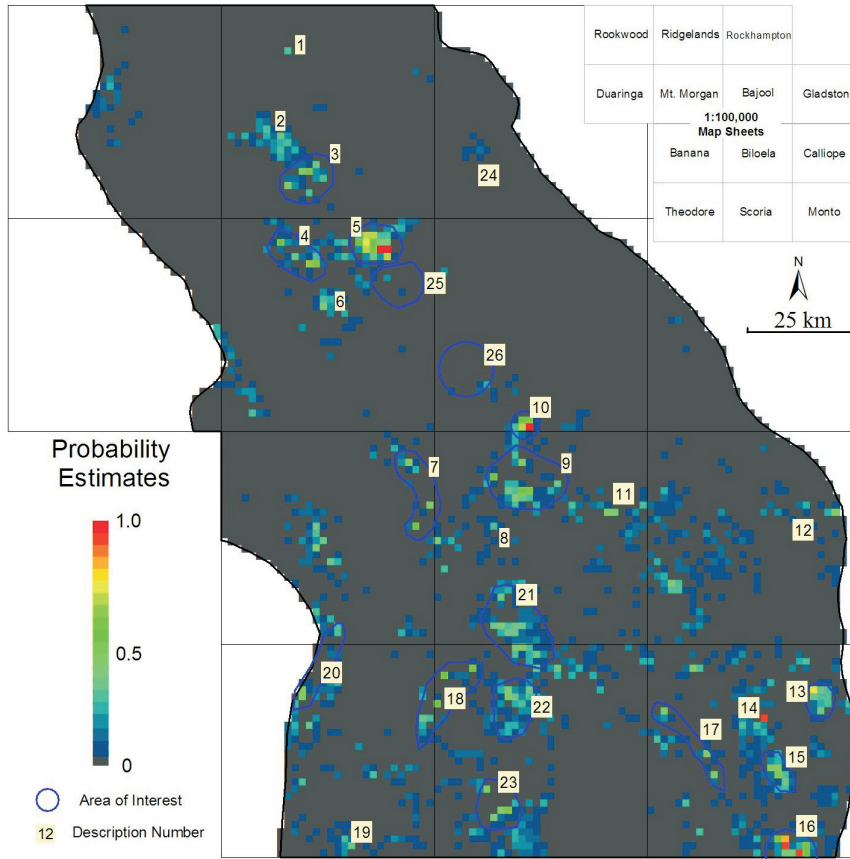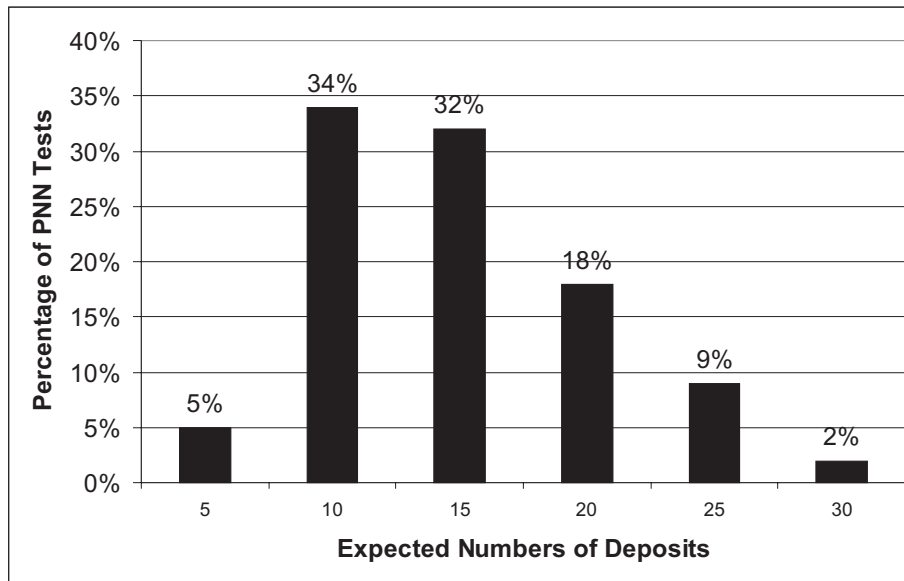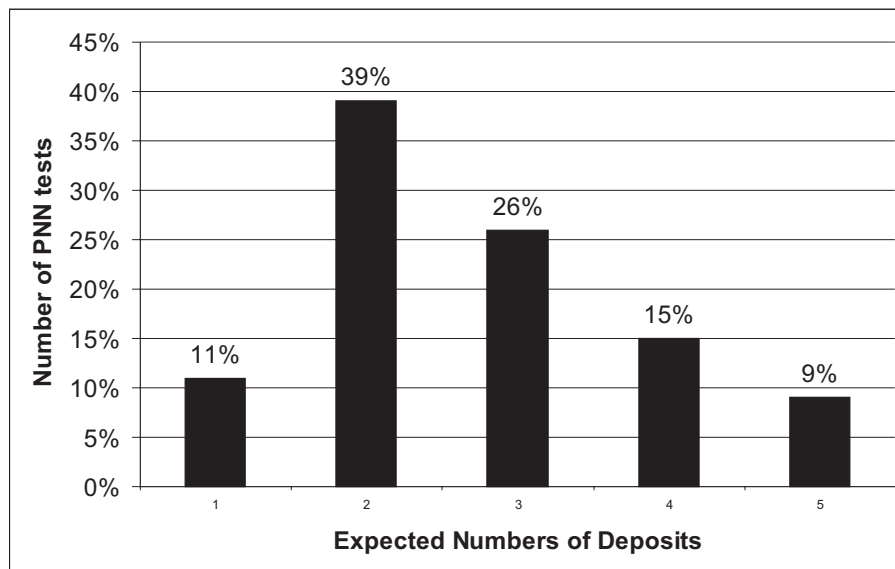
b) VMSkDep class
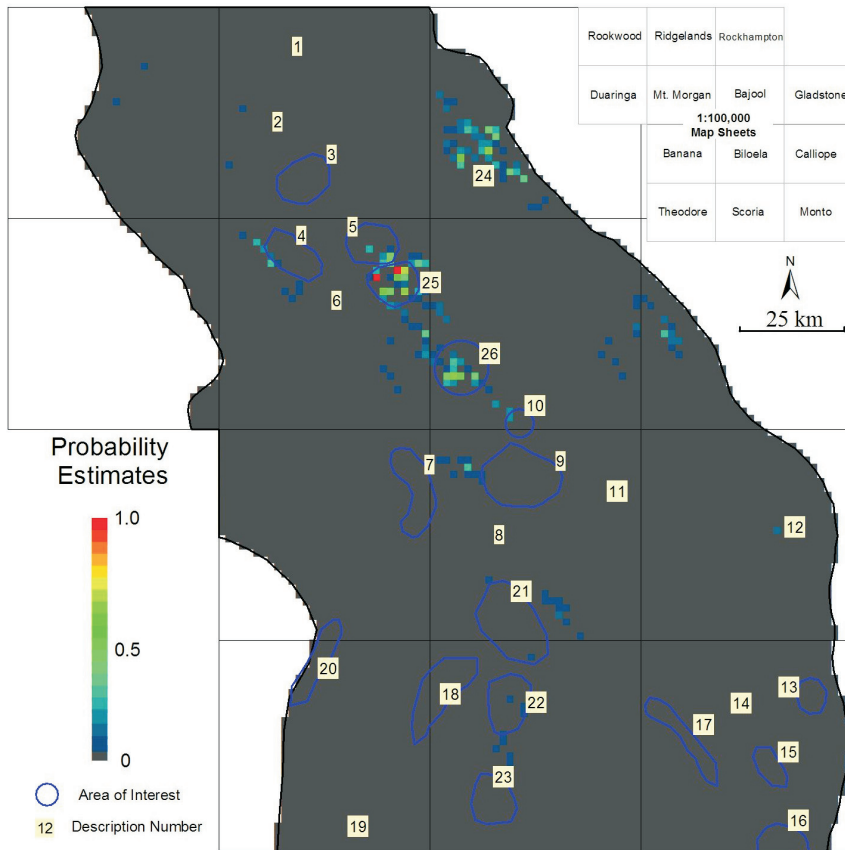


a)  PorpDep class

*Figure 49: Tenement blocks with average probability estimates for the deposit classes.*
*Averages are based on 100 multivariate sigma PNN tests.*

a.) Porphyry Au-Cu-Mo exploration targets



b.) Kuroko VMS exploration targets

*Figure 50: Expected number of exploration targets in 100 multivariate sigma PNN tests*

feeder zones. The western Kuroko VMS occurrence tenement covers rocks of the Chalmers Formation. A Permo-Triassic diorite stock is also exposed in the tenement and may be responsible for several small magnetic highs located in the Chalmers Formation.

25. A cluster of Kuroko VMS deposits tenements occur around and over the Mount Morgan Au-Cu deposit. Several tenements cover Mount Morgan Trondjemite, Mount Warner Volcanics and Raspberry Creek Formation. Three other Kuroko deposit tenements are situated 5km to the west of Mount Morgan again in Mount Warner Volcanics and Raspberry Creek Formation.

26. A broad cluster of Kuroko deposit tenement blocks. These tenements cover the contact rocks of the Raspberry Creek Formation and faulted blocks of mid-Devonian Ginger Creek member. A large east-north-east elongated magnetic anomaly is shown in the aeromagnetics under the southern three tenement blocks. Several questionably magmatic Au vein occurrences occur to the south of the area in the Raspberry Creek Formation (eg **King Soloman** and **Queen of Sheba**).

Some of the tenement areas discussed above are thought to have potential as porphyry or Kuroko VMS regional exploration targets. However, others, for example numbers 6, 17,19

and 20, are considered likely to be the result of inaccuracies in the classification process

The two maps in Figure 49 show the spatial distribution of average probability estimates for the Yarrol tenement blocks. The average is based on the 100 PNN tests discussed earlier. Areas of high probability correspond well to those tenement blocks classified in the deposit classes. There are also tenement blocks that show probabilities for the deposit classes but are not classified as such. They correspond well with tenements classified in the occurrence classes. These probability estimates (Figure 49) are conditional or posterior probabilities[3]. They describe the probability that a certain PNN class will occur given the geological data sampled within a tenement block. The consequence of this is that posterior probabilities can be used to estimate the expected number of deposit exploration targets within the tenement blocks.

The estimates calculated are for numbers of deposit exploration targets and are not deposits as such. An estimate of the expected number of mineral exploration targets within the Yarrol Province is obtained by summing posterior probabilities adjusted for area. Making the assumption that a tenement block contains only one deposit, whose areal extent equals that of the unit cell, and that PNN probabilities are unbiased (Singer & Kouda, 1999), the expected number of exploration targets would be:

$$E(n) = \Sigma p_k A_k \qquad (0.1)$$

Where $p_k$ is the posterior probability in tenement block $k$ and $A_k$ is the area of the tenement block in unit cells. As a tenement block represents a unit cell in the assessment area (see section on sampling support) then the equation (0.1) becomes a summation of the probability of $E(n) = \Sigma p_k$. As the assessment deals with both occurrence and deposit classes, the posterior probabilities for the deposit classes are scaled using the prior probability for a deposit observation within the training dataset, which equals 14/255 (ie the number of training deposit observations over all the training observations).

Figure 50 shows the distribution of the expected numbers of porphyry Au-Cu-Mo exploration targets and Kuroko VMS exploration targets in the 100 multivariate sigma PNN tests. The horizontal axis shows the numbers of expected exploration targets and the vertical axis shows the proportion of PNN tests that estimated this number.

Estimates made for porphyry exploration targets are high, with at least 10% of tests indicating 20 targets. Such a high result may be due to the relatively high misclassification rate for Cu-Au skarn as Cu-Au porphyry, which would mean some of the porphyry targets might actually correspond to skarn targets. Estimates for the number of Kuroko VMS exploration targets indicate in at least 9% of tests, 5 exploration targets could exist in the Yarrol Province. Spatial probability estimates for the 26 target areas shown in Figure 48 identifies targets 3, 4 and 18 as having moderate probabilities and target 13 as having high probability (targets 5, 10, 14, 16 are excluded as known deposits used in the training set).

---

3    The assumptions that the PNN classes are exclusive (one observation belongs to one class only) and are exhaustive (all the class modelled are present) were accepted.

# SECTION 7

# GRADE AND TONNAGE MODELS AND ESTIMATES OF THE NUMBERS OF UNDISCOVERED DEPOSITS IN THE YARROL PROVINCE

## CG Murray, PR Blake & M Scott

Mineral deposit grade and tonnage models and estimates of the number of undiscovered deposits provides the means of translating geologists resource assessments into terms that economists and land planners can use (Singer, 1993a). In this section the results of the prospectivity modelling and interpretations of geology, geophysics and mineral occurrences presented earlier in the report are applied, as per the the USGS three-part resource assessment process, to provide estimates of the numbers of undiscovered deposits in the Yarrol assessment area.

This process involves the use of grade and tonnage models, where tonnages and average grades of whole deposits are samples (Singer, 1993b), to represent the resources of undiscovered deposits. Grade and tonnage models are used to help distinguish a deposit from a mineral occurrence and to provide the basis for estimating the potential value of undiscovered deposits in the Yarrol assessment area. This process is underpinned by the fact that a major source of variation in size of deposits is due to differences between types of deposits (Cox & Singer, 1986). Grade and tonnage models are in the form of frequency distributions of tonnages and average grades of well-explored deposits of each type. Both global (*eg* USGS Bulletin 1693 — Cox & Singer, 1986) and Australian (*eg* Ozpot, in preparation) grade and tonnage models are presented in the following text. The Australian models are included to reflect local deposit characteristics.

The estimation of the number of undiscovered deposits within delineated tracts is done to show explicitly how favourable a tract is for the occurrence of deposits (Singer, 1993a). For a deposit type there is a single number of undiscovered deposits in its permissive area. As this number is unknown subjective estimates are made of the number of deposits

present at the $90^{th}$, $50^{th}$, $10^{th}$ and $5^{th}$ percentile. The percentile estimate represents the percentage chance of that number of deposits occurring — for example, the $10^{th}$ percentile represents the number of deposits for which there is at least a 10% chance of that number of deposits or more occurring (Root & others, 1992). Frequently estimates of deposits in the $90^{th}$ percentile are associated with deposits that are known in the area or deposits that are otherwise almost certain to exist. Estimates in the $10^{th}$ percentile can express the idea that many of the ore-forming processes and depositional environments have come together to form likely deposits in the area, and that most of the surface indicators such as mineral occurrences, and structural intersections actually represent hidden bodies. A wide range between the high and low estimates indicates a paucity of relevant information about the area and/or deposit model, and consequently a high degree of uncertainty. Conversely, a narrow range indicates a high level of confidence in the estimates.

Estimates of the number of undiscovered deposits made here are based on the information in this report, published grade and tonnage data (USGS Bulletin 1693 — Cox & Singer, 1986; Ozpot, in preparation), and on the combined knowledge of a team composed of authors of this section. In all cases team members were mindful of the grade and tonnage model of the deposit type such that about half of the undiscovered deposits estimated are likely to fall above the median grade and tonnage for that deposit type.

The assessment process is dependent on deposit models, and consequently the team was only able to evaluate those mineral resources that occur in deposit types that were relatively well understood. Estimates of

undiscovered deposits were not made for some deposit types because of insufficient knowledge about the model or local controls for the formation of a deposit, or where grade and tonnage models were considered inappropriate and there was insufficient data to develop local models.

## Porphyry deposits

Porphyry Cu, porphyry Cu-Mo and porphyry Cu skarn deposits (Cox & Singer, 1986) are known in the assessment area. Permissive rock types, areas identified as probable targets using PNN analyses and geochemical data were the main basis for estimating the number of undiscovered deposits.

The minimum number of undiscovered porphyry type deposits, consistent with grade and tonnage models (Ozpot, in preparation; Cox & Singer, 1986; Singer & others, 2005) is estimated to be:

| Percentile | 90 | 50 | 10 | 5 |
|---|---|---|---|---|
| Estimated number of deposits | 0 | 0 | 1 | 2 |

## Skarn deposits

Felsic to intermediate plutons and carbonate rocks are widespread in the Yarrol assessment area. Similar and related deposit types are also known to occur here (*eg* polymetallic veins).

There is insufficient data to support an estimate of the expected number of undiscovered skarn deposits. However, the numerous small Cu skarn occurrences and veinlet basemetal mineralisation in carbonate rocks adjacent intrusives such as the Glassford Igneous Complex and the Diglum Granodiorite and the results of the PNN analyses, indicates that small undiscovered deposits are likely to exist in the area. Such deposits may be economical if spatially associated and viewed as a whole rather than individually. Mount Allen in the Kroombit area warrants further exploration.

In the assessment area, small polymetallic replacement deposits are possible where carbonate and calcareous clastic rocks are intruded by calcalkaline plutons and dykes. There are, however, no known examples of polymetallic replacement deposits. No estimate



Figure 51: Porphyry gold, copper deposits (after Ozpot, in preparation)
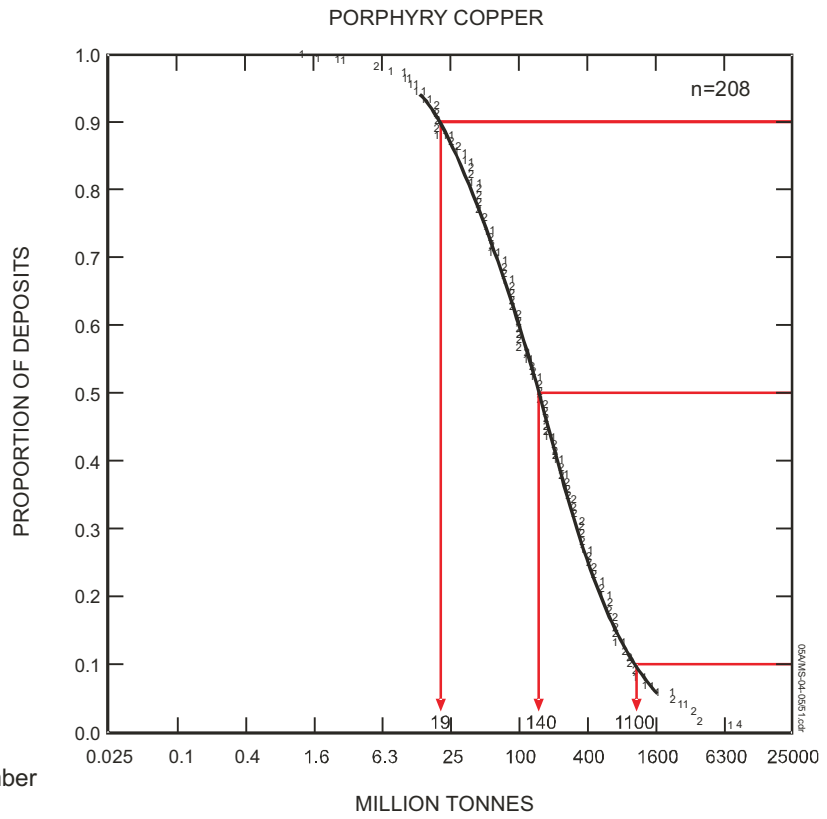
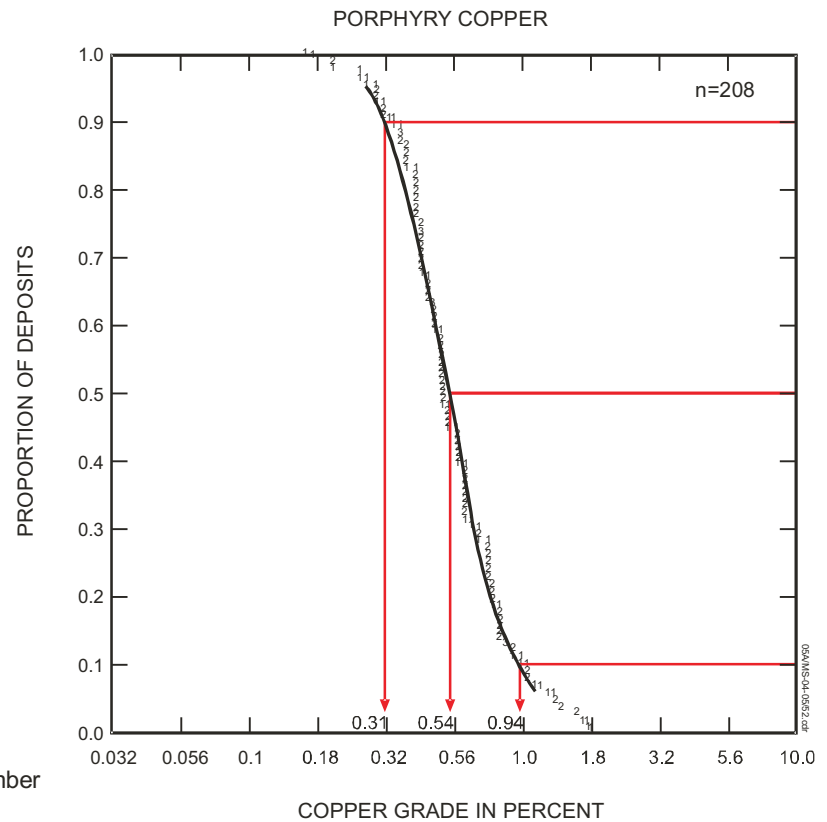*Figure 52: Tonnages of porphyry Cu deposits (after Cox & Singer, 1986)*



*Figure 53: Copper grades of porphyry Cu deposits (after Cox & Singer, 1986)*
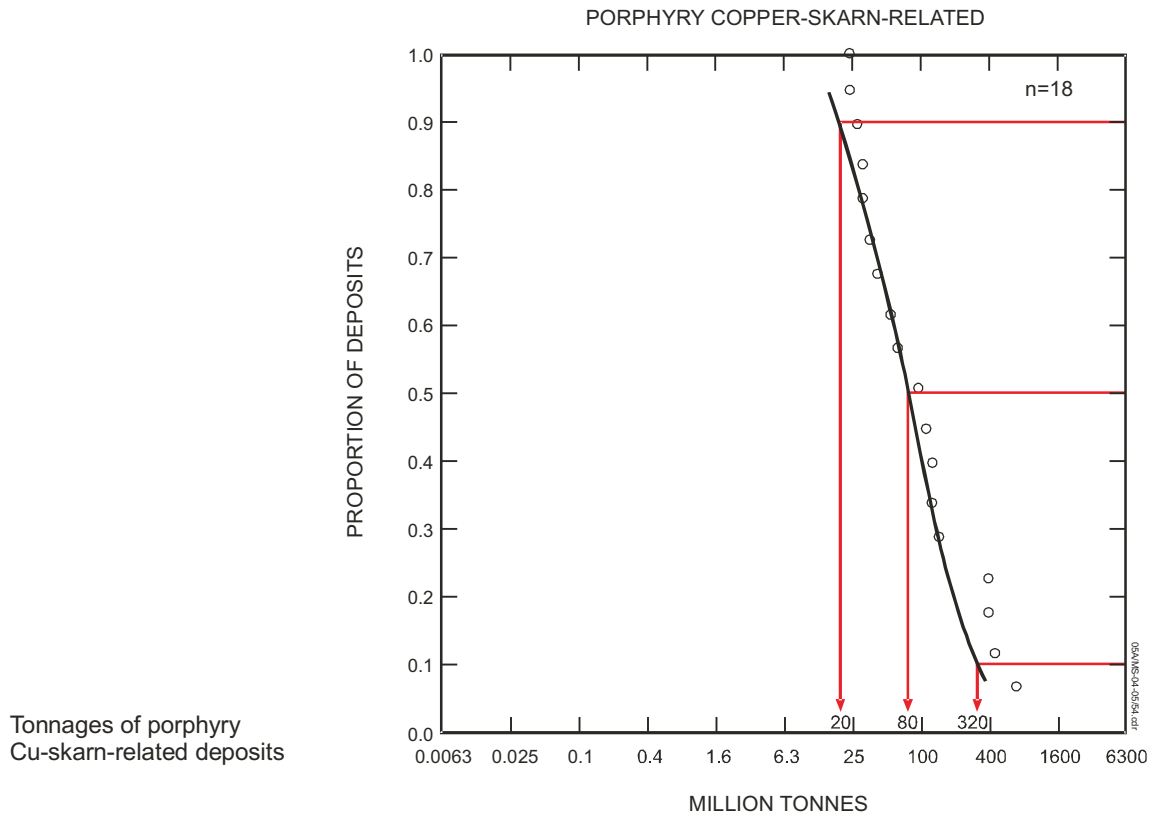
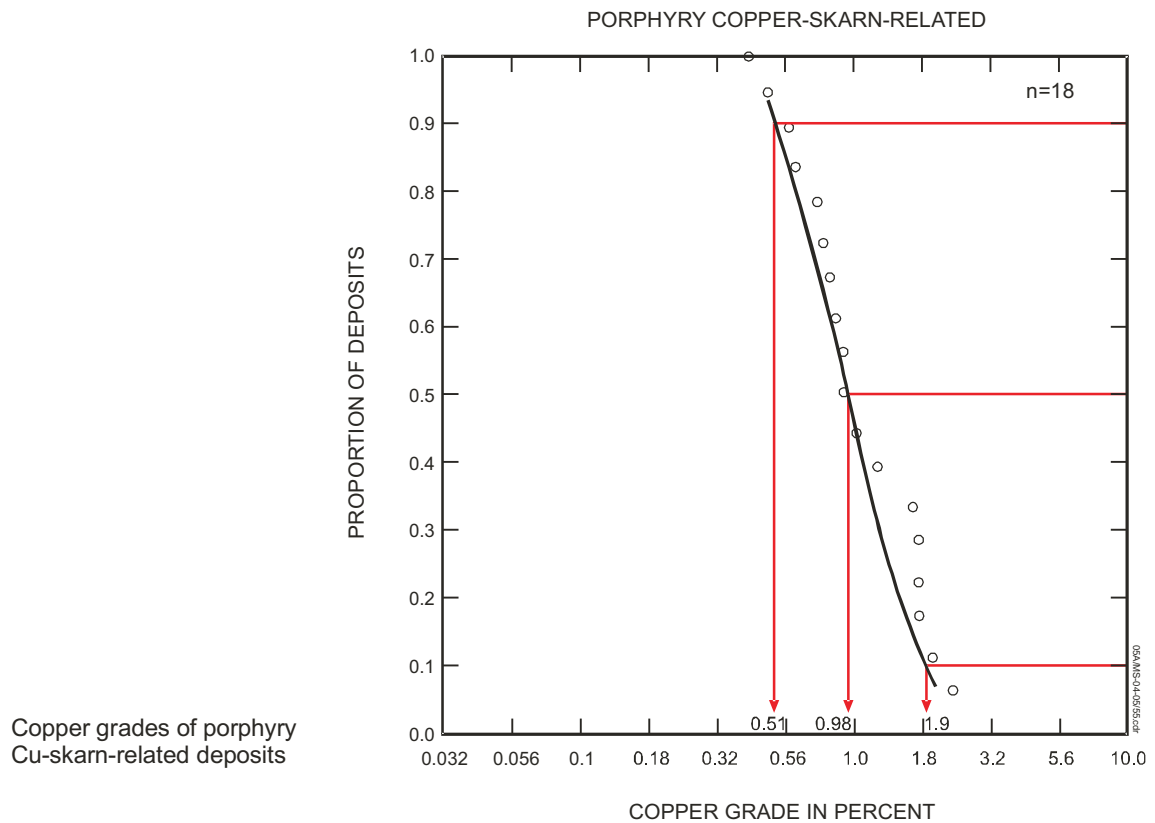Figure 54: *Tonnages of porphyry Cu-skarn-related deposits (after Cox & Singer, 1986)*



Figure 55: *Copper grades pf porphyry Cu-skarn-related deposits (after Cox & Singer, 1986)*
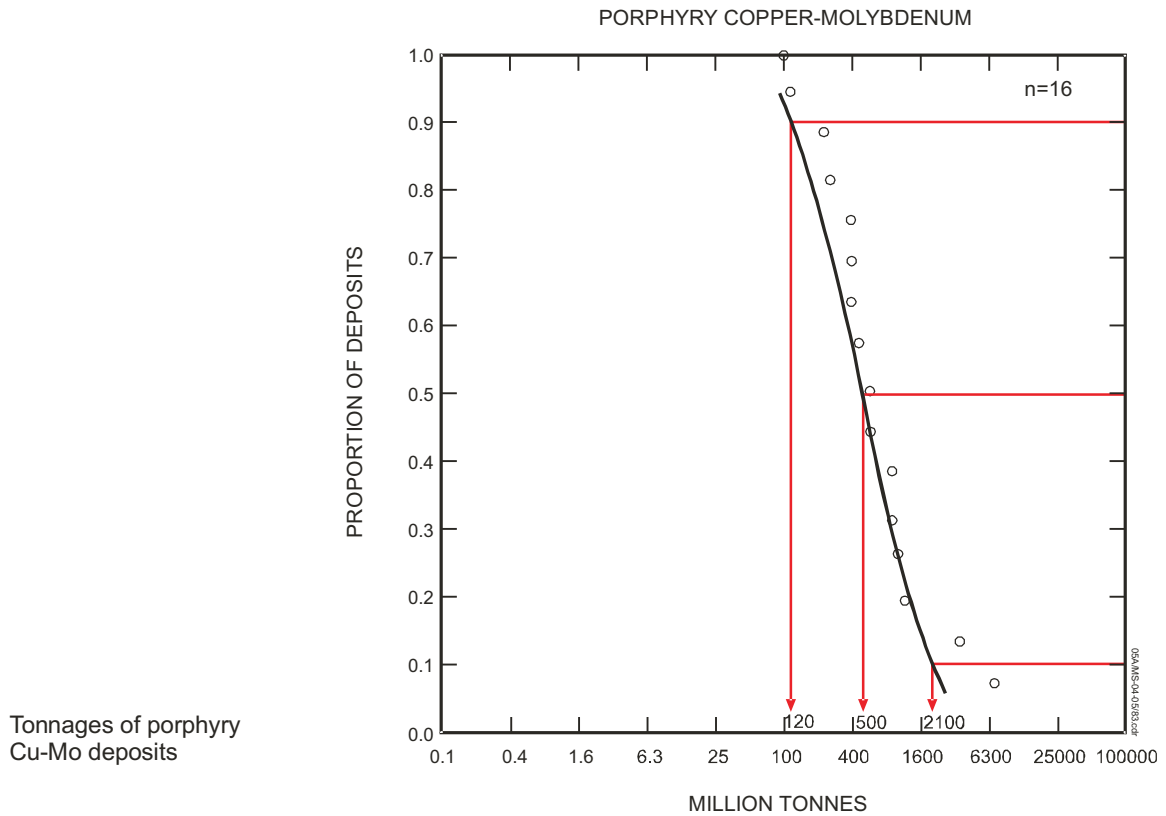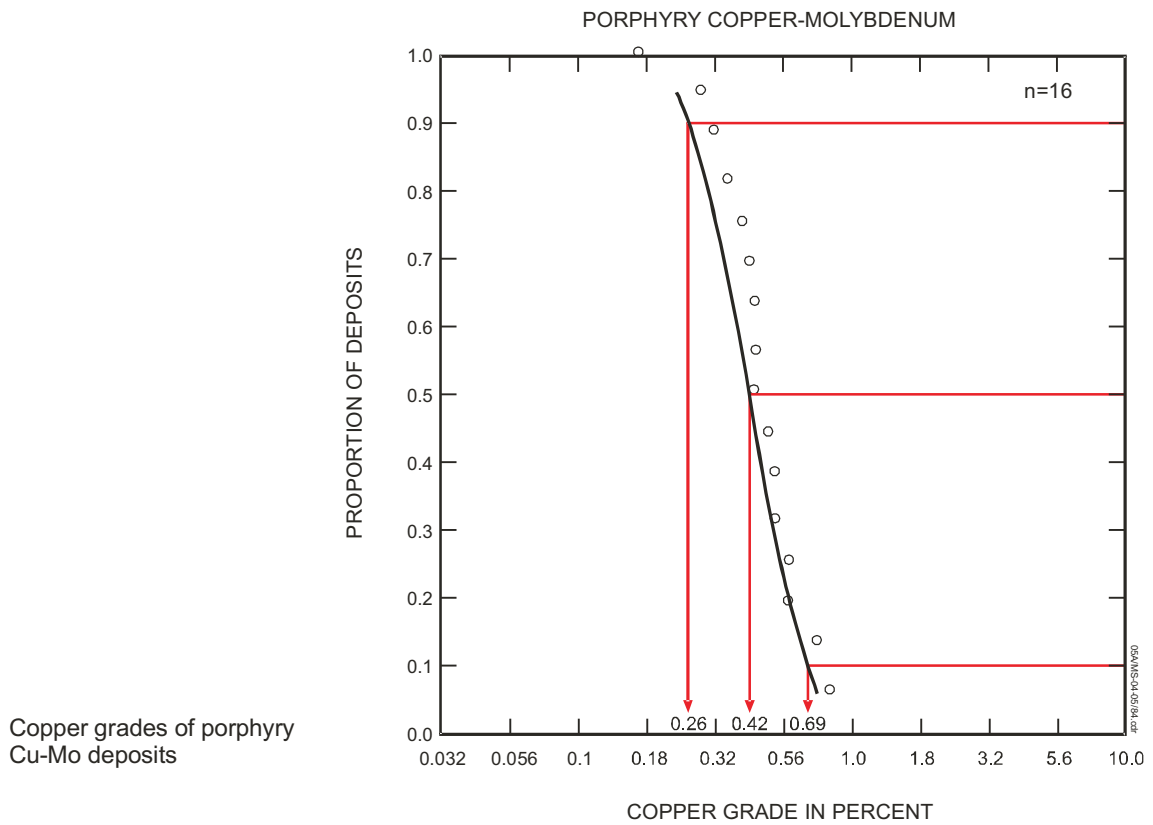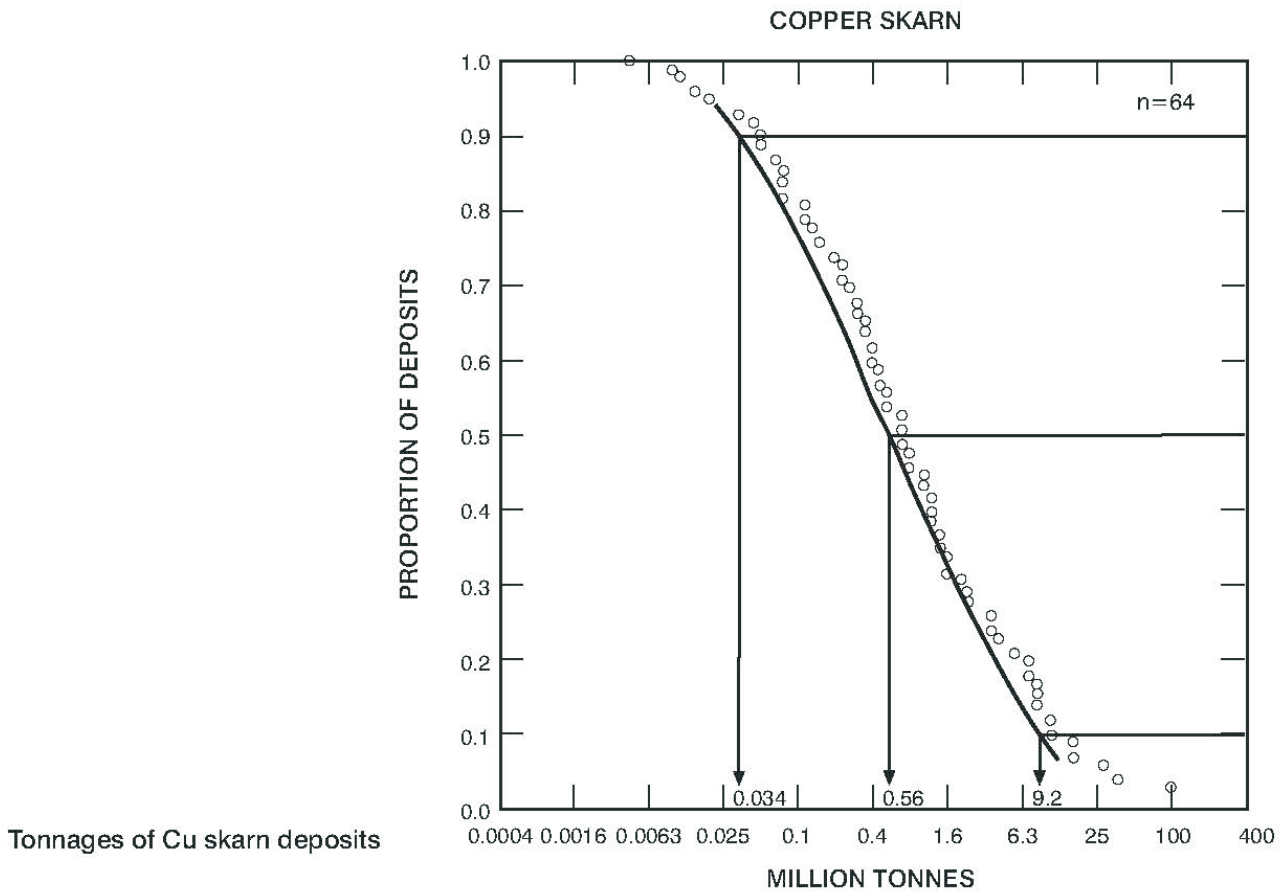
PORPHYRY COPPER-MOLYBDENUM



Tonnages of porphyry
Cu-Mo deposits

*Figure 56: Tonnages of porphyry Cu-Mo deposits (after Cox & Singer, 1986)*

PORPHYRY COPPER-MOLYBDENUM



Copper grades of porphyry
Cu-Mo deposits

*Figure 57: Copper grades of porphyry Cu-Mo deposits (after Cox & Singer, 1986)*

**COPPER SKARN**



Tonnages of Cu skarn deposits

Figure 58: Tonnages of copper skarn deposits (after Cox & Singer, 1986)



Copper grades of Cu skarn deposits
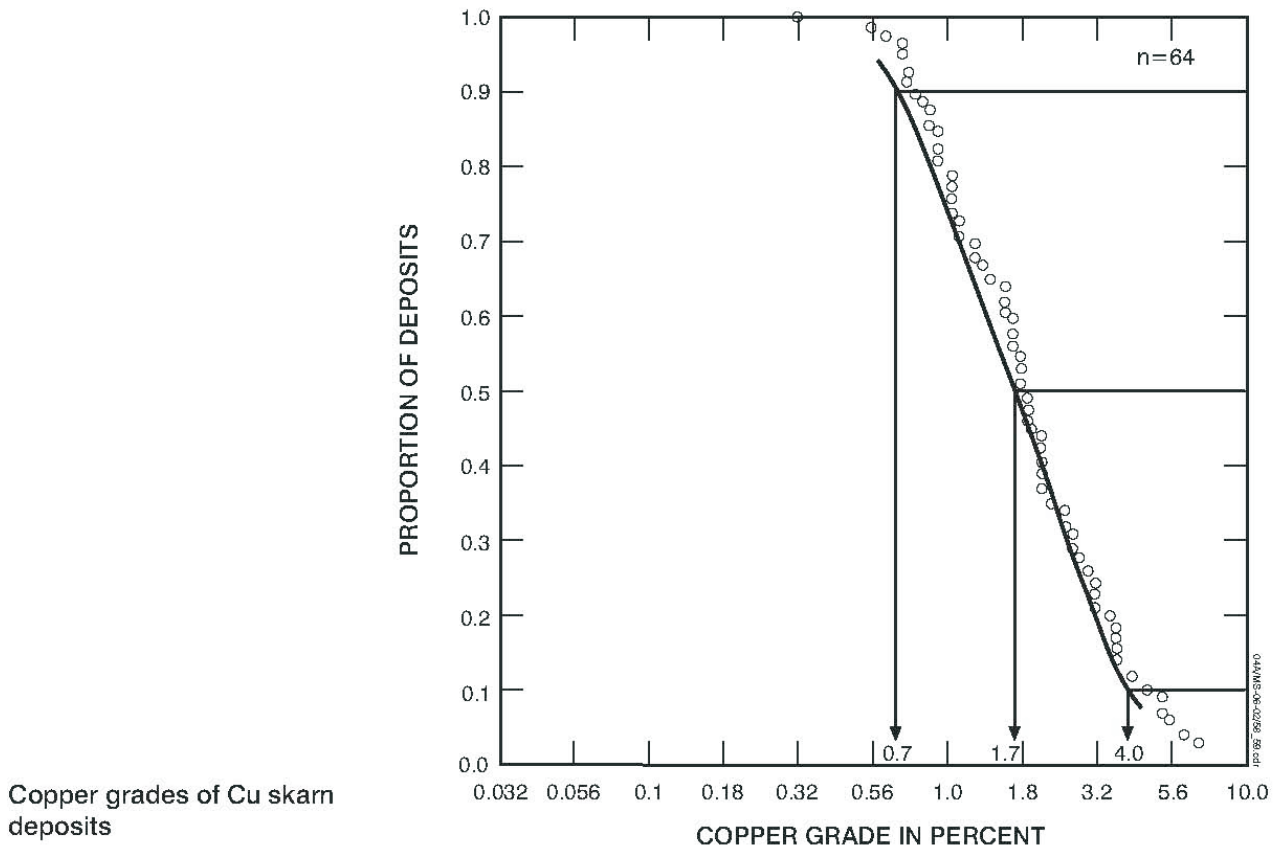
Figure 59: Copper grades of Cu skarn deposits (after Cox & Singer, 1986)

IRON SKARN
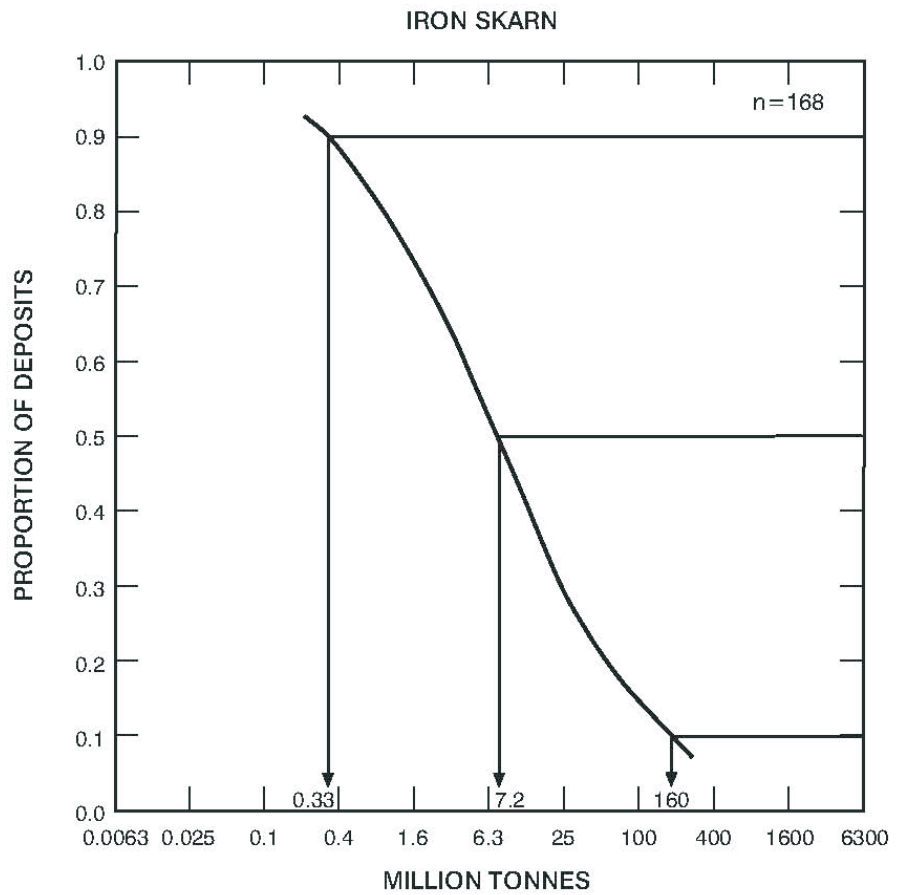


Tonnages of Fe skarn deposits

Figure 60: Tonnages of of Fe skarn deposits(after Cox & Singer, 1986)
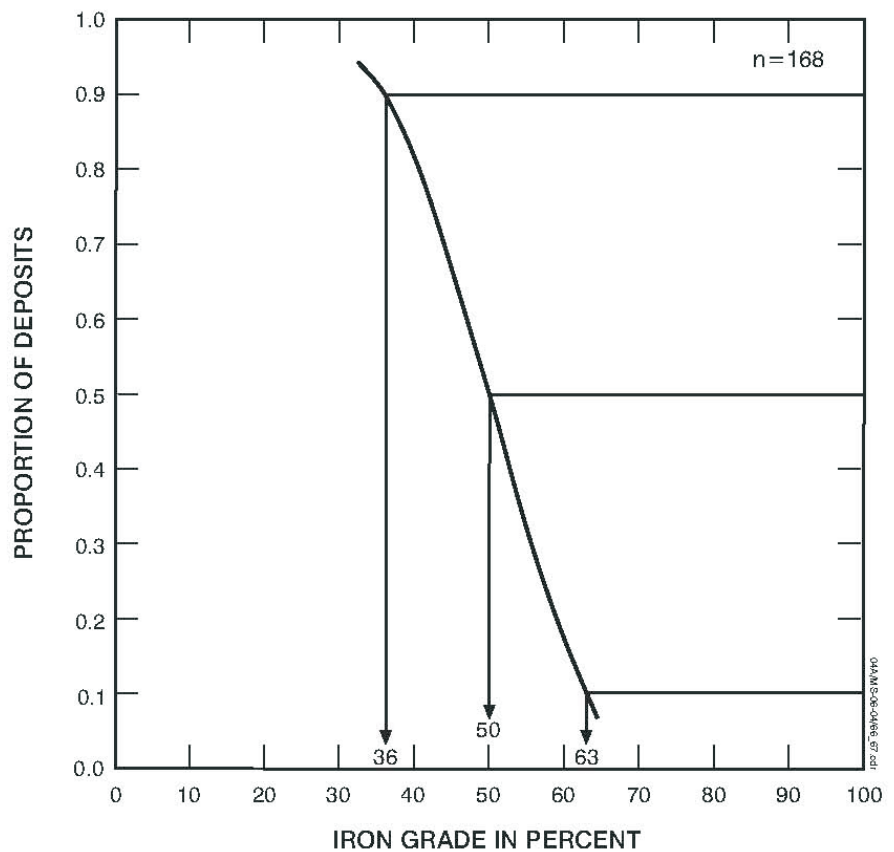


Iron grades of Fe skarn deposits

Figure 61: Iron grades of Fe skarn deposits(after Cox & Singer, 1986)

*Figure 62: Tonnages of carbonate hosted stratabound lead-zinc deposits (after Ozpot, in preparation)*

has been made of the number of undiscovered deposits.

## Polymetallic vein deposits

Polymetallic vein deposits can be associated with intrusive rocks of any age and in a wide range of compositions (Cox & Singer, 1986). This model also includes deposits/occurrences that have limited information and do not obviously fit other deposit types.

Because of the uncertainty attached to occurrences included in this deposit type and a lack of information on the controls of mineralisation and the timing and genesis of lode deposits in the assessment area, an estimate of the expected number of deposits was not attempted.

## Carlin-style replacement deposits

No carlin-style replacement gold mineralisation is known in the assessment area. This type of deposit is associated with the replacement of carbonate rocks adjacent to and along faults or bedding. Some areas matching these conditions are present in the assessment area but these are not spatially significant. No

attempt was made to estimate the number of undiscovered deposits.

## PGE deposits

Several layered ultramafic intrusives have been unsuccessfully explored for PGE mineralisation. However, magnetic interpretation has identified gabbroic bodies at depth (*eg* Rule Gabbro) that are as yet to be explored.

No attempt was made to estimate the number of undiscovered PGE deposits.

## Podiform chromite

Podiform chromite has been mined at Elgalla (2192.5t of oxidised ore), Balnagowan Surface and Balnagowan Lode.

Because of the small size and low grade of known mineralisation in the Yarrol area no estimate has been made of undiscovered podiform chromite deposits.
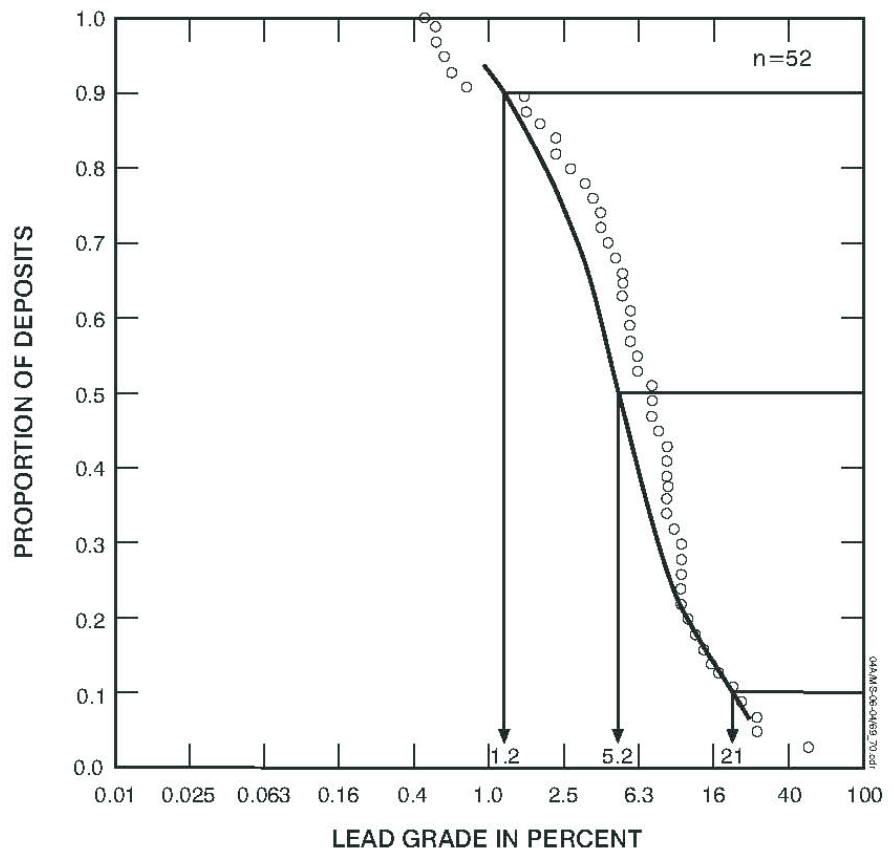
## Epithermal deposits

Whilst tracts of volcanic rocks and an association between volcanics and intrusives of
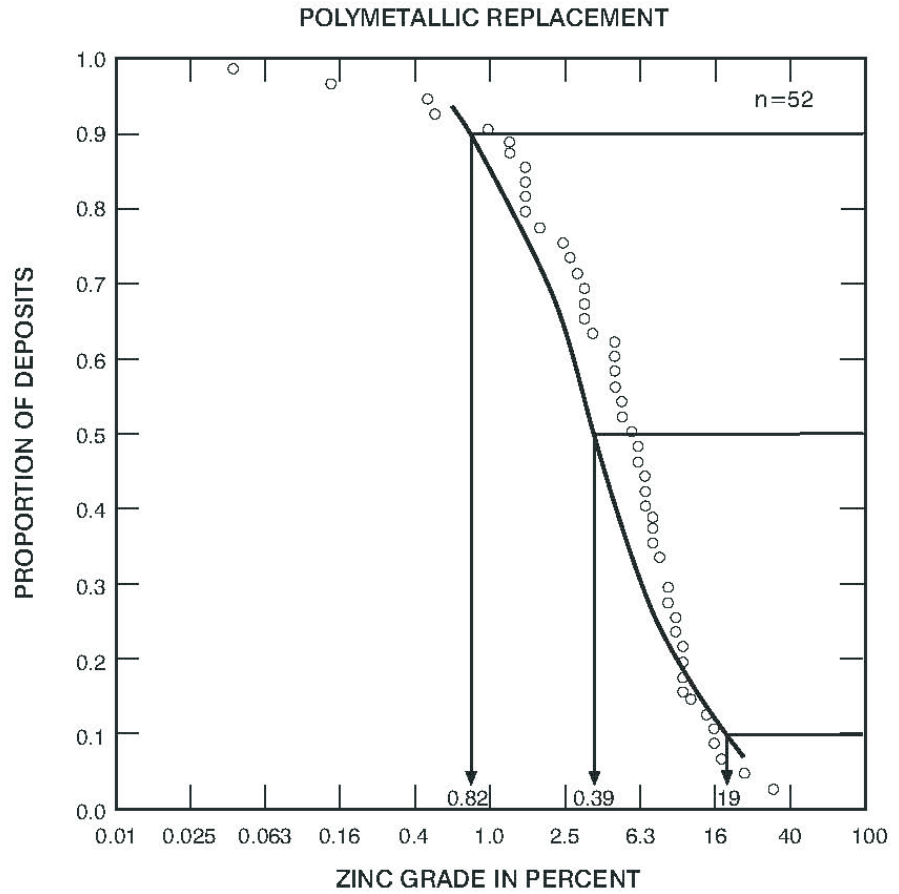
POLYMETALLIC REPLACEMENT
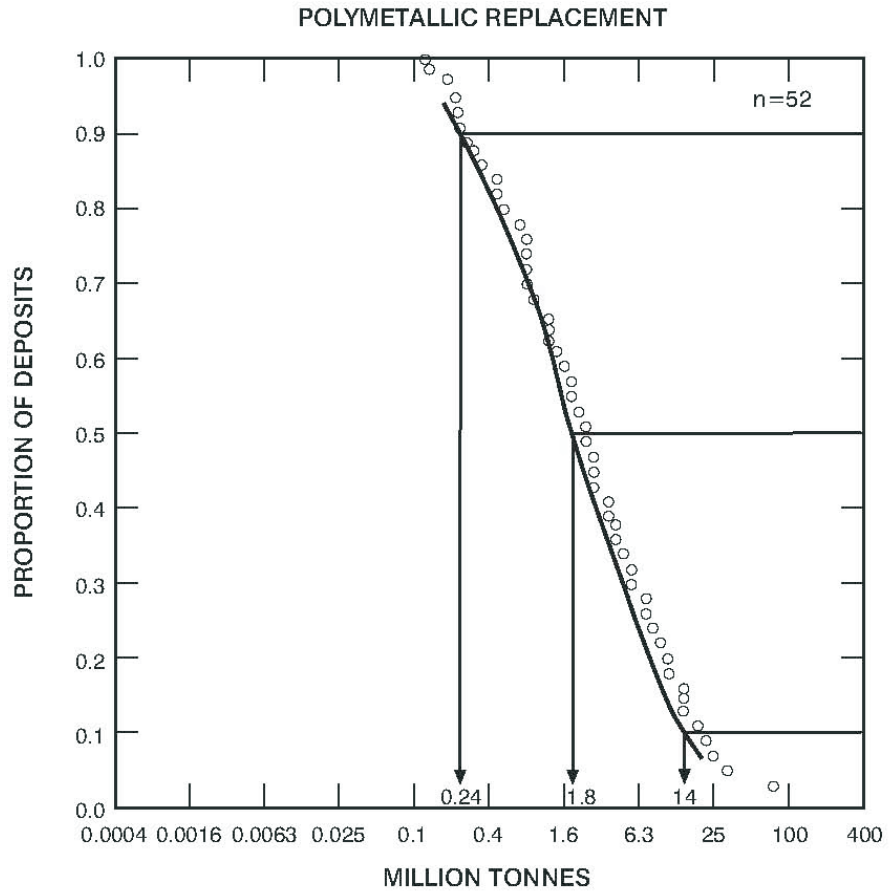


Tonnages of polymetallic
replacement deposits

*Figure 63: Tonnages of polymetallic replacement deposits (after Cox & Singer, 1986)*
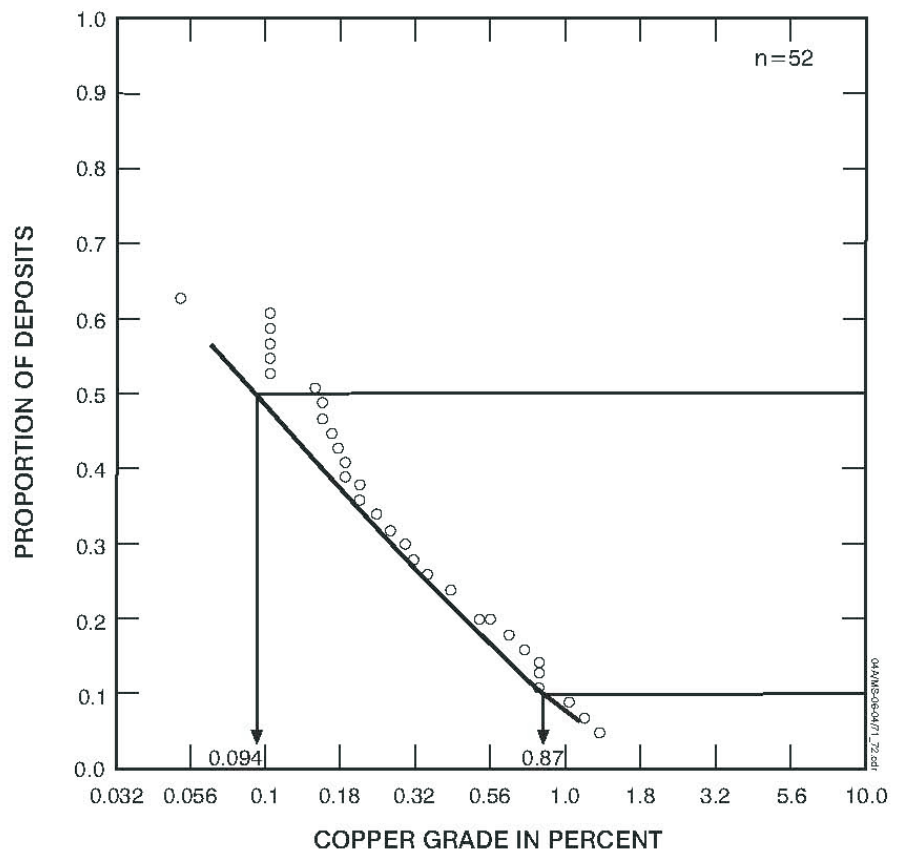


Lead grades of polymetallic
replacement deposits

*Figure 64: Lead grades of polymetallic replacement deposits (after Cox & Singer, 1986)*
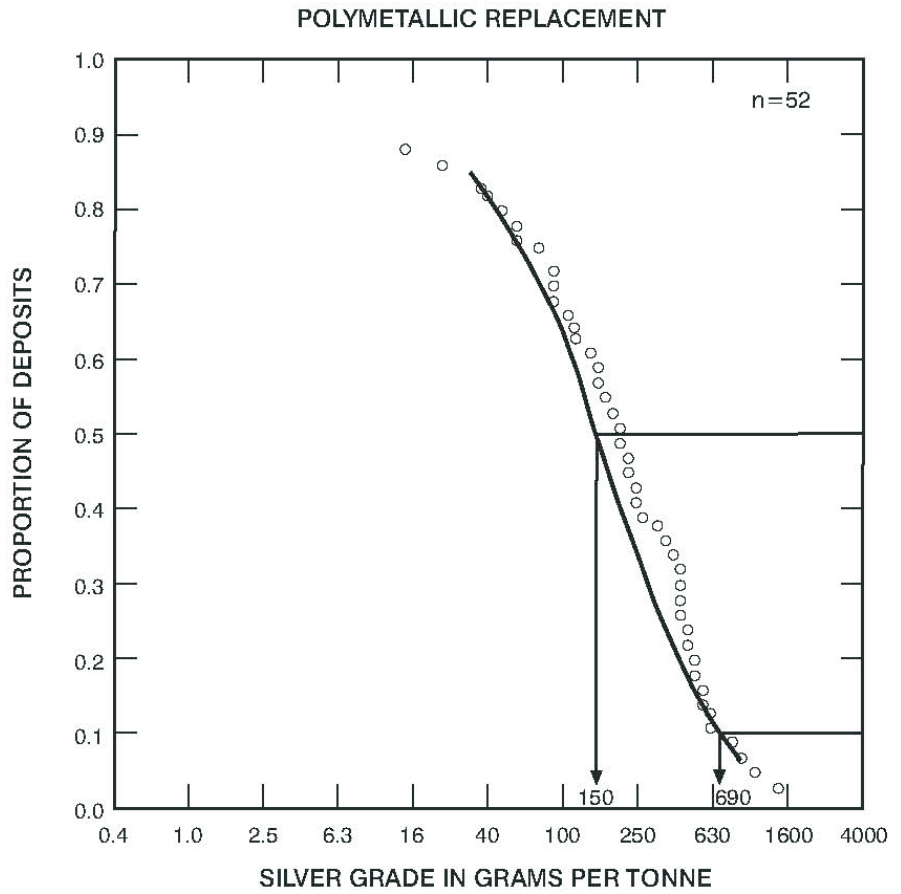
POLYMETALLIC REPLACEMENT

Zinc grades of polymetallic
replacement deposits

*Figure 65: Zinc grades of polymetallic replacement deposits (after Cox & Singer, 1986)*
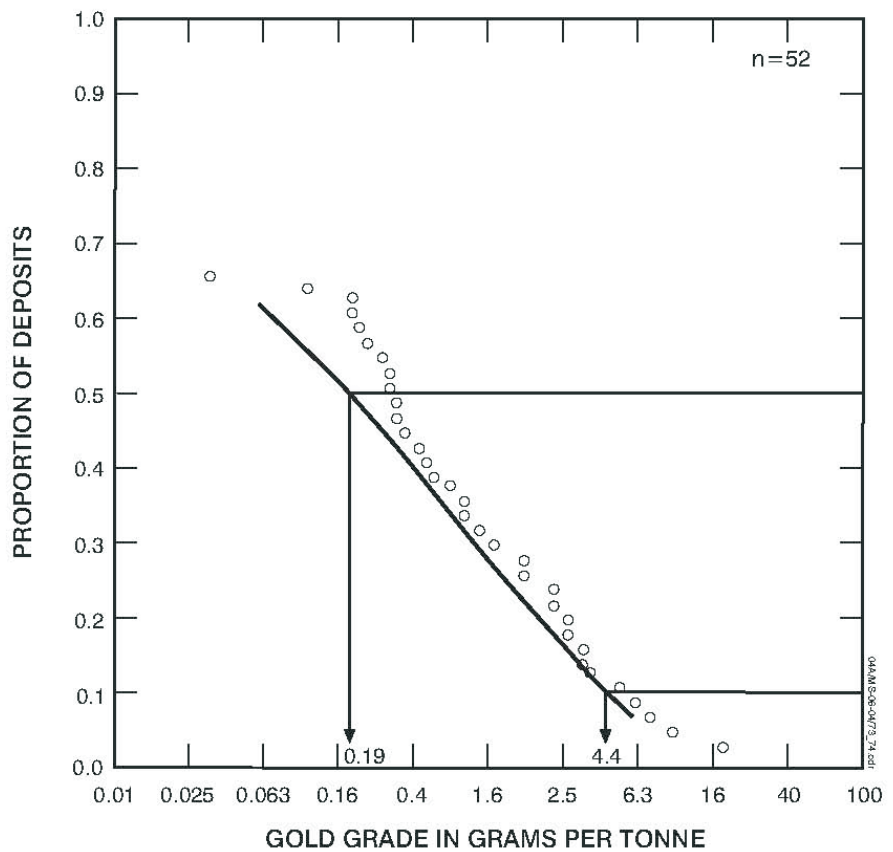
Copper grades of polymetallic
replacement deposits

*Figure 66: Copper grades of polymetallic replacement deposits (after Cox & Singer, 1986)*
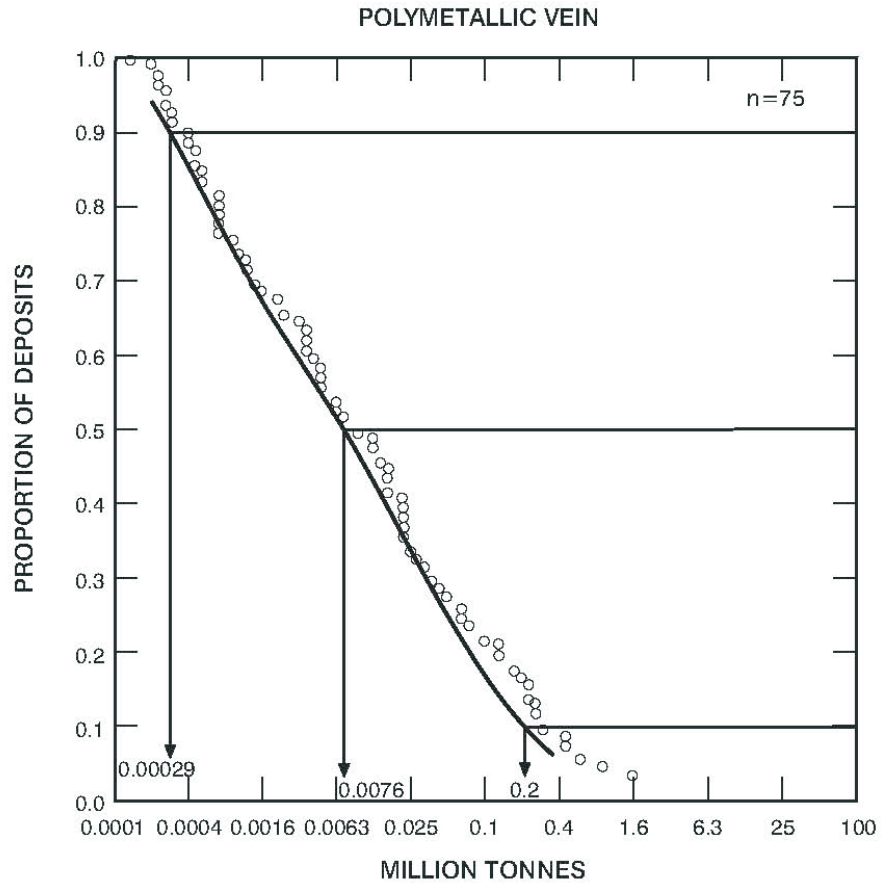
Silver grades of polymetallic replacement deposits

Figure 67: Silver grades of polymetallic replacement deposits (after Cox & Singer, 1986)



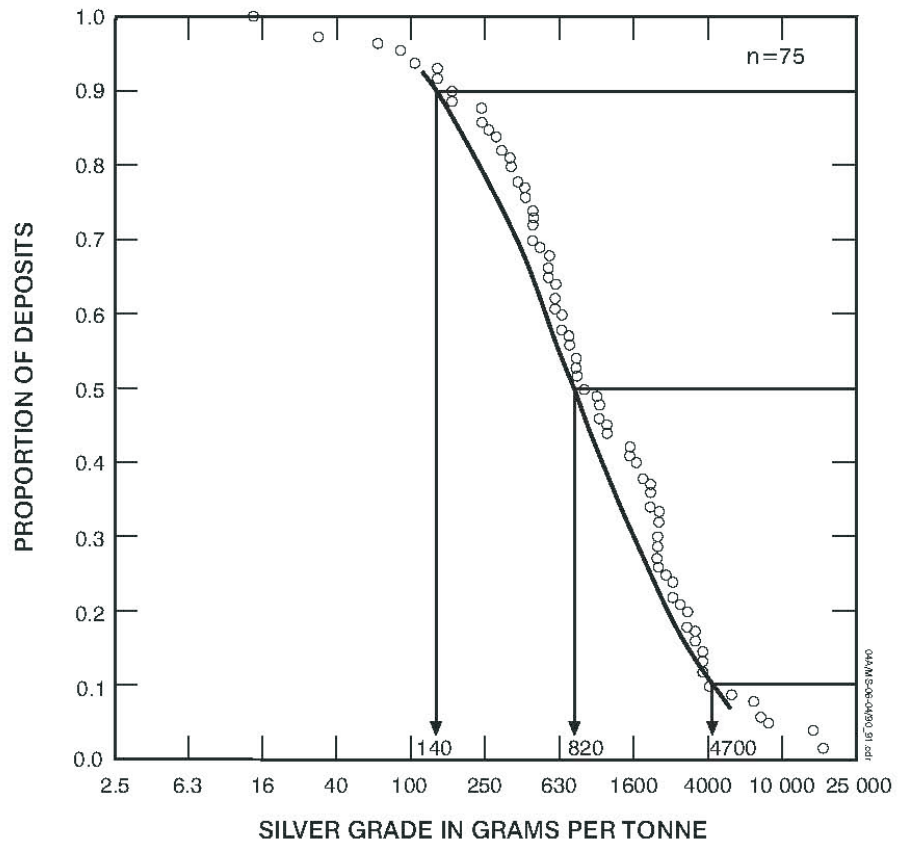Gold grades of polymetallic replacement deposits

Figure 68: Gold grades of polymetallic replacement deposits (after Cox & Singer, 1986)

POLYMETALLIC VEIN



Tonnages of polymetallic
vein deposits

*Figure 69: Tonnages of polymetallic vein deposits (after Cox & Singer,1986)*



Silver grades of polymetallic
vein deposits

*Figure 70: Silver grades of polymetallic vein deposits (after Cox & Singer,1986)*

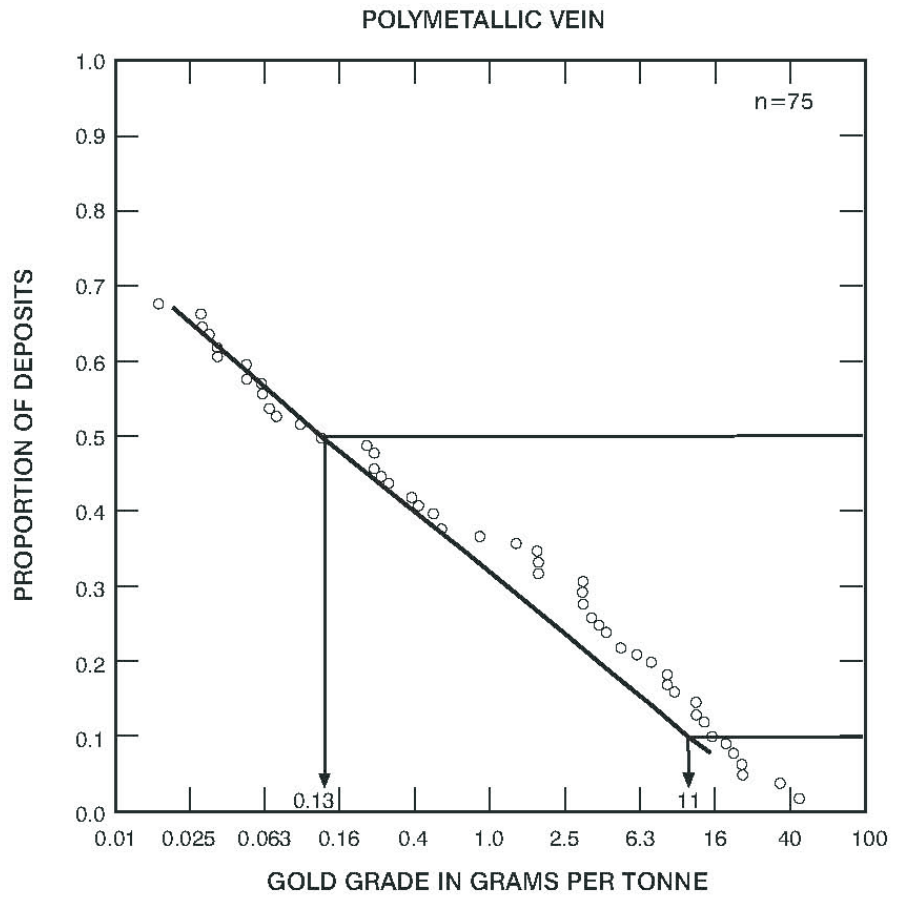**POLYMETALLIC VEIN**



Gold grades of polymetallic
vein deposits

*Figure 71: Gold grades of polymetallic vein deposits (after Cox & Singer, 1986)*
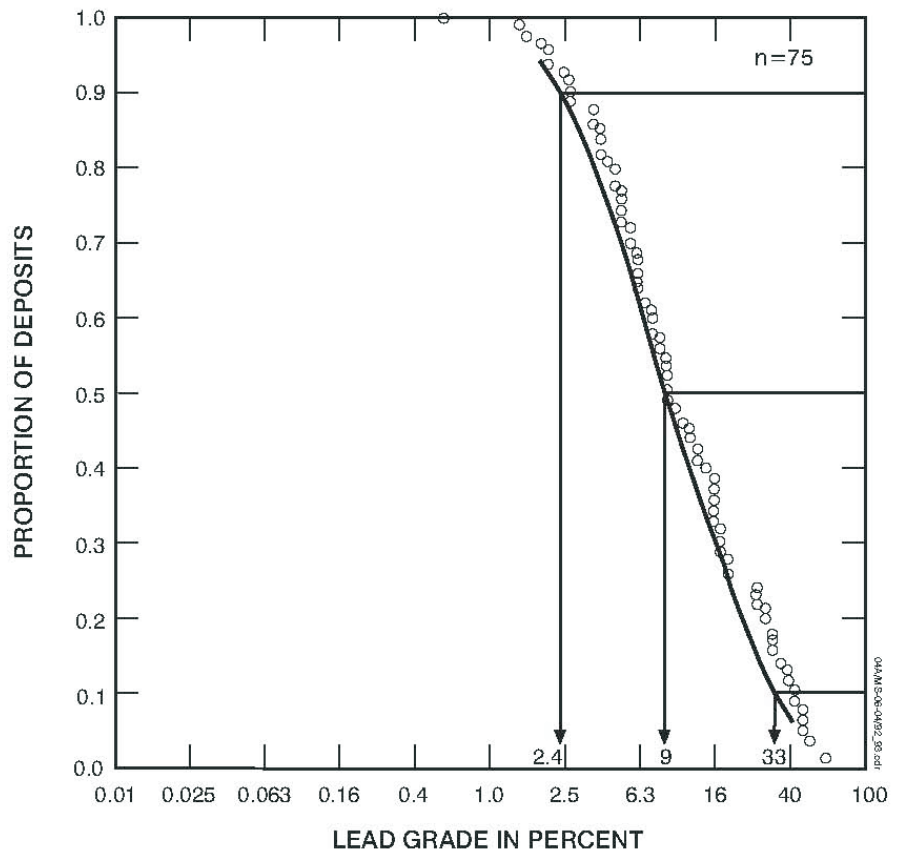


Lead grades of polymetallic
vein deposits

*Figure 72: Lead grades of polymetallic vein deposits (after Cox & Singer, 1986)*
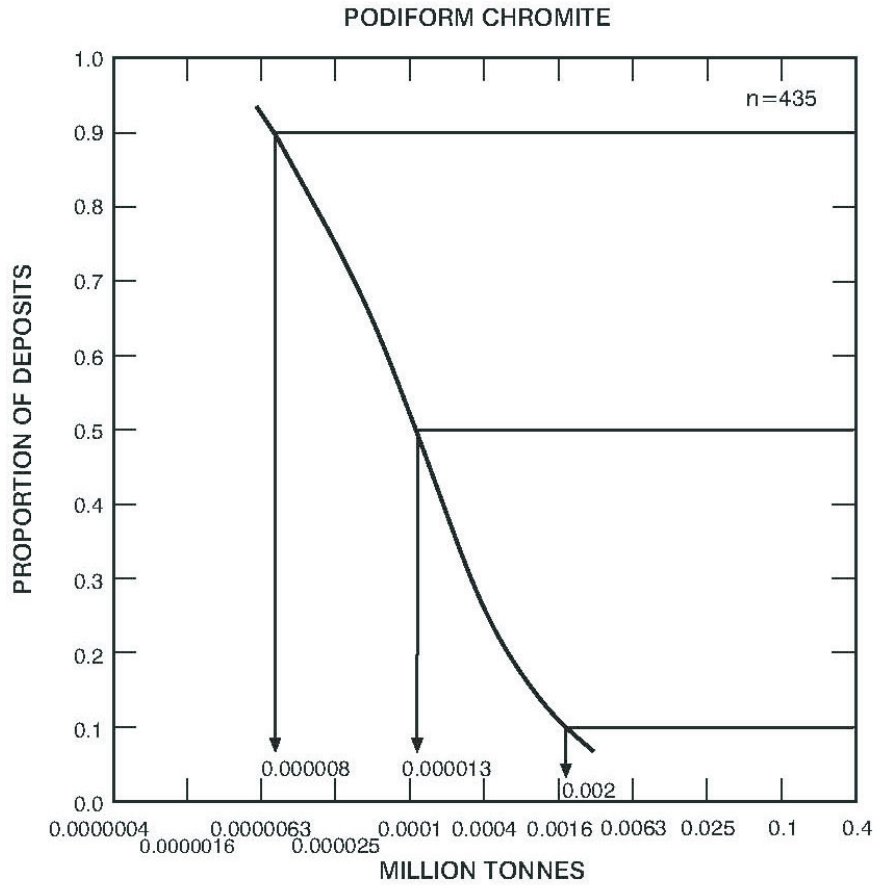
Tonnages of Podiform chromite
deposits from California and
Oregon, U.S.A.

*Figure 73: Tonnages of podiform chromite deposits in the USA (after Cox & Singer, 1986)*



Chromite grades of podiform
chromite deposits from
California and Orogen, U.S.A.

*Figure 74: Chromite grades of podiform chromite deposits in the USA (after Cox & Singer, 1986)*

**Epithermal Gold Deposits**
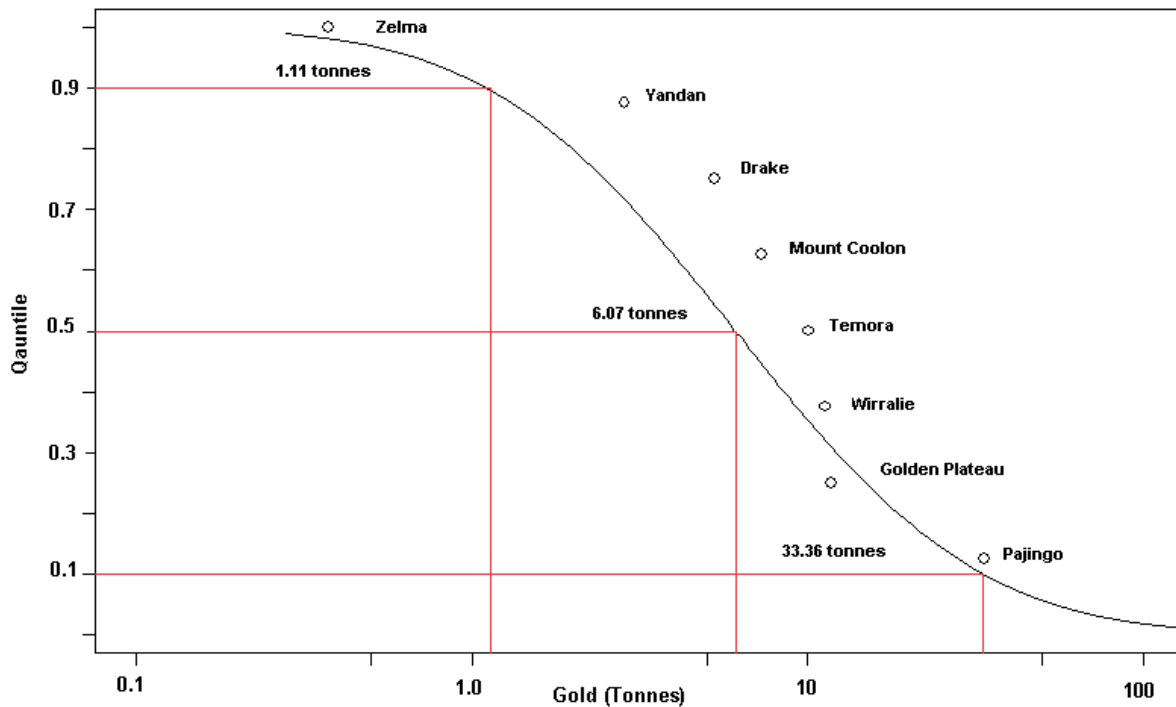


*Figure 75: Tonnages of epithermal gold deposits (after Ozpot, in preparation)*

about the same age is apparent and possible eruptive centres have been identified (*eg* Winterbourne Volcanics in the Kroombit area) no epithermal deposits are known in the area and only one occurrence. Economic deposits, however, are known to occur outside the assessment area in rock units that extend into it or their equivalents (*eg* Cracow, North Arm).

The minimum number of undiscovered epithermal deposits, consistent with grade and tonnage models (Ozpot, in preparation) is estimated to be:

| Percentile | 90 | 50 | 10 | 5 |
|---|---|---|---|---|
| Estimated number of deposits | 0 | 0 | 1 | 1 |

## *Lateritic nickel*

The areal extent of tract 3, lateritic nickel, is not great within the assessment area and because of the relative ease of exploring for lateritic deposits and because the Yarrol assessment area has been well-explored for this type of deposit, it is considered as having a low probability for future discoveries. No estimate

for undiscovered lateritic nickel deposits has been attempted.

It is noted that the development of potential deposits to the north of the assessment area could result in the economic development of lateritic nickel mineralisation in the Yarrol area, with it providing additional resources to nearby operations.

## *Kunwarara-type magnesite*

This type of deposit can be expected to occur in loosely consolidated sediments due to weathering and erosion of nearby serpentinite and subsequent enrichment through diagenesis.

No grade and tonnage model exists for the Kunwarara-type magnesite deposit and there is insufficient data on the genesis of economic mineralisation. Consequently no estimate of the number of undiscovered deposits has been made. However, Yaamba is a large active prospect that is likely to prove economical and the Jim Crow Basin also represents geological conditions that has potential for similar mineralisation. Consequently, there exists an

excellent possibility for the discovery of at least one deposit in the tract.

## LSAUQ and listwanite deposits

Both low sulphide gold-quartz and listwantite veins occur in the assessment area. The region also contains, for LSAUQ in particular, a significant area of suitable geological setting and host rocks permissive for additional deposits. However, because of the small tonnage of these deposits in the general model (Bliss & Cox, 1986) and because important deposits of this type are not known in Yarrol, undiscovered deposits were not estimated.

## Basaltic copper

The Cretaceous Alton Downs Basalt, mafic volcanics in Devonian Mount Hoopbound Formation, and the Carboniferous to Permian Camboon Volcanics and Mount Benmore Volcanics, all record local concentrations of native copper and copper sulphide mineralisation that are interpreted to be basaltic copper occurrences.

No grade and tonnage model exists for basaltic copper and occurrences known in the assessment area and adjacent areas are not considered to have economic potential.

Consequently, no estimate has been made for undiscovered basaltic copper.

## Cu-Zn VMS subtype

The presence of rifting settings and basaltic volcanism, local intermediate to felsic volcanics, and marine sedimentary rock units indicates that the assessment area is permissive for Cu-Zn VMS. The coincidence of favourable rock units and regional geochemistry highs in Cu, Pb and Zn are used to estimate the minimum number of undiscovered Cu-Zn VMS deposits consistent with grade and tonnage models.

| Percentile | 90 | 50 | 10 | 5 |
|---|---|---|---|---|
| Estimated number of deposits | 0 | 0 | 1 | 2 |

## Kuroko VMS

Felsic volcanic hosted Kuroko-style VMS occur with the Yarrol assessment area. The most significant of these is Mount Morgan, but numerous other deposits and occurrences occur within the assessment area including: Mount Chalmers, Botos, Striker 2, Hunter1/2/18, Tungamull Prospect. The geological setting and host rocks, whilst favourable for additional deposits, are not



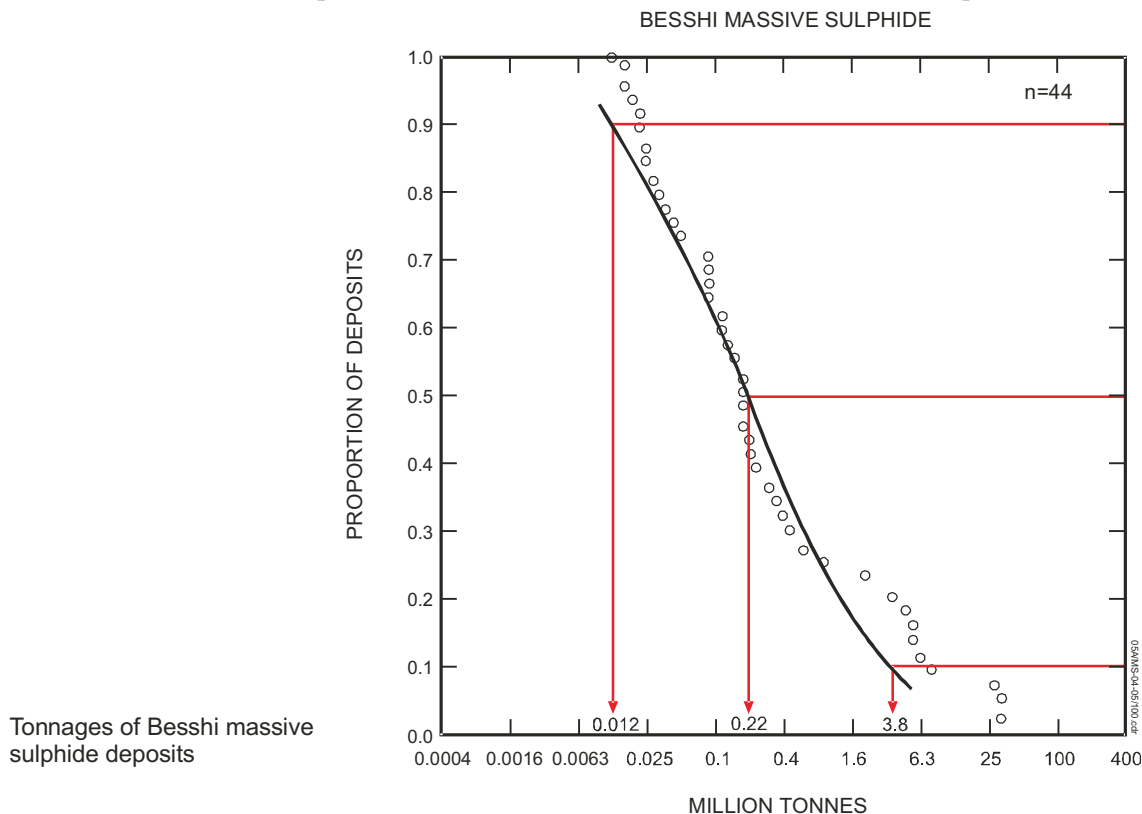Figure 76: Tonnages of Besshi massive sulphide deposits (after Cox & Singer, 1986)

BESSHI MASSIVE SULPHIDE



Copper grades of Besshi massive sulphide deposits
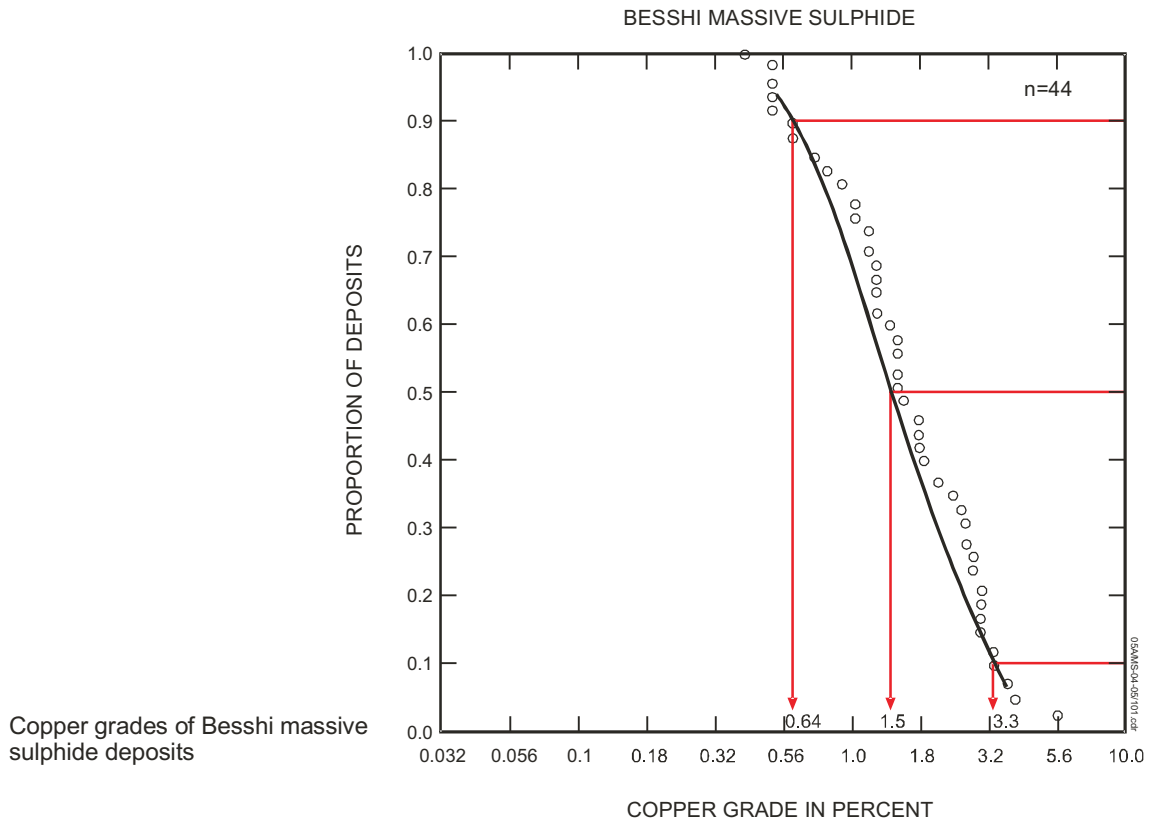
*Figure 77: Copper grades of Besshi massive sulphide deposits (after Cox & Singer, 1986)*

## Volcanic Associated Massive Sulphide Deposits
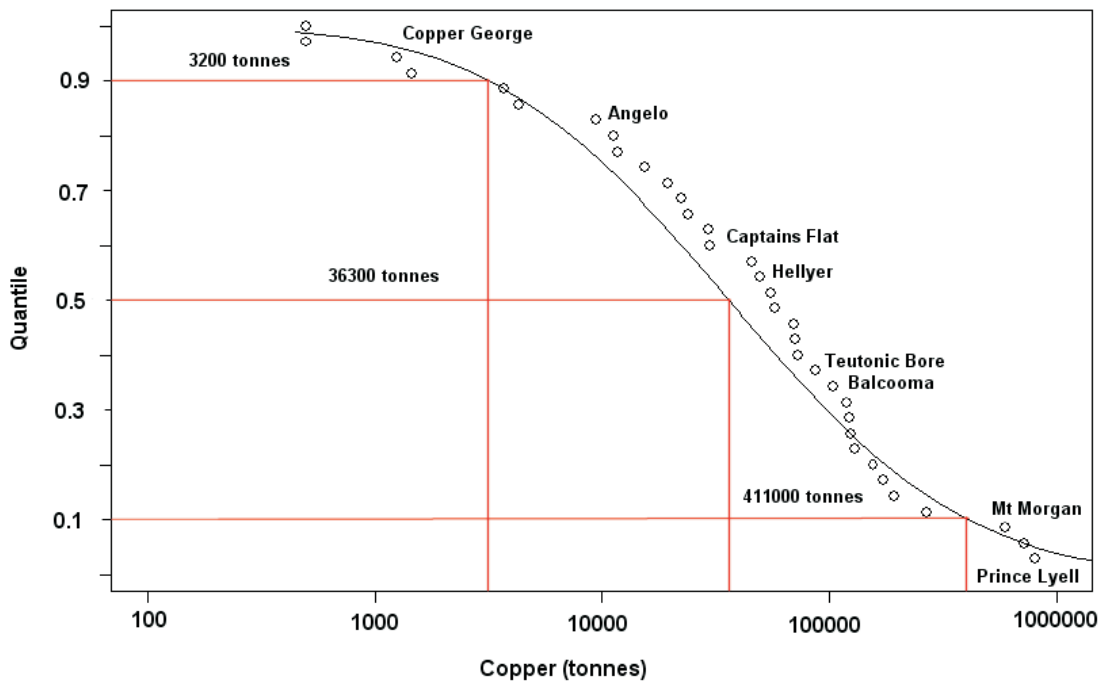


*Figure 78: Tonnages of Kuroko massive sulphide deposits (copper) (after Ozpot, in preparation)*

## Volcanic Associated Massive Sulphide Deposits
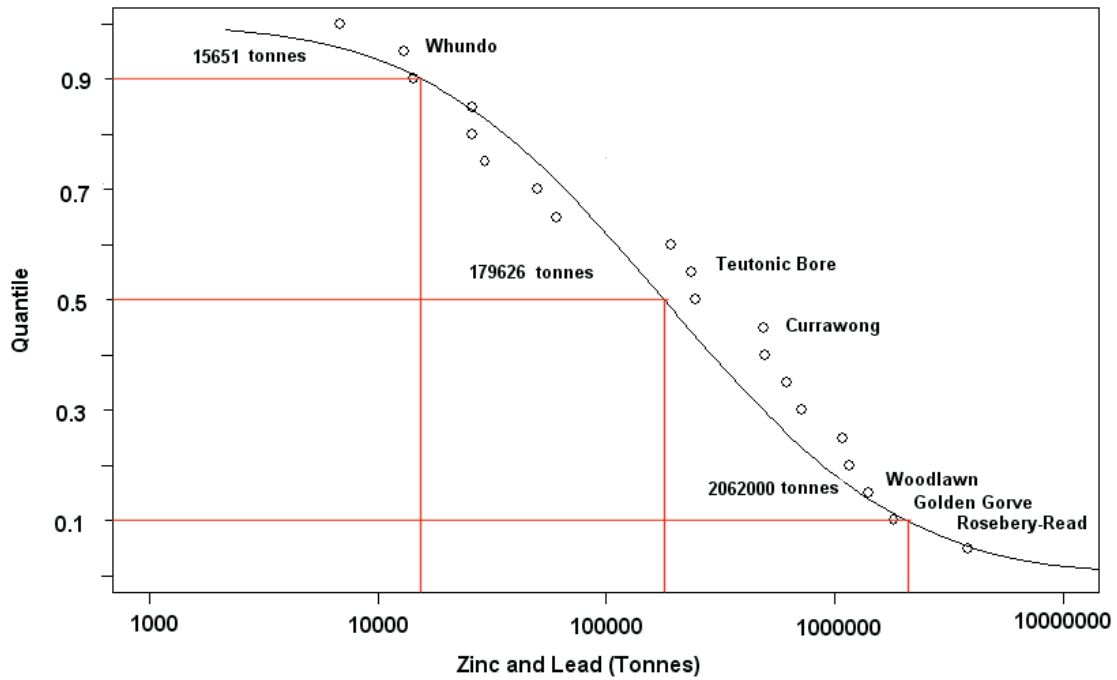


*Figure 79: Tonnages of Kuroko massive sulphide deposits (zinc and lead) (after Ozpot, in preparation)*

extensive. Therefore, the probability of undiscovered Kuroko-type deposits is correspondingly low. Based on the geology, geochemistry and PNN analysis the minimum number of undiscovered Kuroko VMS deposits consistent with grade and tonnage models is:

| Percentile | 90 | 50 | 10 | 5 |
|---|---|---|---|---|
| Estimated number of deposits | 0 | 0 | 0 | 1 |

## *Volcanogenic manganese*

Known manganese ore occurrences are recorded on the Gladstone and Rockhampton sheets, in the Wandilla and Doonside Formations.

It is considered that there is limited economic potential for this style of mineralisation and no grade and tonnage model is available. No estimate of the number of undiscovered deposits has been made.

## *Gold on flat faults*

Because of the small tonnage of these deposits and the absence of grade and tonnage models, the number of undiscovered deposits has not been estimated.

# APPENDIX 1

## WEIGHTS OF EVIDENCE

The following is an overview of weights of evidence based on work recorded in Bonham-Carter (1994) and Singer & Kouda (1999).

The general idea employed in weights of evidence involves prior and posterior probabilities. The goal is to estimate the posterior probability of deposit occurrence given the presence or absence of evidence. By assuming that the prior probability is constant over the study region, Bayes' Rule is applied to generate a posterior probability that a unit cell contains a deposit. This posterior probability is of interest, whether it is larger or smaller than the prior probability, as it reflects the favourability of the unit cell.

Before outlining the application of Bayes' Rule in weights of evidence, the underlying assumptions need to be stated:

1) Each mineral deposit/occurrence within the study area is assigned to a small unit cell of area $ukm^2$.

2) The total number of unit cells containing a deposit is represented by N(D), where N() is the count of unit cells and D refers to the presence of deposits.

3) Cells either contain a deposit or not.

4) The total area of the region being studied is $tkm^2$. The total number of cells, N(T) = t/u unit cells.

5) The average density of known deposits in the area is then N(D)/N(T). This ratio is taken as the prior probability of a cell containing a deposit, P(D).

6) In the j-th binary predictor map, $B_j$, the area with the pattern present is denoted as $N(B_j)$ unit cells and $N(B_j') = N(T) - N(B_j)$ is the area with the pattern absent.

7) The prior probability that a unit cell contains a deposit is assumed to be constant over the study region.

In combining evidence from several maps, the weights are calculated independently for each map, and then combined. This requires an assumption of conditional independence. The conditional independence assumption produces a simplified model that can be useful for prediction and for indicating the relative contributions of the separate sources of evidence.

As indicated above, the Bayesian approach allows the prediction of the presence of a set of point objects. The point objects (mineral deposits) are treated as being a small area object either occurring or not within a small unit cell. The favourability of existence of a deposit given the presence of evidence can be expressed by Bayes' Rule as the conditional probability of a deposit occurring, (given the j-th binary pattern):

$$P(D/B_j) = P(D \cap B_j)/P(B_j) \qquad (1.1)$$

where $P(D/B_j)$ is the conditional probability of a deposit given the presence of the j-th binary pattern. In order to obtain an expression relating the posterior probability of a deposit in terms of the prior probability and a multiplication factor, the conditional probability of being on the binary map $B_j$, given the presence of a deposit, is defined as:

$$P(B_j/D) = P(B_j \cap D)/P(D) \qquad (1.2)$$

Because $P(B_j \cap D)$ is the same as $P(D \cap B_j)$, equations 1.1 and 1.2 can be combined to solve for $P(D/B_j)$, satisfying the relationship:

$$P(D/B_j) = [P(B_j/D) \, P(D)]/P(B_j) \qquad (1.3)$$

This states that the conditional (posterior) probability of a deposit, given the presence of the binary pattern, equals the prior probability of the deposit P(D) multiplied by the factor $P(B_j/D)/P(B_j)$.

A similar expression can be derived for the posterior probability of a deposit occurring given the absence of a variable (indicated by the apostrophe beside the $B_j$):

$$P(D/B_j') = [P(B_j'/D)P(D)]/P(B_j') \qquad (1.4)$$

The same model can be expressed in an odds form, with weights of evidence using the

natural logarithm of odds, known as logits. Equation 1.4 expressed as odds becomes:

$$P(D/B_j)/ P(D'/B_j) = [P(D) \ P(B_j/D)]/[P(D'/B_j) \ P(B_j)] \quad (1.5)$$

where the apostrophe beside the D refers to the absence of deposits. From the definitions of conditional probability:

$$P(D'/B_j) = P(D'\cap B_j)/P(B_j) = P(B_j/D')P(D')/P(B_j) \quad (1.6)$$

Substituting this expression for $P(D/B_j)$ into the numerator of the right hand side of the equation yields:

$$P(D/B_j)/ P(D'/B_j) = [P(D)/P(D')] \ [P(B_j)/P(B_j)]$$
$$[P(B_j/D)/ \ P(B_j/D')] \quad (1.7)$$

The odds of a deposit are equal to $P(D)/(1-P(D)$ or $P(D)/P(D')$, so substituting odds into equation 1.7 gives:

$$O(D/B_j) = O(D) \ P(B_j/D) \ / \ P(B_j/D') \quad (1.8)$$

where $O(D/B_j)$ is the conditional (posterior) odds of D given $B_j$, $O(D)$ is the prior odds of D, and $P(B_j/D)/ \ P(B_j/D')$ is known as the sufficiency ratio or LS. In weights of evidence, the natural logarithms of both sides of equation 1.8 are taken. Recasting these equations in loglinear form results in the following expressions for the posterior logit (posterior log odds) of a cell containing a deposit on the basis of the j-th binary pattern:

$$posterior \ logit(D/B_j)=prior \ logit(D)+W_j^+ \quad (1.9)$$

and

$$posterior \ logit(D/B'_j)=prior \ logit(D)+W_j' \quad (1.10)$$

where the positive weight of evidence is defined as:

$$W_j^+ = ln[P(B_j/D)/P(B_j/D')] \quad (1.11)$$

and the negative weight of evidence as

$$W_j'=ln[P(B'_j/D)/P(B'_j/D')] \quad (1.12)$$

The contrast C for the j-th map is an overall measure of spatial association between the deposits and the binary pattern:

$$C_j=|W_j^+ -W_j'| \quad (1.13)$$

It is assumed that either a cell contains a deposit or does not contain a deposit, so that:

$$P(D/B_j)=1-P(D'/B_j) \quad (1.14)$$

If n binary predictor maps are used as evidence, the posterior logit can be expressed as

$$posterior \ logit \ (D/B_1^{k(1)}\cap B_1^{k(2)}....B_1^{k(n)})$$
$$= prior \ logit(D) + \sum_{j-1}^{n} W_j^{k(j)} \quad (1.15)$$

where the superscript k(j) is + for the presence or – for the absence of the j-th binary pattern.

The variances for the weight formulae are approximately:

$$s^2 \ (W_j^+)=[1/N(B_j\cap D)]+[1/N(B_j\cap D')] \ \text{and}$$
$$s^2 \ (W_j')=[1/N(B'j\cap D)]+[1/N(B'_j\cap D')] \quad (1.16)$$

where $N(B_j\cap D)$ is the number of unit cells where both deposits and the j-th binary pattern are present, and the other terms are similarly defined.

Equation 1.15 assumes conditional independence (CI) for predictor maps with respect to the deposits. In practice, this assumption is commonly violated to some degree, particularly if a large number of maps are being combined. If the assumption is violated, the posterior probability will be either over or under estimated. The CI value can be checked using statistical tests or by testing the final favourability map to determine whether the total number of predicted deposits is equal to the total observed number. In the latter case, should an overestimation >10–15% occur, then pairwise tests (chi-squared or G) of independence can be carried out to reveal whether particular map pairs are in serious violation. Wright & Bonham-Carter (1996) indicate that datasets in serious violation can still be used in the modelling, as in practice, the rank order of the polygons by posterior probability is not greatly affected.

In weights of evidence, predictor (evidence) maps are usually reduced to binary form for ease of interpretation. Binary conversion can be done subjectively using geological judgement, or statistically to determine a threshold that maximises the spatial association between the resultant binary map

pattern and the data pattern. The latter approach objectively determines optimal thresholds between an anomaly and the background by establishing the maximum spatial association between the deposits and each evidence pattern. The contrast, C, is the measure of overall spatial association between the binary pattern and the deposits. To quantify this relationship, weights are calculated using Bayes' Rule for cumulative distances (equations 1.11 and 1.12). For maps with an ordinal, interval or ratio level of measurement, weight calculations are made at successive cut-offs using cumulative areas. Each cut-off is the threshold value between the pattern being present and the pattern being absent. Decisions on threshold, however, are often not straightforward because there may be no clear maximum on a contrast curve, in which case subjective judgement is used. Another guide to the interpretation of the contrast curve comes from estimates of variances of the contrasts. The variance of C is the sum of the variances of the weights. When the ratio of C to its standard deviation (square root of variance) is large (>1.5), the contrast value is considered to be relatively reliable. The ratio of C to its standard deviation is used in a relative sense, S(C) indicating the errors associated with C due to the small number of points or due to small areas. Bonham-Carter & others, (1990) discuss aspects of variances of weights and contrasts in detail.

The final product of the 'weights of evidence' technique is a combined map either in a weight form or as a posterior probability map. In analysing results presented in this form, the limitations of the technique need to be recognised. Weights of evidence is based on a statistical model and assumes that the known

deposits are an adequate sample of known and undiscovered deposits in the region. A significant limitation in the weights of evidence technique is the requirement of a well-explored training site with known deposits. This limitation is common to other 'data-driven' methods, which use statistical measures to characterise the spatial associations between known deposits and map patterns based on local data only. In areas in which limited exploration has been done and where only a few occurrences are known, the estimates of weights will be in error and will have large variances. Bonham-Carter (1994) claims that, in partly explored regions where a reasonable sample of deposits and mineral occurrences are known, the estimates may be sufficiently stable and that adding new as yet undiscovered deposits with essentially the same characteristics as those of known deposits will not greatly alter the weights. The addition of undiscovered deposits can be modelled by increasing the prior probability, which does not change the ranking of areas by posterior probability. Conditional independence (CI) is another problem, often resulting in the posterior probabilities being too large. However, the use of weights and the ranking of areas provides results not affected by CI. According to Bonham-Carter (1994) the weight values should be considered scores and not probabilities when CI is violated. It should be noted that whilst the actual values for weights and contrasts are not very sensitive to the unit cell size or CI, they can be sensitive to the choice of the study region (Bonham-Carter, 1994), and this needs to be considered in the interpretation. The validity of these weights can be confirmed independently and the weights are readily reproducible.

# THE PROBABILISTIC NEURAL NETWORK

The artificial neural network represents an algorithm approach to information analysis that unlike most traditional mathematic models, has the ability to handle complex information, learn patterns and generalise data relationships.

The Probabilistic Neural Network (PNN) is a type of artificial neural network that is based on a powerful statistical approach to classification. The following outline is based on work by Masters (1995).

## *Probabilistic Classification*

Given a set of multivariate geological data points $x$, referred to here as the set of geological observations $X$ (where $x \subset X$ and where bold lower case represents a vector and bold upper case is a matrix) subsets can be identified as $X^{(k)}$, which contains observations that are known to belong to an class (eg a mineral deposit or mineral occurrence) and $X^{(j)}$, which contains observations that belong to an unknown class where $x_k \subset X^{(k)}$ and $x_j \subset X^{(j)}$. The aim is to use $X^{(k)}$ as a training dataset to obtain an estimation of the probability density

function (PDF) $p_i(x_j)$, for all i=1,...,c classes; describing the probability of an unknown geological observation, $x_j \subset X^{(j)}$ belonging to the $i^{th}$ class.

The classification problem assumes that an unknown geological observation $x_j$ must belong to a known population, in this case a population described by one of the classes. If the true PDF $p_i(x_j)$ is known for all i=1,...,c classes, then a Bayes optimal decision rule can be used to classify the unknown observation in the $i^{th}$ class if

$$P_i L_i p_i(x_j) > P_{\hat{i}} L_{\hat{i}} p_{\hat{i}}(x_j) \qquad (2.0)$$

and $i = \hat{i} \; \forall i, \hat{i} \in c$. Here $P_i$ is a constant describing the prior probability for the $i^{th}$ class and $L_i$ is a constant for the loss (sometimes referred to as cost) associated with the misclassification of the $i^{th}$ class. Under these conditions the application of the decision rule in Equation (2.0) minimises the expected cost of a misclassification, for the largest PDF, making it an optimal decision rule.

Equation (2.0) can be used to create a characteristic function or "hard membership function" $\mu(x_j)$ where

$$\mu(x_j) = \begin{cases} 1 & if\ x_j\ belongs\ i^{th}\ event\ class \\ 0 & otherwise \end{cases} \qquad (2.1)$$

When applied to all the $q$ unknown observations in $X^{(j)}$ the resulting $c \times q$ matrix of hard membership functions is referred to as a crisp partition matrix $U^{(j)}$. If $L_i = L_{\hat{i}}$ what is required is knowledge of the PDFs, which must be estimated.

## *Non-Parametric Density Estimators*

Modelling $p_i(x)$ traditionally assumes that the PDF has a certain form, for example a normal distribution or a Poisson distribution. Parameters for these distributions, such as mean and covariance, can be calculated or estimated using the observations in the training set. However, for natural phenomena, such a geology, the underlying distributions are often complex and multi-modal.

Parzen (1962) details a class of univariate, non-parametric PDF estimators that asymptotically converge to the true underlying density function as the sample size approaches infinity. For a set of $k=1,..., n$ random univariate observations, belonging to a single population, Parzen's estimation of the density function for that population is

$$p(x) = \frac{1}{n\sigma} \sum_{k=1}^{K} W\left(\frac{x-x_k}{\sigma}\right) \qquad (2.2)$$

where the weighting function, or "kernel", $W(y)$ is bounded,

$$\sup_{-\infty < y < +\infty} |W(y)| < \infty \qquad (2.3)$$

rapidly approaches zero as its argument increases in absolute value

$$\int_{-\infty}^{\infty} |W(y)| dy < \infty$$
$$\lim_{y \to \infty} |yW(y)| = 0 \qquad (2.4)$$

and is properly normalised

$$\int_{-\infty}^{\infty} W(y) dy = 1 \qquad (2.5)$$

The value sigma $\sigma$, or scaling parameter, in Equation (2.2), defines the width of the kernels about each of the $x_k$ observations. For appropriate asymptotic behaviour, the width of the kernel must become narrower as the number of observations $n$ increases. Thus, for $\sigma$ expressed as a function of $n$, the following conditions must be true:

$$\lim_{n \to \infty} \sigma(n) = 0$$
$$\lim_{n \to \infty} n\sigma(n) = \infty \qquad (2.6)$$

The most commonly used kernel that satisfies Equations (2.3), (2.4) and (2.7) is the Gaussian function, which converts Equation (2.2) to

$$p(x) = \frac{1}{\sqrt{2\pi\sigma^2}} \sum_{k=1}^{K} \exp^{-\left(\frac{x-x_k}{2\sigma^2}\right)} \qquad (2.7)$$

Whilst other kernels can be used (refer Specht, 1990, table 1), the Gaussian function is the most commonly used function because it is well behaved and easy calculated (Masters, 1995).

An appropriate value for the smoothing parameter is important to the estimator's performance. Refer to the six data points in Figure 1a, here the data can be visually placed into two groups of three points along the x-axis. In Figure 1b the density estimate is calculated with a very small smoothing parameter and the benefits of aggregation are lost as the individual training points produce separation in the estimate. The PNN will over fit and its ability to generalise (that is, to recognise incomplete or complex patterns in training datasets) is lost as only observations
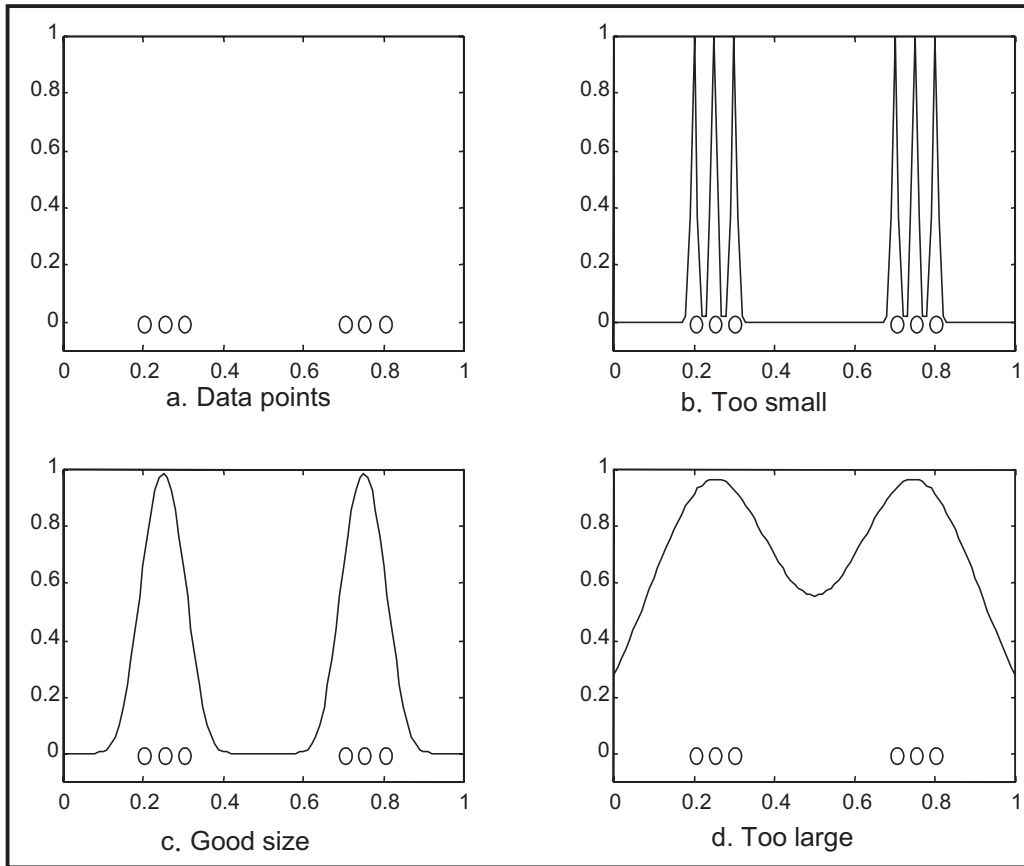
*Figure 1: Effects of the smooth parameter on the shape of the kernel in a (Parzen, 1962 ) density estimator*

very close to the observations that form the neuron weights are recognised. In Figure 1d the opposite occurs. Here a very large smoothing parameter is used and as a result the influence of the training points becomes blurred and kernels cannot be easily separated. In this case the PNN over generalises with the distal points that should belong to other groups being captured and incorrectly classified. Figure 1c shows a more appropriate smoothing parameter where the two groups can be easily separated by the two kernels. At the same time the kernels are wide enough to cover the data points and some area about them. An estimator based on these kernels is able to generalise, but does not under fit or over fit. Finding an appropriate smoothing parameter is discussed below in the section on the PNN models.

The extension of Parzen's estimator to the multivariate case involves the use of multivariate kernels, with multiple smoothing parameters for each variable. Cacoullos (1966) details the multivariate extension of Parzen's estimator and shows that in the multivariate case, where $x$ is a $m$ variable vector, a multivariate kernel becomes the product of univariate kernels

$$W(y_1, \ldots, y_m) = \prod_{q=1}^{m} W_q(y_q) \qquad (2.8)$$

Effects of the smooth parameter on the shape of the kernel in a (Parzen, 1962 ) density estimator.

By using a Gaussian kernel, where $e^{y_1} e^{y_2} = e^{y_1 + y_2}$, the multivariate estimator can be expressed as

$$p(x) = \frac{1}{(2\pi)^{m/2} \sigma^m K} \sum_{k=1}^{K} e^{-\left( \frac{|x - x_k|^2}{2\sigma^2} \right)}$$

$$(2.9)$$

The assumption that all of the smoothing parameters are equal ($\sigma = \sigma_1 = \sigma_2 = \ldots \sigma_m$) is made in Equation (2.9) and this may be an over simplification of the problem of estimating complex PDFs.

The use of multiple smoothing parameters can be important in probability neural network applications where it can improve the network's performance and provide a measure of the importance for each of the variables.
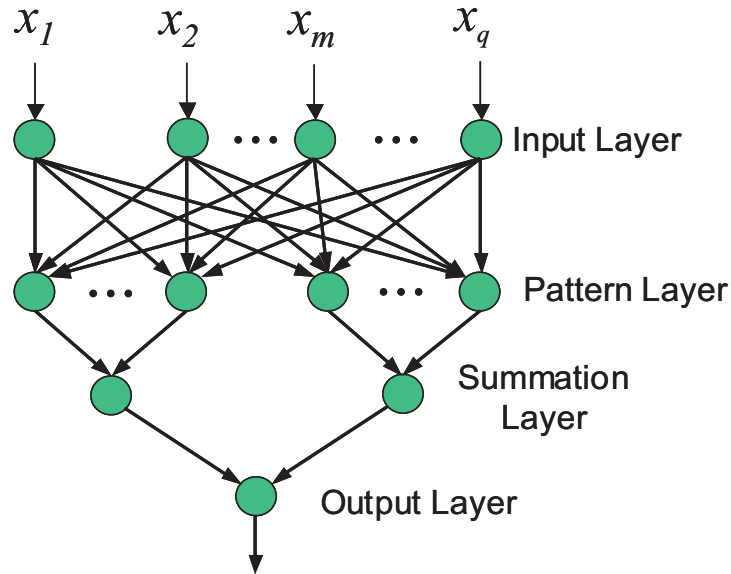
*Figure 2: Basic PNN architecture for a two class classifier (after Specht, 1990)*

## *The Probabilistic Neural Network - Models*

The PNN architecture is shown in Figure 2.

Basic PNN architecture for a two class classifier (after Specht, 1990)

The PNN shown in Figure 2 has an input layer with m inputs, each corresponding to a variable in the multivariate input vector x. The next layer is the pattern layer that contains n neurons each corresponding to one of the $k^{th}$ known geological observations in the training set. The summation layer contains $c$ neurons each corresponding to the $i^{th}$ class. These three layers define the estimator shown in Equation (2.9) as applied in parallel to $c$ classes. The network works by presenting an input vector $x_j$, to the pattern layer (via the input layer), which computes the distances between the input and various training class neurons. The distances are then passed through the activation function or kernel and summed for each class. The summations are then passed to the output layer, or decision layer, where according to Bayes optimal decision rule, Equation (2.0), the maximum ith summation is used to classify $x_j$ as belonging to the $i^{th}$ class. Output here represents a hard membership function, where the $i^{th}$ class is assigned one and the other classes assigned zero.

For computation purposes the restriction implied by Equation (2.5), where the weight function must be normalised, can be lifted. This is possible if the constants in Bayes's decision rule, Equation (2.0), are equal for all classes. In this case the overall network output would be the same whether an estimate of the true PDF or a density function is used. Here $f(x)$ represents a (multiple of a) density function and is used to avoid confusion with PDF denoted by $p(x)$. If a constant smoothing parameter is used for all classes and its associated multiplies are incorporated into this constant, then for an unnormalised Gaussian function, the estimator in Equation (2.9) can be generalised for the $k^{th}$ training class to

$$f(x_j) = \frac{1}{K} \sum_{k=1}^{K} e^{-\left(\frac{\|x_j - x_k\|}{\sigma}\right)} \qquad (2.10)$$

where $\|\cdot\|$ is the Euclidean distance[1] and $n$ equals the number of observations in the $i^{th}$ training class only. If both the known and unknown observations are represented by unit length vectors, then the calculation of Euclidean distance can be replaced by the dot product calculation $x_j^T \cdot x_k$, where T indicates a transpose vector[2].

---

1    The Euclidean distance is not mandatory. Other distances are possible but are almost never used (Masters, 1995).
2    Here the transpose is a row vector and the dot product produces a scalar value called the inner product. Refer books on vector calculus.

## PNN Training

The process of training the PNN is essentially one of finding an optimal smoothing parameter such that it reduces the network's misclassification error while still allowing enough flexibility in the class density estimators for the network to generalise. As in the case of the univariate estimators, an optimal smoothing parameter produces a density estimate that does not over fit (see Figure 1b), nor over generalise (see Figure 1d).

The optimisation of a network with a single smoothing parameter requires an error function, which is simply a count or sum of the classification errors. A classification error can be obtained by re-classifying the training dataset where classification is known, using the PNN. However, when all the training data is used to assess classification errors, optimisation will result in over fitting and loss of generalisation because the PNN is presented with observations whose exact patterns are already stored in the network architecture. To overcome this a Jackknife method is applied, where one of the known observations is excluded from network training, and is presented to the network for classification with the error recorded. This is equivalent to turning off one neuron and then using it to test the other neurons. This is done systematically for all the neurons (all the observations in the training dataset) and the errors for each are summed. The sum of errors is then used as a measure of the network's performance.

This operation can be repeated for various smoothing parameters and the error sums compared to find the best or optimal smoothing parameter. The problem then becomes one of determining which smoothing parameter values are to be tested. As Equation (2.10) uses a single smoothing parameter for all variables and all classes, the search for an optimal value is a one dimensional minimisation problem and a line search method can be used. The most commonly used approach is a Golden Section[3] search which iteratively reduces a scaled search interval using the smallest real root of the quadratic $\gamma^2 - 3\gamma + 1 = 0$; $\gamma = (3 - \sqrt{5})/2 \approx 0.382$ and its complement $1 - \gamma \approx 0.618$. Searching stops, and the smoothing parameter is accepted as optimal, once an acceptable classification error

is reached or the reduction of the search interval becomes too small.

While the use of a single smoothing parameter makes for a fast and simple network it has several drawbacks, notably a reduction in network performance when dealing with complex data and difficult classification problems. An alternative is to use multi-smoothing parameters for the geological variables and the classes.

A major improvement to the classification ability of the PNN can be achieved through the use of multiple variable or multivariable smoothing parameters. While there is a concession in computation time, the performance is greatly improved as the network architecture now has a more "realistic" structure. The use of multivariable smoothing parameters can also overcome some of the problems associated with a training set that is heavily biased to specific variables. For example in predicting the presence of an undiscovered mineral deposit a geochemical variable such as gold (soil content) might be far more important to the classification process than a geophysical metric such as total magnetic response, however using a PNN based on Equation (2.10) both are given equal weighting.

Multivariate smoothing parameters use one parameter for each variable in the observation vector. The use of Equation (2.10) is no longer valid as it determines the vectorial distance (Euclidean distance) between the known and unknown observation and then smooths. Smoothing now occurs when individual variable distances are calculated and then summed to give the overall distance between the observations. If the observation vector contains m variables, where q represents one variable, the distance between the $k^{th}$ known observation and unknown observation[4] $x$ is expressed by the distance function,

$$\delta(x, x_k) = \sum_{q=1}^{m} \left( \frac{x - x_{kq}}{\sigma_q} \right)^2 \qquad (2.11)$$

Using a Gaussian function for the kernel the density estimator becomes

$$f(x) = \frac{1}{K} \sum_{k=1}^{K} \exp\left(-\delta(x, x_k)\right) \qquad (2.12)$$

---

3    Golden Section is a common numerical optimisation technique and is only briefly discussed here.
4    The subscript $j$ for the $j^{th}$ unknown observation has been left off to avoid confusion and an unlabelled observation vector $x$ infers the observation being sought.

Training this new PNN model is more difficult as the optimisation operation becomes a multi-dimensional minimisation problem. The use of a simplistic integer error function based on the sum of classification errors is no longer efficient. A better error function is obtained by measuring the distance between the estimated hard membership function $\mu(x)^*$ and a true hard membership function $\mu(x)$, using the multivariate smoothing parameters (see Equation (2.1)). The true hard membership function is known for the training dataset. For $c$ classes it is represented by a $c$-dimension bit vector with the $i$th element equal to 1 and other elements equal to zero, if Equation (2.1) is true. The issue is finding the estimate $\mu(x)^*$.

Schioler & Hartman (1992) details a method for obtaining a conditional estimate of $\mu(x)^*$ using the PNN as a conditional mapping function. A mapping function simply maps the independent variable vector X to a class membership vector Y, such that for an unknown X an estimate of Y can be obtained. If the mapping is regressional, then the expected least squares error is minimised and the estimate of Y is optimal. In the situation where this mapping represents the joint pdf between X and Y, $p_{XY}(x, y)$, then an optimal estimate of Y for X becomes the conditional expectation of Y given X; and can be expressed as

$$E_{Y|X}(x) = \frac{\int_{-\infty}^{\infty} y \cdot p_{XY}(x,y)dy}{\int_{-\infty}^{\infty} p_{XY}(x,y)dy} \qquad (2.13)$$

Note that for each $x$ in X the single integral is used and Equation (2.13) represents an integral for each $y$ element in Y. X and Y are used to produce a $m + c$ length vector, representing the stochastic joint variable $\Lambda=(X,Y)$ (Schioler, 1992). Assuming that X is an independent variable and using Parzen's estimator in Equation (2.12) to obtain the joint density function $f_\Lambda(x,y)$ an estimation of the (hard) membership function conditional to the observation $x$ is

$$\mu(x)^* = \frac{\int_{-\infty}^{\infty} y \cdot f_\Lambda(x,y)dy}{\int_{-\infty}^{\infty} f_\Lambda(x,y)dy} \qquad (2.14)$$

Schioler & Hartman (1992) showed that if a Gaussian kernel is used for $f_\Lambda(x,y)$ then Equation (2.14) can be simplified by removing the integrals and summing the kernels. The result is that if a Parzen neuron is used the activation function $\gamma(x)$ for the $i$th neuron becomes

$$\gamma_i(x) = \sum_{k=1}^{n} \mu_i(k) \exp(-\delta(x, x_k)) \qquad (2.15)$$

and the conditional estimate becomes

$$\mu_i(x)^* = \frac{\gamma_i(x)}{\psi(x)} \qquad (2.16)$$

where the denominator is the sum of all neuron activations

$$\psi(x) = \sum_{i=1}^{c} \gamma_i(x) \qquad (2.17)$$

For any $i$th class, Equation (2.16) is essentially a measure of Bayesian confidence. For example for the $i$th class the numerator activation function in Equation (2.16) represents only its density function (as $\mu_i(k)=1$, $\mu_{\bar{i}}(k)=0 \ \forall i \neq i$) and only distances to the observations belonging to the $i$th classes are summed. The denominator on the other hand, sums for all known observations and for all $c$ classes. This assumes that all events are exhaustive (the training set contains all classes) and mutually exclusive (an observation in the training set can belong only to one class).

Masters (1995) describes a continuous error function

$$e_i(x) = \left[1 - \mu_i(x)^*\right]^2 + \sum_{\bar{i} \neq i} \left[\mu_{\bar{i}}(x)^*\right]^2 \qquad (2.18)$$

which is essentially a measure of how much $\mu_{\bar{i}}(x)^*=1$ and all the $\mu_{\bar{i}}=0$. Masters presents the derivatives for Equation (2.18) with respect to the variable smoothing parameters in Equation (2.11). For the $q$ variables, each with a smoothing parameter, the 1st and 2nd order derivatives are respectively;

$$\frac{\partial e_i(x)}{\partial \sigma_q} = 2\left[\mu_i(x)^* - 1\right]\left[\frac{\partial \mu_i(x)^*}{\partial \sigma_q}\right] + 2\sum_{i \neq k} \mu_k(x)^* \frac{\partial \mu_k(x)^*}{\partial \sigma_q} \qquad (2.19)$$

$$\frac{\partial^2 e_i(x)}{\partial^2 \sigma_q^2} = 2\left[\mu_i(x)^* - 1\right]\left[\frac{\partial^2 \mu_i(x)^*}{\partial \sigma_q^2}\right] + 2\left[\frac{\partial \mu_i(x)^*}{\partial \sigma_q}\right]^2$$
$$+ 2\sum_{k \neq i}\left[\mu_k(x)^* \frac{\partial^2 \mu_k(x)^*}{\partial \sigma_q^2}\right] + 2\sum_{i \neq k}\left[\mu_k(x)^* \frac{\partial \mu_k(x)^*}{\partial \sigma_q}\right]^2 \qquad (2.20)$$

As $\mu(x)$ is based on the Gaussian distance function in Equation (2.12) and recognising $\exp^{a+b} = \exp^a + \exp^b$, then 1st and 2nd partial derivatives for the functions of $\mu_i(x)^*$, with respect to the smoothing parameters, $\sigma_q$ can be expressed as:

$$\frac{\partial \mu_i(x)^*}{\partial \sigma_q} = \frac{\nu_{iq}(x) - V_q(x)\mu_i(x)^*}{\psi(x)}$$ (2.21)

$$\frac{\partial^2 \mu_i(x)^*}{\partial \sigma_q^2} = \frac{w_{iq} - W_q(x)\mu_i(x)^*}{\psi(x)}$$
$$+ \frac{2V_q^2(x)\mu_i(x)^* - 2\nu_{iq}(x)V_q(x)}{\psi^2(x)}$$ (2.22)

where

$$\frac{\partial \gamma_i(x)}{\partial \sigma_q} \equiv \nu_{iq}(x) = 2\sum_{k=1}^{n} \mu_i(k)\exp[-\delta(x,x_k)] \cdot \frac{(x_q - x_{iq})}{\sigma_q^3}$$

$$\frac{\partial \psi(x)}{\partial \sigma_q} \equiv V_q(x) = \sum_{i=1}^{c} \nu_{iq}(x)$$ (2.23)

$$\frac{\partial^2 \gamma_i(x)}{\partial \sigma_q^i} \equiv w_{iq}(x)$$

$$= 2\sum_{k=1}^{n} \mu_i(k)\exp[-\delta(x,x_k)] \cdot \left[ 2\frac{(x_q - x_{iq})^4}{\sigma_q^6} - 3\frac{(x_q - x_{iq})^2}{\sigma_q^4} \right]$$

$$\frac{\partial^2 \psi(x)}{\partial \sigma_q^2} \equiv W_q(x) = \sum_{i=1}^{c} w_{iq}(x)$$ (2.24)

Note that the functions in Equations (2.23) and (2.24) use individual variable distances for each observation. For computation efficiency these equations can be simplified by removing redundant calculations related to common smoothing factors. The result is that the error function in Equation (2.18) can be minimized for the multivariable smoothing parameters using Equations (2.19) to (2.24).

In cases where the classes have natural variations in scale or importance, the use of multiclass smoothing parameters is suited for finding complex patterns. Multiclass smoothing parameters, however, do increase the number of computations required to optimise the $q$ (variables) x $c$ (classes). There are also issues associated with the interactions between the smoothing parameters when variable and class numbers are large. Optimisation of a large system of parameters may not reach true stability. The high number of parameters can also lead to over fitting. The use of validation, via another set of labelled observations, is then required to gauge a network's performance.

For multi-class smoothing parameters the distance function in Equation (2.11) needs to be redefined to include not only the separate variable smoothing parameters but also separate class smoothing parameters:

$$\delta_i(x,x_k) = \sum_{q=1}^{m} \left( \frac{x_q - x_{kq}}{\sigma_{iq}} \right)^2$$ (2.25)

The activation function must also account for multiple smoothing parameters associated with each class. The multiclass activation function, for the Parzen estimator in Equation (2.15), when extended to multiclass function becomes:

$$\gamma_i(x) = \frac{1}{\sigma_{i1}\sigma_{i2}\cdots\sigma_{iq}} \sum_{k=1}^{n} \mu_i(k)\exp\left(-\delta_i(x,x_k)\right)$$ (2.26)

The process of finding the partial derivatives of the new multiclass activation function with respect to the multiclass smoothing parameters involves the definition of two new functions:

$$\upsilon_{iq}(x) = 2\sum_{k=1}^{n} \mu_i(k)\exp\left[-\delta_i(x,x_k)\right] \frac{(x_q - x_{kq})^2}{\sigma_{iq}^3}$$ (2.27)

$$\omega_{iq} = 2\sum_{k=1}^{n} \mu_i(k)\exp[-\delta_i(x,x_k)]\cdot$$

$$\left[2\frac{\left(x_q - x_{kq}\right)^4}{\sigma_q^6} - 3\frac{\left(x_q - x_{kq}\right)^2}{\sigma_q^4}\right]$$

$$(2.28)$$

Except for the inclusion of a new distance function Equations 2.25 and 2.27 are identical to Equations 2.23 and 2.24, and represent unnormalised partial derivatives of the activation function in Equation 2.26. As $\mu_i(k)=1$ only when the $k^{th}$ observation belongs to the $i^{th}$ class, the variable difference summation is done only over the $i^{th}$ class. By creating a new parameter $\tau_i = \sigma_{i1} + ... + \sigma_{iq} + ... \sigma_{im}$ both Equations 2.27 and 2.28 can be normalised and used to find the $1^{st}$ and $2^{nd}$ partial derivatives for the activation function in respect to the class/variable smoothing parameters:

$$\frac{\partial \gamma_i(x)}{\partial \sigma_{iq}} \equiv \nu_{iq} = \frac{\upsilon_{iq}(x)}{\tau_i} - \frac{\gamma_i(x)}{\sigma_{iq}}$$

$$(2.29)$$

$$\frac{\partial^2 \gamma_i(x)}{\partial \sigma_{iq}^2} \equiv w_{iq}(x) = \frac{\varpi_{iq}(x)}{\tau_i} + 2\frac{\gamma_{iq}(x)}{\sigma_{iq}} - 2\frac{\upsilon_{iq}(x)}{\tau_i \sigma_{iq}}$$

$$(2.30)$$

Many of the partial derivatives for the activation functions above are equal to zero, as in many cases a known observation does not belong to a class ie $i \neq k$. It follows then that:

$$\frac{\partial \psi(x)}{\partial \sigma_{kq}} = \sum_{i=1}^{c} \nu_{ikq}(x) = \nu_{kq}$$

$$\frac{\partial^2 \psi(x)}{\partial \sigma_{kq}^2} = \sum_{i=1}^{c} w_{ikq}(x) = w_{kq}$$

$$(2.31)$$

These parameters can then be used to modify the multi-variable partial derivatives in Equations (2.21) and (2.22) to obtain the partial derivatives of estimated (hard) membership functions, with respect to multi class/variable smoothing parameters:

$$\frac{\partial \mu_i(x)^*}{\partial \sigma_{kq}} \equiv \frac{\nu_{ikq}(x) - \nu_{kq}(x)\mu_i(x)^*}{\psi(x)}$$

$$(2.32)$$

$$\frac{\partial^2 \mu_i(x)^*}{\partial \sigma_{iq}^2} \equiv \frac{w_{ikq} - w_{kq}\mu_i(x)^*}{\psi(x)} +$$

$$\frac{2\nu_{kq}^2(x)\mu_i(x)^* - 2\nu_{ikq}(x)\nu_{kq}(x)}{\psi^2(x)}$$

$$(2.33)$$

These derivatives can be then used in the error derivatives (Equations 2.19 and 2.20 ) and to optimise the error function in Equation (2.18).

Network optimisation involves minimising errors in the search for optimal smoothing parameters. This requires the selection of an appropriate starting point for the search for optimal smoothing parameters, then a method is chosen that uses the error derivatives defined above to iteratively optimise the smoothing parameters. Masters (1995) suggests that a Golden line search, using a Parzen estimator (single constant smoothing parameter), can be used to find a starting value for the multiple smoothing parameters. Once starting points are located finding a minima then requires a move down hill away from this point (unless it is the minima). The use of simplistic gradient descent update is slow and in some cases can "bounce" around minima without locating them. Another approach is the conjugate gradient descent method[5] that uses: if $g_l$ is a negative gradient and $d_l$ a direction, both at point $l$, then

$$\beta = \frac{(g_l - g_{l-1})\cdot g_l}{g_{l-1}\cdot g_{l-1}}$$

$$(2.34)$$

$$d_l = g_l + \beta d_{l-1}$$

Note that the dot product used in Equation (2.34) implies that the first vector term is transposed. The algorithm begins by taking $g_0$ and $d_0$ as equal to the negative gradient at the starting point. While the conjugate gradient method does not require $2^{nd}$ order derivatives they can be used to scale the (line) search used in Equation (2.34). If the $2^{nd}$ order error partial derivatives in Equation (2.20) are used as the diagonal in a Hessian[6] matrix $H$, while the other entries (the mixed partial derivatives) are left as zero, then

---

5   Conjugate gradient behaves as $2^{nd}$ order descent while not requiring the $2^{nd}$ derivatives.
6   Hessian is matrix of $2^{nd}$ order partial derivatives, whose diagonal contains only pure partials derivatives while upper/lower triangles are mixed partials derivates.

$$t_i = -\frac{g_l \cdot d_l}{d_l^T H_l d_l} \tag{2.35}$$

The new distance given by $t_l$ should move the error from point $l$, along the direction $d_l$, to a better minimum at the new point $l+1$. The process of optimisation then becomes an iterative one where the error is calculated at point $l+1$ and the conjugate gradient method is applied to find the next minima. This continues until an appropriate error is reached or the gradients become very small or equal zero. The smoothing parameters calculated by this process then represent optimal values and can be used in the new trained PNN to classify the unknown observations and obtain estimates of their class density functions.

## *Bayesian weights and Bayesian confidences*

From Equation (2.0) the prior probabilities and cost are equal for all classes and thus can be ignored in the Bayesian decision rule. However, if this assumption is incorrect and class prior probabilities and/or misclassification costs are different then these have to be incorporated in the PNN training. This can be useful if data for the various classes is biased, in which case a set of Bayesian weights $\{P_i, i=1,..., c\}$ can be used to incorporate this information. Note that $P_i$ here can include both the prior probabilities and the costs in Equation (2.0) via simple multiplication, or can represent either the prior probability or cost, depending on what is known about the classes being studied. The weights are then used to modify Equations (2.16) and (2.17), so that the Bayesian estimate becomes:

$$\mu_i(x)^* = \frac{P_i \gamma_i(x)}{\psi(x)} \tag{2.36}$$

and the sum of class activations equals

$$\psi(x) = \sum_{i=1}^{c} P_i \gamma_i(x) \tag{2.37}$$

The result is that the error function in Equation (2.18) is not affected and its partial derivatives do not change. Also the partial derivatives of the activation function in Equations (2.23) and (2.24) (and their multi-class counterparts in Equations (2.29) and (2.30) are not changed. The only modification of the partial derivatives is that output functions $v_{iq}$ and $w_{iq}$ (or unnormalised functions in the case of multi-class smoothing, $\upsilon_{iq}$ and $\varpi_{iq}$) need to be multiplied by the weights.

If estimates of density generated by a trained PNN need to be Bayesian confidence estimates representing conditional estimates of the density function that the $i^{\text{th}}$ class occurs given observation $x$ occurs, then

$$P(i|x) = \frac{P_i f_i(x)}{\sum_{i=1}^{c} P_i f_i(x)} \tag{2.38}$$

If prior probabilities and losses represented by the Bayesian weight Pi are equal for all classes then they can be removed from both the denominator and numerator. If such weights have been used in training it is appropriate to use them in conditional density estimates.

Equation (2.38) is valid as a conditional estimate if the training dataset $X^{(j)}$ is exhaustive (contains observations for all the classes) and mutually exclusive (observations can only belong to one class). In mineral potential analyses this implies that training data should contain geological observations for all the deposit and barren classes to be found in the unknown data and that each observation must belong to one class only. Both conditions are often not met because data and geological understanding is incomplete. However if both conditions are expected then the PNN can be used to generate conditional estimates.

## REFERENCES

BONHAM-CARTER, G.F., 1994: *Geographic Information Systems for geoscientists:modeling with GIS*. Pergamon.

CACOULLOS, T., 1966: Estimation of a multivariate density. *Annals of the Institute of Statistics Mathematical*, **18**(2), 179–189.

MASTERS, T., 1995: *Advance algorithms for neural networks a C++ source book*. John Wiley and Sons, New York.

PARZEN, E., 1962: On estimation of a probability density function and mode. *Annals of Mathematical Statistics*, **33**, 1065–1076.

SCHIOLER, H. & HARTMAN, U., 1992: Mapping neural network derived from the Parzen window estimator. *Neural Networks*, **5**(6), 903–909.

SPECHT, D. F., 1990: Probabilistic neural network. *Neural Networks*, **3**, 109–118.

SINGER, D. A. & KOUDA, R., 1999: A comparison of the weights-of-evidence method and probabilistic neural networks. *Natural Resources Research*, **8**(4), 287–298.